GLR Control Charts for Monitoring Correlated Binary Processes

Ning WANG

Dissertation submitted to the Faculty of the

Virginia Polytechnic Institute and State University

in partial fulfillment of the requirements for the degree of

Doctor of Philosophy

in

Statistics

Marion R. Reynolds, Jr., Chair

Ran Jin

Inyoung Kim

William H. Woodall

December 5, 2013

Blacksburg, Virginia

Keywords: Abrupt Change; Average Time to Signal; Change Point; CUSUM Chart; Generalized Likelihood Ratio; Markov Chain; Initial State; Statistical Process Control; Steady State.

GLR Control Charts for Monitoring Correlated Binary Processes

Ning WANG

Abstract

When monitoring a binary process proportion p, it is usually assumed that the binary observations are independent. However, it is very common that the observations are correlated with ρ being the correlation between two successive observations.

The first part of this research investigates the problem of monitoring p when the binary observations follow a first-order two-state Markov chain model with ρ remaining unchanged. A Markov Binary GLR (MBGLR) chart with an upper bound on the estimate of p is proposed to monitor a continuous stream of autocorrelated binary observations treating each observation as a sample of size $n = 1$. The MBGLR chart with a large upper bound has good overall performance over a wide range of shifts. The MBGLR chart is optimized using the extra number of defectives (END) over a range of upper bounds for the MLE of p. The numerical results show that the optimized MBGLR chart has a smaller END than the optimized Markov binary CUSUM.

The second part of this research develops a CUSUM-$p\rho$ chart and a GLR-$p\rho$ chart to monitor p and ρ simultaneously. The CUSUM-$p\rho$ with two tuning parameters is designed to detect shifts in p and ρ when the shifted values are known. We apply two CUSUM-$p\rho$ charts as a chart combination to detect increases in p and increases or decreases in ρ. The GLR-$p\rho$ chart with an upper bound on the estimate of p, and an upper bound and a lower bound on the estimate of ρ works well when the shifts are unknown. We find that the GLR-$p\rho$ chart has better overall performance.

The last part of this research investigates the problem of monitoring p with ρ remains at the target value when the correlated binary observations are aggregated into samples with $n > 1$. We assume that samples are independent and there is correlation between the observations in a sample. We proposed some GLR and CUSUM charts to

monitor p and the performance of the charts are compared. The simulation results show MBNGLR has overall better performance than the other charts.

Acknowledgements

My sincere gratitude and special thanks go to my advisor, Dr. Marion R. Reynolds Jr., who has provided his guidance, support and patience throughout my dissertation research. I also thank Dr. Reynolds for his countless hours of editing and suggestions to help me complete this dissertation.

I would like to thank Dr. Ran Jin, Dr. Inyoung Kim, and Dr. William H. Woodall for their interest in my research and insightful suggestions on the future directions of my work.

Many people in Department of Statistics have helped and encouraged me in various ways. I especially want to thank Dr. Jeffery Birch and Dr. Eric Vance for their advice and help throughout my study and work in the department. My thanks also go to all the graduate students in Dr. Reynolds' research group.

I give my most special thanks to my parents. Without their unlimited love supports, none of my work would be possible.

Table of Contents

List of Tables

List of Figures

Chapter 1. Introduction

Statistical process control (SPC) applies statistical methods to monitor or control a process. The SPC idea was first proposed by Walter A. Shewhart in 1920s and was used to improve the quality in manufacturing during World War II. In recent years, SPC has been widely used in a variety of areas, such as public health, the transportation industry, and environmental management.

As an intuitive idea, variation exists in any production process where a product is required to meet some specified requirements. The causes of variation can be divided into two categories: common causes and special causes. The common cause variation is some inherent variation that is usual and has been identified previously; and special cause variation is unusual, not identified before, and caused by some identifiable factors. The existence of special cause variation can impact the quality of the product and needs to be detected and controlled as quickly as possible in a production process.

To detect a special cause of variation, control charts have been widely used in industry for a long time. As a production process keeps going on, a control chart is applied to detect special causes by visually displaying a control statistic from the process. This control statistic differs with different types of control charts. The control limits are specified according to the requirements of the controlled process. Samples from the production process are taken at regular time intervals and the statistics calculated are compared with the control limits. A process without the presence of any special cause of variation is said to be in-control. If a process is out-of-control and a special cause is detected by a sample statistic falls outside of the control limits, then remedial measures are needed to move the process back to the in-control state. A control chart is expected to detect such changes as quickly as possible to reduce the loss due to excessive variation in the process. The change of a parameter from the original value to some larger or smaller value in a process is called a shift in the parameter. Another type of change where the process is changing gradually is called a drift. We will only consider the shift case in this dissertation.

Traditionally, there are several types of control charts used for monitoring observations following the normal distribution, such as control charts based on the sample averages. The Shewhart $\overline{X}$-Chart proposed by Shewhart (1931) using the sample average $\overline{X}$ as the chart statistic is the most widely used control chart due to the simplicity of the chart construction. Shewhart-type charts are very effective when the parameter shift is large, however, when a shift is small, Shewhart-type charts with control statistic calculated only from the current sample are not effective. Page (1954) proposed the CUSUM chart using the cumulative sum of the observation as the control statistic. With a tuning parameter included, the CUSUM chart can be tuned to detect a small shift. Another control chart that is also effective for detecting a small shift is the exponential weighted moving average (EWMA) chart proposed by Roberts (1959). To detect a wide range of shifts effectively, combinations of control charts have been used in the literature, such as a combination of a Shewhart-type chart and a CUSUM chart (Westgard, 1977).

Besides the monitoring of normal observations, control charts have been widely applied to proportion-related data, such as Bernoulli observations, geometric observations and binomial observations. In a production process, suppose that items are examined and classified as either defective (nonconforming) or non-defective (conforming) by some criteria specified by the manufacturer. The quality of an item is represented by a binary variable X. Let $X_k = 0$ if the k^{th} item is non-defective, and $X_k = 1$ if the k^{th} item is defective. The long-run proportion of defective items p is considered to be some value p_0 if the process is in-control. A control chart is applied to monitor the proportion and an increase in the proportion refers to the case in which the quality of the process output has decreased due to the increased number of defectives. A decrease in the proportion means that the quality has improved. It is usually more important to detect an increase in the proportion rather than a decrease from the point of view of the manufacturers who need to satisfy the requirements of the customer. In this dissertation we will consider the problem of monitoring a proportion and will focus on the detection of increases in this proportion.

In practice, p_0 is estimated in Phase I where a sufficiently large data set is collected. This data set is used retrospectively to estimate p_0 and then construct the control limit. The process enters Phase II once we determine that the observations are from a stable process and are representative of an in-control process. In Phase II, the control chart is applied in real time to the

data taken in sequence and the control statistic is compared with the control limits. A signal is given once the control statistic falls outside of the control limits.

In practice, different sampling plans can be applied to obtain observations for inspection. The sampling plan requires the specification of the sample size and the frequency with which samples are taken. Suppose, for example, that a process produces one item every 5 seconds and consider two general types of sampling plans that could be used.

The first general type of sampling plan only inspects items during specified periods of time. For example, suppose that 60 consecutive items are inspected every 8 hours, and these 60 items are considered to be a sample. The time to produce 60 items is 5 minutes, and this is short enough that shifts are unlikely to occur within a sample. As another case suppose that samples of 300 consecutive items are inspected every 8 hours. Producing one sample requires 25 minutes and this time is longer than in the first case. Therefore, shifts are more likely to happen within samples for this case. When items are inspected as samples, a control chart with a control statistic based on a sample statistic can be applied.

The second general type of sampling plan that could be used in practice is called "continuous inspection". One example for "continuous inspection" is when all produced item are examined, i.e. 100% inspection. The inspection takes place once an item is produced and available for inspection. The 100% inspection in this example requires that the time for inspecting one item is less than 5 seconds. However, "continuous inspection" can also happen with less than 100% inspection. In this example, 720 items are produced in one hour, but it may happen that only 60 of them can be inspected, because the inspection time of each item takes 1 minute. In this case, the inspection stream we get is still continuous with items 1 minute apart but only 1/12 of the items are being inspected. When inspecting continuously, we can use a sample size of $n = 1$ or artificially aggregate observations into samples with $n > 1$.

In tradition, the process proportion is monitored by the Shewhart p-chart or an equivalent Shewhart np-chart, which is based on samples of size $n > 1$. The Shewhart p-chart plots the proportion of defectives in a sample on the chart and the control limits are usually set at three standard deviations from p_0. An equivalent Shewhart np-chart plots the number of defectives in each sample on the chart. Gan (1993) and Reynolds and Stoumbos (2000) considered a binomial

CUSUM chart based on a likelihood ratio statistic for the case in which the observations are aggregated into samples. Compared with the Shewhart-type charts, the binomial CUSUM chart can be tuned to detect small shift sizes and is much more flexible in the selection of control limits.

For the situation in which there is a continuous stream of inspected items, Reynolds and Stoumbos (1999) proposed the Bernoulli CUSUM chart based on a sample size of $n = 1$. The Bernoulli CUSUM chart plots a point after the inspection of each individual item, and thus does not need to wait until the number of observations required to make a sample of $n > 1$ have been obtained in order to make a decision. Thus, the time to detect most changes is faster compared with the binomial CUSUM chart. The charts discussed here all assumed that the observations are independent from each other. General reviews of control charts for monitoring a proportion are given by Woodall (1997) and Szarka and Woodall (2011).

In practice, the binary observations from a process are frequently not independent and thus cannot not be treated as Bernoulli observations if $n = 1$ and the number of defectives in a sample of $n > 1$ will not have a binomial distribution. In recent decades, there has been some work done for the case where the observations are not independent. Alwan and Roberts (1995) discussed the misspecification of control limits when autocorrelation exists among normal observations. Deligonul and Mergen (1987) showed that neglecting the dependence of observation for small lot sizes may cause bias in estimating control limits for the p-chart. It is a very common to model autocorrelated binary observations using a two-state Markov chain model, in which the value of observation X_k only depends on the value of the previous observation X_{k-1}. Thus, in this model the current observation can be generated from the previous observation using the transition probabilities.

For the two-state Markov chain model, Blatterman and Champ (1992) showed that when using a Shewhart chart the time required for detection for any shift in the proportion increases as the correlation increases, and thus it is reasonable to consider the effect of correlation when monitoring correlated binary data when using a Shewhart chart. It is noted that they used an equivalent geometric-type random variable for process monitoring. The statistic to be plotted, Y_t, is the number observations needed to observe the t^{th} defective items after the $(t-1)^{th}$ defective observation. The random variable Y is considered to be a variable of the geometric

type, but is not a standard geometric variable due to the existence of correlation between the binary observations. When the binary observations are independent and Y follows a geometric distribution, the Geometric CUSUM chart developed by Bourke (1991) can be applied to monitor a proportion. Reynolds and Stoumbos (1999) and Megahed et al. (2011) showed that a Geometric CUSUM chart is equivalent to a Bernoulli CUSUM chart with some appropriate settings to the headstart.

Champ, Blatterman and Rigdon (1994) proposed a CUSUM chart based on Y_t for monitoring the Markov dependent data and showed that the CUSUM chart has better performance than the Shewhart type chart. Shepherd et al. (2007) proposed a control chart that is a special case of the "sets method" (originally proposed by Chen (1978)). This control chart plots Y_t and will be signal if a specified number of consecutive values of Y_t fall below the control limit. The chart proposed by Shepherd et al. (2007) is most effective when the in-control proportion p_0 is very small.

Mousavi and Reynolds (2009) discussed the robustness of the Shewhart p-chart and the binomial CUSUM chart when there is autocorrelation among the binary observations and showed that the in-control performance is not robust as the correlation changes. Thus, they proposed a Markov Binary CUSUM (MBCUSUM) chart using likelihood-ratio-based statistics for the monitoring process. The MBCUSUM chart was shown to have better overall performance than the traditional charts that ignore any autocorrelation in the observations. Comparing the MBCUSUM chart with the chart proposed by Shepherd et al. (2007), the MBSUCUM chart has better performance expect for very large shifts relative to extremely small in-control p_0 values.

When the process is not monitored continuously, only samples or segments of the process taken at times t_1, t_2 ... are inspected. Then a sample statistic can be defined as $T_s = X_{t_s} + \cdots + X_{t_s+n-1}$. The time distance $t_s - t_{s-1}$ is assumed to be sufficiently large so that the T_s statistics can be assumed to be approximately independent and identically distributed. A possible correlation structure within a sample has been discussed by Madsen (1993) and assumes that any two observations in the sample have the same correlation, i.e. $Corr[X_i, X_j] = \rho$. Altham (1978) proposed a distribution for T_s when the correlation ρ is very small. Both of the two distributions for T_s are not realistic for use in practice (see more details in Weiss (2009)). Weiss

(2009) suggested using a distribution for T_s, called the Markov Binomial distribution MB (n, p, ρ), which assumes that within the same sample, the sequence $X_{t_s} \ldots X_{t_s+n-1}$ follows a two-state Markov chain model. Weiss (2009) also developed a Markov np-chart and Markov EWMA chart based on this distribution for T_s. It was concluded that the Markov EWMA chart with appropriate tuning parameters can detect any change in a proportion, but the Markov np-chart cannot detect a decrease in a proportion when p_0 and n are both small. It is also shown by Weiss (2009) that the in-control performance of the traditional Shewhart-type and EMWA charts is not robust when correlation exists.

Besides the statistical monitoring of correlated binary data using samples of $n > 1$, situations with grouped correlated binary observations are also discussed in other areas. In the structured finance area, the distribution of an idealized portfolio of n assets with the same probability on each asset and same correlation between any two assets is known as Moody's correlated binomial default distribution (Mori, Kitsukawa and Hisakado (2009)). Hisakada, Kitsukawa and Mori (2006) also proved that the distribution is beta-binomial when any of the two observations in a sample are correlated. The correlated binomial model and the beta-binomial model have been used in the analysis of the certain toxicological experiment by Kupper and Hasman (1978) and microarray experiments involving comparisons of thousands of genes by Gupta and Tao (2010). Weiss (2009) discussed the inspection of binary data by groups under several assumptions about the data distributions.

Based on the discussion in the literature, the traditional types of control charts (Shewhart, CUSUM, and EWMA) that do not account for the correlation in the process are not robust to correlation, and are thus not reasonable to apply to correlated binary data. The control charts that account for the correlation have better performance than the traditional types of charts, especially the MBCUSUM chart when there is a continuous stream of inspected items.

Another type of chart that has been used in recent years to detect changes in a distribution is the generalized likelihood ratio (GLR) chart, which is based on a sequential likelihood ratio test. The GLR algorithm was initially proposed by Lorden (1971) and then was generalized by Blostein (1991). In recent years the GLR chart has been discussed in research papers, but has not been widely used in industry due to the complexity in calculation and the fact that it is unknown

to most practitioners. In research, the GLR chart has been well developed for the case of normal observations, such as monitoring the normal process mean and/or variance. See, for example, Willsky and Jones(1976), Basseville and Nikiforov (1993), Lai (1995, 1998,2001), Apley and Shi (1999), Capizzi (2001), Hawkins et al.(2003), Runger and Testik (2003), Reynolds and Lou (2010), Reynolds et.al (2013) and Wang and Reynolds (2013) for more details.

Huang, Wang and Reynolds (2012) proposed a Bernoulli GLR chart to detect an increase in a proportion when there is continuous inspection and the binary observations are independent. The Bernoulli GLR chart uses a generalized likelihood ratio based on the past m observations where m is called a window size. An upper bound on the estimate from the MLE is imposed to avoid an undefined Bernoulli GLR statistic. The Bernoulli GLR chart is shown to have overall better performance in detecting a range of increases in a proportion than the Shewhart CCC-chart, the Bernoulli CUSUM chart, and Bernoulli EWMA chart. Huang, Wang and Reynolds (2013) showed that the Bernoulli GLR chart is easier to design and has much faster detection of small shifts than the Bernoulli CUSUM chart and has almost the same performance for other shifts.

Huang, Reynolds, and Wang (2012) proposed a binomial GLR chart to detect an increase in a proportion when the observations are grouped into samples. It was shown that the binomial GLR chart can be approximated by a countable set of Bernoulli CUSUM charts, and thus can detect a wider range of shifts faster than a single binomial CUSUM chart which is tuned to detect just a particular size of shift. The binomial GLR chart does not require users to specify values of numerous control chart parameters, which greatly reduces the effort needed to design and implement this chart. They also showed that the binomial GLR chart has very good overall performance for detecting a wide range of shift sizes. The Bernoulli GLR and the binomial GLR charts are both designed to detect an increase in the proportion of defectives when the binary observations are independent. And both charts can beat the CUSUM charts with better overall out-of-control performance. The two GLR charts are easy to design, as the control limits of the charts can be easily obtained from a linear equation once the false alarm rate is fixed. From the aspect of designing control charts, it is much easier to design a GLR chart than to design a CUSUM chart.

The two GLR charts for the cases of $n = 1$ and $n > 1$ are based on the assumption that the observations are independent. However, in practice, due to the nature of the production

process and the nature of the raw materials, the items produced may be correlated with each other and it will be more reasonable to assume that autocorrelation exists among the binary observations.

The goal of this dissertation is to develop GLR charts for monitoring correlated binary observations which follow the two-state Markov chain model. In this dissertation, we first consider the situation of continuous inspection ($n = 1$) and develop a Markov binary GLR chart with an upper bound imposed on the estimated shift $\hat{p}_1$. The performance of the Markov binary GLR chart in detecting increases in p is compared to the MBCUSUM chart. The Markov binary GLR chart and the MBCUSUM chart are optimized over different values of the upper bound and the pre-determined shift size, respectively. A loss function is proposed based on the extra number of defectives produced when there is a shift in p above p_0 and is used as a criterion to optimize the two types of charts.

In the work described in the previous paragraph, the correlation is assumed to be unchanged as the proportion increases. The correlation in a two-state Markov Chain model is related to the transition probabilities, and it is possible that a particular combination of correlation and proportion does not exist. In addition, it is possible in a real process that a special case results in a change in both simultaneous p and ρ. Therefore, the second part of the dissertation focuses on the monitoring process under a more general assumption and allows for p and ρ shift simultaneously. We propose several different types of charts for monitoring both p and ρ and evaluate the performance of these proposed charts.

The third part of the dissertation considers the case in which observations are grouped into samples of $n > 1$ and the time interval between any two consecutive samples is long enough that the samples can be considered to be independent. A Markov binomial GLR chart is proposed for monitoring using the number of defectives in the samples. This Markov binomial GLR chart is compared with the Markov np-chart, the Markov CUSUM chart and Markov Shewhart-CUSUM chart combinations when the sample size takes different values. An EGLR chart based on an EWMA estimator instead of the MLE is also proposed to compare with the other charts.

The structure of this dissertation is as follows. In the next chapter, we provide a literature review of some commonly used control charts for monitoring a proportion, and a summary of

work that have been done previously for the GLR chart. The review also includes background information on process monitoring, the sampling plan, and the performance metrics that will be used to compare different control charts for detecting shifts in a proportion. Chapter 3 is devoted to the derivation of the Markov binary GLR chart when $n = 1$ and an explanation of the chart design with an upper bound. The extra number of defectives (END) is defined in this chapter and used to optimize the Markov binary GLR chart and the MBCUSUM chart with respect to the upper bound and the pre-specified shift size, respectively. A real data example is used to illustrate how practitioners can apply the Markov binary GLR chart. Chapter 4 discusses the monitoring process for proportion and correlation and we propose the CUSUM-$p\rho$ and GLR-$p\rho$ chart. The performance of the charts is studied for various directions of the shifts. Chapter 5 discusses the derivation and design of the Markov binomial GLR chart when $n > 1$. The proposed chart is compared with the Markov Shewhart, the Markov Binomial CUSUM, the Markov Shewhart-CUSUM combination, and the EGLR charts. Some preliminary analysis from simulation is discussed as well. In Chapter 6, we summarize current results and outline some future work.

Chapter 2. Background

2.1 The Data Structure and the Sampling Plan

For quality characteristics, the data are measured in two forms: a continuous form and a discrete (or count) form. The continuous form is frequently known as variables data while the discrete form is known as attributes data. Count data can be are collected in a production process, where a defective item is represented as "1" and a non-defective item is represented as "0". For example, with a filling process for milk cartons that normally contain 8 oz, a milk carton is mark as "1" if it contains less than 7.98 oz and "0" otherwise. As each of the cartons is examined, we observe a sequence of binary data with "1" and "0". Another example is testing whether a light bulk works or not, which generates a binary observation. If the probability of being defective is a constant for each of the subjects and we can assume that the subjects are independent from each other, then we can model the binary observations using a Bernoulli model with the parameter p being the probability that a subject examined is defective. However, the independence assumption among subjects is not always true if we consider that mechaniced defects usually worsen over time. Thus observing a defective may impact the probability of observing another defective item in the future. Broadbent (1958) showed that the quality of observations is usually serially dependent. Thus, we will assume in this dissertation that the data can be modeled as a two-state Markov Chain, in which the current observation is dependent upon the previous observation once the defective probability p and the correlation among observations ρ are fixed.

Consider a sequence of $X_1, X_2, X_3 \ldots$ of binary observations with the proportion of defectives equal to p. Let 0 and 1 be the two states of the Markov chain model and $p_{ij}, i, j = 0,1,$ be the transition probability of the process entering state j from state i. Therefore, the model can be defined using

$$p_{01} = P(X_k = 1 | X_{k-1} = 0)$$

$$p_{10} = P(X_k = 0 | X_{k-1} = 1) \qquad (2.1)$$

By the properties of the two-state Markov chain, the proportion of defectives p and the correlation ρ between consecutive observations can be expressed as follows:

$$p = \frac{p_{01}}{p_{01} + p_{10}}$$

$$\rho = 1 - (p_{01} + p_{10}) \tag{2.2}$$

Then the four transition probabilities are:

$$p_{00} = 1 - p(1 - \rho)$$

$$p_{01} = p(1 - \rho)$$

$$p_{10} = (1 - p)(1 - \rho)$$

$$p_{11} = 1 - (1 - p)(1 - \rho) \tag{2.3}$$

It is noted that the correlation ρ defines the correlation between X_k and X_{k-1} and the correlation between X_k and X_{k+t} is $\rho_k = (1 - p_{01} - p_{10})^t = \rho^t$ for $t = 1, 2, 3 \ldots$. For more details, see Shepherd et al. (2007).

To design a control chart for monitoring binary data modeled as a two-state Markov chain, we need to specify an appropriate sampling plan including the sample size n and the frequency of taking a sample. In this proposal, we consider two sampling plans; one is single items once they are produced and available for inspection, i.e. $n = 1$. Another is taking inspected observations as a sample with $n > 1$. The sampling plans for the two cases were studied by Reynolds and Stoumbos (1999) and it was shown that the Bernoulli CUSUM designed for $n = 1$ is generally better than the Shewhart np −chart and binomial CUSUM chart when monitoring observations from subgrouping.

When $n = 1$, it is assumed that the observations are inspected as a continuous stream and p_0 can increase to p_1 after the τ^{th} observation and before the $(\tau + 1)^{th}$ observation. In the process example introduced earlier with items produced every 5 seconds, 100% inspection could be applied here assuming that the inspection time for each item is less than or equal to 5 seconds.

When $n > 1$, we will take n observations at one time as a sample, and wait for a time period to take another sample of the same size. In practice, it is sometimes infeasible to inspect all the observations and thus it is reasonable to use part of the items grouped into samples for inspection. However, it is sometime difficult to select an appropriate sample size. In this dissertation, we consider taking a relatively large sample and waiting a relatively long time to take another sample of the same size, for instance, use $n = 100$ and take samples every 4 hours. We can also use a relatively small size n and take samples more frequently, for example, use $n = 10$ and take samples every 24 minutes. In the situations that we consider, the sampling plans with different sample sizes are assumed to have the same total number of observations in the same period of time. In the two examples above, both sampling plans inspect 600 items in 24 hours. If an item is produced every 5 seconds, then in the two cases producing one sample takes about 8 minutes and 50 seconds, respectively. The time to take a sample is relatively small compared to the time between samples. Therefore, in this proposal, when $n > 1$, we will assume there is a long enough time interval between two consecutive samples that the shift will occur between samples.

2.2 Measures of Control Chart Performance

A control chart is considered to be effective if a shift in p from p_0 can be detected quickly after it occurs, and a small number of false alarms will be produced when the process is actually in-control. When p does not change, too many false alarms would reduce the confidence in the control chart detecting a shift if there is one. Thus to apply a control chart to a real process, one would want a low false alarm rate, and could calculate the average number of observations or samples needed to observe one false alarm. The average number of samples used to give a false alarm when the process is in-control here is called the in-control ANSS (Average Number of Samples to Signal). Another equivalent metric is the ANOS (Average Number of Observations to Signal), which is equal to ANSS $* n$. These metrics have been used, for example in Huang, Reynolds, and Wang (2012) in the context of detecting a shift in p for binomial observations. The ANOS metric is useful when comparing control charts where observations are grouped into samples of different sizes. The In-Control ANOS value (ICANOS) measures the number of observations taken from the process for examination until a false alarm is given.

In an out-of-control process, it is frequently assumed that the shift in p occurs immediately after the monitoring process starts, and then the ANOS (ANSS) is called the initial-state ANOS(ANSS). In practice, it is more reasonable that a process will operate as in-control for a period of time to reach a steady state and then the shift in p_0 will occur due to some special cause. The metrics SSANOS (Steady State ANOS) and SSANSS (Steady State ANSS) are defined, respectively, as the average number of observations and samples to signal from the time point that the shift occurs, assuming the process has already reached a steady state. In this proposal, we use the SSANOS as the metric to compare the out-of-control performance of different charts with the same sampling plan. When the sampling plans are different, the same SSANOS values may refer to different times required to detect a signal. For instance, suppose samples of $n = 100$ are taken every 4 hours. If it takes two samples to signal, then this is 200 observations, but the time from the shift to the signal must be between 4 and 8 hours, and the average should be 6 hours. This assumes that a sample can be taken in negligible time and that the time that the shift occurs in the interval between samples has a uniform distribution. If samples of $n = 200$ are taken every 8 hours and it takes one sample to signal then this is 200 observations, but the time from the shift to the signal must be between 0 and 8 hours, and the average should be 4 hours.

When there is a time interval d between taking samples and the time to take a sample is short enough that we assume the shift does not occur within a sample, we can use the steady state average time to signal (SSATS) instead of the SSANOS. This metric defines the average time needed to detect a signal. The SSATS is based on the assumption that the distribution of the shift within d is uniform. Thus, the expected position within the interval is the midpoint and the $\text{SSATS} = \text{SSANSS} * d - \frac{d}{2}$.

Usually the SSANOS and SSATS are used to compare the performance of two control charts, however, it is difficult to draw conclusions about the overall performance when the SSANOS or SSATS for one chart is smaller for some shifted values than the other chart but is larger for some other shifted values. In this case, a loss function can be used to evaluate the performance of the control charts. Loss functions are widely used in decision theory of statistic and measure the loss associated with an event. In SPC when comparing different control charts, we will not usually find a chart that is uniformly best over all shifts. Then the extra quadratic loss (EQL) can be used to evaluate the performance of a control chart when the process variable is

continuous as well as in making comparisons among different charts. For example, Reynolds and Lou (2010) used EQL for a control chart for monitoring the normal process mean. It is noted that it may not be necessary to use the loss function as the primary method to compare different control charts if the chart performance comparisons are very easy to determine. In this dissertation, we will use the Extra Number of Defectives (END) defining the expected loss due to the increase in the proportion of defectives as a measure of the performance of the control charts. When the proportion increases, the process produced more defectives and therefore there is more loss to the process. A control chart that performs well will have less loss when detecting the shifts. Therefore, a small value of END represents better performance for the control chart. More discussion of the END will be given later in Chapter 3.

2.3 Detection of Shifts in a Proportion with Binary Data

In this section, we will introduce several traditional types of control charts used to detect a shift in p associated with binary data obtained from various sampling plans. In Phase II, the control chart can be considered as a sequence of hypothesis tests. The null hypothesis states that p remains at the target value p_0. At sampling point k, the alternative hypothesis states that p has shifted to some $p_1 > p_0$ at some time $\tau < k$. The samples are drawn at regular time intervals and after sample k is obtained the control statistic is calculated for the above hypothesis test. A signal is given when the sample statistic falls outside the control limit and this is an indication that a shift has been detected at that time point.

2.3.1 Shewhart-Type Charts

The simplest control chart to apply in practice is the Shewhart p-chart or the equivalent Shewhart np-chart. Consider a sequence of independent binary observations which are grouped into samples of size n. Then the number of defectives in sample i, say B_i, follows a binomial(n, p) distribution and the Shewhart-type charts can be applied using the binomial observations B_i. The Shewhart p-chart uses the proportion of defectives within a sample, $\frac{B_i}{n}$, as the control statistic and plots this sample proportion on the control chart after each sample is collected. When the sample size is large enough, the in-control distribution $\frac{B_i}{n}$ can be approximated by a normal

$N\left(p_0, \frac{p_0(1-p_0)}{n}\right)$ distribution. Then a Shewhart p-chart can be constructed with the centerline being p_0, and the LCL (lower control limit) and UCL (upper control limit) are:

$$\text{LCL} = p_0 - Z_{\alpha/2}\frac{p_0(1-p_0)}{n}$$

$$\text{UCL} = p_0 + Z_{\alpha/2}\frac{p_0(1-p_0)}{n}$$

where $z_{\alpha/2}$ satisfies $P(Z > z_{\alpha/2}) = \alpha/2$ and Z follows the standard normal $N(0,1)$ distribution. This control chart is designed to detect both increases and decreases in p. The traditional choice is $Z_{\alpha/2} = 3$, which is known as the three-sigma rule and corresponds to $\alpha = 0.0027$, which corresponds to a relatively small false alarm rate. This control chart signals if $\frac{B_i}{n} <$ LCL or $\frac{B_i}{n} >$ UCL is observed for a sample. If we are only interested in an increase in p, there will be only one control limit $\text{UCL} = p_0 + Z_\alpha \frac{p_0(1-p_0)}{n}$ and the chart signals if $\frac{B_i}{n} >$ UCL. The equivalent Shewhart np-chart uses B_i as the control statistic that is plotted. The construction of a Shewhart np-chart is similar as a Shewhart p-chart. The Shewhart-type of charts usually require $n > 1$. This chart could in theory be applied to the case of $n = 1$, and presumably the chart would signal whenever a detective is observed. However, there is usually not enough evidence gathered to conclude that the process has changed just based on a sample of $n = 1$, and thus the Shewhart-type charts require a reasonably large n to have reasonable performance.

Based on the assumption that binary data that follows a two-state Markov chain model, Shepherd et al. (2007) proposed a Shewhart-type chart based on plotting the geometric-type random variable Y_t . It is shown by Shepherd et al. (2007) that the sequence $Y_1, Y_2, \ldots$ is independent and the sequence $Y_2, Y_3, \ldots$ is identically distributed. There is only a lower control limit for this Shewhart-type chart to detect an increase in p from the in-control value p_0 to the out-of-control value p_1. The chart used different control limits for Y_1 and $Y_t, t \geq 2$ because their distributions are slightly different. Shepherd, Champ, Rigdon and Fuller (2007) proposed another chart based on $Y_t, t = 1,2,3$ .... This chart has a better performance than the Shewhart-type chart they proposed in the same paper. This chart gives a signal if two consecutive values of Y_t fall below the control limit.

Another Shewhart-type chart, the Markov np-chart, proposed by Weiss (2009) uses correlated observations as samples with $n > 1$ when the time between samples is large enough that the sample can be assumed to be independent. The chart plots the number of defectives, $T_s = X_{t_s} + \cdots + X_{t_s+n-1}$, in each sample on the control chart. The distribution of T_s follows a Markov binomial distribution $MB\ (n, p, \rho)$. With the in-control proportion p_0, the the centerline for this control chart is np_0 and the control limits are:

$$\text{LCL} = \max(0, np_0 - 3\sqrt{np_0(1-p_0)\frac{1+\rho}{1-\rho}(1-\frac{2\rho(1-\rho^n)}{n(1-\rho^2)})})$$

$$\text{UCL} = \min(0, np_0 + 3\sqrt{np_0(1-p_0)\frac{1+\rho}{1-\rho}(1-\frac{2\rho(1-\rho^n)}{n(1-\rho^2)})})$$

Given the specific control limits, the ANSS can be computed from:

$$\text{ANSS} = (1 - \sum_{j=\text{LCL}}^{\text{UCL}} P(\ T_s = j))^{-1}$$

The Shewhart-type charts are sensitive to large shifts in p but have difficulty detecting relatively small shifts.

2.3.2 The Markov EWMA Chart

Weiss (2009) proposed a Markov EWMA chart based on the random variable T. Let $\text{round}(x)$ be the nearest interger to x. Let $Z_0 = \text{round}(np_0)$ and the Markov EWMA statistic is define as

$$Z_s = \text{round}\ (\lambda T_s + (1-\lambda)Z_{s-1})$$

where $0 < \lambda \leq 1$. The Markov EWMA chart is equivalent to a Markov np-chart if $\lambda = 1$. Weiss (2009) provides the upper and lower control limits for different values of the combinations of (n, p_0, ρ) under several different tuning parameters λ. It was shown that the choice of λ can affect the attainable range of the statistic Z_s, and that a value of Z_s below the lower or above the upper control limits can only be reached if $\lambda > \frac{1}{2(k+1)}$ or $\lambda > \frac{1}{2(n-k+1)}$. Compared with the Markov np-chart, the Markov EWMA chart is superior in the sense that with an appropriate

tuning parameter λ, the Markov EWMA chart can detect both increases and decreases in p relatively fast.

2.3.3 The Markov Binary CUSUM Chart

The above Markov np-chart and Markov EWMA chart are both applied to samples of correlated binary observations where there is enough time between samples that the samples can be treated as independent. For the case in which inspection is continuous Masouvi and Reynolds (2009) proposed a Markov Binary CUSUM (MBCUSUM) chart to detect an increase in p when ρ remains constant by plotting a likelihood ratio based control statistic after inspecting each observation. The MBCUSUM chart is thus based on samples of size $n = 1$. Assuming that the binary observations can be modeled as a two-state Markov Chain, the joint density of $X_1, X_2, \dots X_k$ can be written as:

$$f(x_1, x_2, \dots x_k|p, \rho) = f(x_1|p) \prod_{i=2}^{k} f(x_i|x_{i-1}, p, \rho)$$

where $f(x_i|x_{i-1}, p, \rho)$ is the probability mass function of the i^{th} binary observation and $f(x_i|x_{i-1}, p, \rho) = f(x_1|p, \rho)$ when $i = 1$. Then a CUSUM control statistic is defined as

$$C_k = \max\{0, C_{k-1}\} + Q_k, \quad k = 1,2,3, \dots$$

with $C_0 = 0$ where

$$Q_k = ln\frac{f(x_k|x_{k-1}, p_t, \rho)}{f(x_k|x_{k-1}, p_0, \rho)}, \quad k = 1, 2, 3, \dots$$

and p_t is the pre-determined shifted value of p that the MBCUSUM chart is tuned to detect. In most application the shift that will occur will be unknown and p_t is considered as a tuning parameter that must be specified. A signal is given if $C_k > h_C$, where h_C is the control limit of the MBCUSUM chart. In calculating the properties of this chart, the statistic Q_k can be approximated by a new statistic Q_k^* which is adjusted to take on only integer values (more details are discussed in Mousavi and Reynolds (2008)). Then the MBCUSUM statistic is

$$C_k^* = \max\{0, C_{k-1}^*\} + Q_k^*, \quad k = 1,2,3, \dots$$

where $C_0^* = 0$ and a signal would be given if $C_k^* > h_C^*$. The control limit h_C^* can only take the multiple of an integer that is used to adjust Q_k, see Mousavi and Reynolds (2008) for details.

The MBCUSUM chart is designed for correlated binary observations following a two-state Markov chain model, and therefore the in-control performance will not have the same problem as the traditional Shewhart np-chart and the CUSUM chart which does not take account of the effect of correlation. The MBCUSUM chart with a tuning parameter p_t has overall better performance than the traditional types of charts as well as the chart proposed by Shepherd, Champ, Rigdon and Fuller (2007). In Chapter 3, the MBCUSUM chart will be discussed as a competitor with the proposed correlated binary GLR chart.

2.3.4 The GLR Algorithm

The MBCUSUM chart that is discussed above assumes that a shift p_t is pre-determined and the chart is designed to detect such a shift. In a GLR algorithm, it is assumed that the size of the shift that occurs at time τ is unknown and the maximum likelihood estimate $\hat{p}_{MLE}$ is calculated and used in the likelihood ratio statistic. The GLR statistic R_k is defined as:

$$R_k = ln \frac{\max\limits_{0 \le \tau < k, p_0 < p_1 < 1} L_k(\tau, p_0, p_1, \rho | X_1, X_2, \dots X_k)}{L_k(\infty, p_0, p_0, \rho | X_1, X_2, \dots X_k)}$$

where L_k is the likelihood function. A GLR chart signals if $R_k > h$, where h is the pre-specified control limit. The above formula cannot be rewritten as a recursive formula as in the case of the CUSUM algorithm and the EWMA algorithm. The major drawback of the GLR method is that it involves the optimization of p_1 at each sampling time k over all past observations. This could be very computationally intensive, especially when the MLE of p_1 does not have a closed form expression and an iterative numerical algorithm has to be applied. To ease the computational burden, a modification is to apply a window to the GLR statistic. Instead of maximizing the ratio over all past observations, we consider the maximization over the past m observations in a window. The maximization is taken over the past m observations if $m < k$ or over the all the past observations if $m \ge k$. The idea of window was first proposed by Willsky and Jones (1976) where they use $\max(0, k - m_1) \le \tau < k - m_2$ as the window over which the maximization is taken. In the literature, it is stated that a large enough m_2 should be used to guarantee that $\hat{p}_1$ can be estimated from the assumed out-of-control samples (given the sample size of $n = 1$). The

selection of values m_1 and m_2 has been a difficult problem in the literature. In some recent work on the GLR chart, $m_2 = 0$ has been used and m_1 is chosen to be large enough to achieve a chart performance similar to the case in which there is no window. We will use this idea in our GLR chart for monitoring correlated binary data as in Reynolds and Lou (2010), Reynolds et.al (2013), and Huang, Reynolds and Wang (2012). The selection of m_1 will be discussed in later chapters and the notation m will be used as the window size.

Chapter 3. A GLR Chart for Monitoring Correlated Binary Data when $n = 1$

3.1 Parameters Estimates for the Two-State Markov Chain Model

Consider a sequence X_1, X_2, X_3 ... of binary observations which follow the two-state Markov chain model with long run proportion p, where the first observation X_1 satisfies $p = P(X_1 = 1)$ and $1 - p = P(X_1 = 0)$. The transition probabilities $p_{ij}, i, j = 0,1,$ can be determined from Equation (2.1). By the properties of this model (see Bhat and Lal (1990)), the long run proportion of defective p and the correlation ρ between consecutive observations are given in terms of the transition probabilities in Equation (2.2).

In the monitoring process, the control chart will be applied to Phase II, where the in-control values of the parameters have been well estimated in Phase I or are known. The parameter estimators for p_0 and ρ are given by:

$$\hat{p}_0 = \frac{\hat{p}_{01}}{\hat{p}_{01} + \hat{p}_{10}}$$

$$\hat{\rho} = 1 - (\hat{p}_{01} + \hat{p}_{10}) \tag{3.1}$$

where the transition probabilities p_{01} and p_{10} are estimated from:

$$\hat{p}_{ij} = \frac{N_{ij}}{N_{i0} + N_{i1}} \tag{3.2}$$

where N_{ij} is the number of transitions from state i to state j for $i, j = 0,1$ in the Phase I data set. Usually, to obtain an accurate and precise estimate of the parameters, a reasonably large data set is required in Phase I.

3.2 Derivation of the Markov Binary GLR Control Statistic

In the Phase II monitoring process, at each sample, we want to do a sequence of tests to see if there is any shift that occurs at the τ^{th} binary observation. At observation k, the hypothesis test is based on all the past observations $X_1, X_2, \ldots . X_k$. The hypothesis test is:

$$H_0: p = p_0 \text{ for } X_i,\ i = 1,2, \ldots k$$

$$H_1: p = p_0 \text{ for } X_i,\ i = 1,2, \ldots \tau$$

$$p = p_1 \text{ for } X_i,\ i = \tau + 1, \tau + 2, \ldots k$$

The alternative hypothesis H_1 states that the shift in p occurs at some time between observations τ and $\tau + 1$, where $\tau < k$. Then the likelihood function after the k^{th} binary observation under the null hypothesis is:

$$L_k(\infty, p_0, p_0, \rho | X_1, X_2, \ldots X_k) = f(x_1, x_2, .., x_k | \infty, p_0, p_0, \rho)$$

$$= f(x_1 | p_0, \rho) \prod\nolimits_{i=2}^{k} f(x_i | x_{i-1}, p_0, \rho)$$

where $f(x_i | x_{i-1}, p_0, \rho)$ is the conditional density of X_i for $i = 2, 3,4, \ldots$ and the marginal density function of X_1 is $f(x_1 | p_0, \rho)$ when $i = 1$. Under the alternative hypothesis, the likelihood function is

$$L_k(\tau, p_0, p_1, \rho | X_1, X_2, \ldots X_k) = f(x_1, x_2, .., x_k | \tau, p_0, p_1, \rho)$$

$$= \begin{cases} f(x_1 | p_1, \rho) \prod\limits_{i=\tau+2}^{k} f(x_i | x_{i-1}, p_1, \rho), & \tau = 0 \\ f(x_1 | p_0, \rho) \prod\limits_{i=\tau+1}^{k} f(x_i | x_{i-1}, p_1, \rho), & \tau = 1 \\ f(x_1 | p_0, \rho) \prod\limits_{i=2}^{\tau} f(x_i | x_{i-1}, p_0, \rho) \prod\limits_{i=\tau+1}^{k} f(x_i | x_{i-1}, p_1, \rho), & \tau \geq 2 \end{cases}$$

The Markov binary GLR statistic at the k^{th} binary observation is defined as the maximized log-likelihood ratio under the alternative hypothesis over the null hypothesis, i.e.

$$R_k = \max_{\tau, p_1} \log[\frac{L_k(\tau, p_0, p_1, \rho | X_1, X_2, \dots X_k)}{L_k(\infty, p_0, p_0, \rho | X_1, X_2, \dots X_k)}]$$

$$= \max_{\tau} \log[\frac{L_k(\tau, p_0, \hat{p}_1, \rho | X_1, X_2, \dots X_k)}{L_k(\infty, p_0, p_0, \rho | X_1, X_2, \dots X_k)}]$$

$$= \max_{\max(0, k-m) \le \tau < k} \sum_{i=\tau+1}^{k} \frac{f(x_i | x_{i-1}, \hat{p}_1, \rho)}{f(x_i | x_{i-1}, p_0, \rho)}$$

where $\hat{p}_1 = max(p_0, p_{MLE})$ and p_{MLE} is defined as the maximum likelihood estimator of p_1, under the restriction that $p_1 \geq p_0$. The Markov binary GLR statistic is maximized over the τ and p_1. In this expression, $f(x_i | x_{i-1}, \hat{p}_1, \rho) = f(x_i | \hat{p}_1, \rho)$ and $f(x_i | x_{i-1}, p_0, \rho) = f(x_i |\, p_0, \rho)$ when $i = 1$ and we will use $f(x_i | x_{i-1}) = f(x_i)$ in the later section for $i = 1$.

The Markov binary GLR statistic requires the calculation of $\hat{p}_{MLE}$, the MLE estimate of p_1, and then maximizes R_k over all possible shift points τ in the window of size m. For the correlated binary case, it is difficult to obtain closed form expressions for $\hat{\tau}$ and $\hat{p}_1$ and a grid search method was applied here. It is noted that $p_0 \leq \hat{p}_{MLE} \leq 1$ and a problem arises with the MBGLR statistic when we allow $\hat{p}_{MLE}$ to be at or close to 1. When the process is in control there is a reasonable probability of having a sequence of consecutive defective items that result in $\hat{p}_{MLE} = 1$ and an inflated value of R_k that is above the control limit h and thus produces a signal (a false alarm) by the Markov binary GLR chart. In particular, suppose that there is a $\hat{\tau}$ such that $X_{\hat{\tau}} = 0$ and $X_i = 1$ for $i = \hat{\tau} + 1, \hat{\tau} + 2 \dots k$. This means that the last $k - \hat{\tau}$ items are defective. Then the likelihood ratio statistic is

$$R_k = \prod_{i=\hat{\tau}+1}^{k} \frac{f(x_i | x_{i-1}, p_1, \rho)}{f(x_i | x_{i-1}, p_0, \rho)} = \frac{f(1|0, p_1, \rho)}{f(1|0, p_0, \rho)} \prod_{i=\hat{\tau}+2}^{k} \frac{f(1|1, p_1, \rho)}{f(1|1, p_0, \rho)}$$

$$= \frac{\hat{p}_{01} \prod_{i=\hat{\tau}+1}^{k-1} \hat{p}_{11}}{p_{01} \prod_{i=\hat{\tau}+1}^{k-1} p_{11}} = \frac{\hat{p}_{MLE}(1-\rho) \prod_{i=\hat{\tau}+1}^{k-1} (1 - (1 - \hat{p}_{MLE})(1-\rho))}{p_0(1-\rho) \prod_{i=\hat{\tau}+1}^{k} ((1 - (1 - p_0)(1-\rho))}$$

$$= \frac{1}{p_0 \big(1 - (1 - p_0)(1-\rho)\big)^{k - \hat{\tau} - 2}}$$

When $k-\tau > 2-\frac{\ln(hp_0)}{\ln(1-(1-p_0)(1-\rho))}$, we have $R_k > h$ and the Markov binary GLR chart will produce a false alarm. For particular combinations of p_0, ρ, and h, the probability of this happening is high enough when the process is in control that false alarms will be too frequent.

The situation with $\hat{p}_{MLE} = 1$ will result in many false alarms when $p = p_0$ unless h is increased. But increasing h hurts the ability to detect shifts in p. To avoid the problem associated with this extreme case, one can put a restriction on the value of τ and prevent τ from getting close to the current observation to get a small R_k. In the literature, the GLR algorithm may not use the observations very close to the current one but the observations in a window, i.e. $\max(0, k-m_1) \le i < k-m_2$. Therefore, to avoid the problem of $\hat{p}_{MLE} = 1$, we can prevent the change point from getting too close to the current observation. This can be done by selecting a large enough m_2 to make the change point relatively far away from the current observation.

Another way to avoid the problem with $\hat{p}_{MLE} = 1$ is to impose a restriction in the form of an upper bound on $\hat{p}_{MLE}$ to avoid the possibility of it being equal to 1. Huang, Wang and Reynolds (2012) found in the independent Bernoulli observation case that the GLR statistic is undefined when $\hat{p}_{MLE} = 1$ and compared the chart performance with the two kinds of restrictions. It was found that there is not much difference in the performance of the control charts when detecting a large shift size. When the shift size is small, the upper bound restriction on $\hat{p}_{MLE}$ has a better performance than the chart with the restriction on τ. Thus, we will impose an upper bound p_{ub} for $\hat{p}_{MLE}$ to avoid it attaining the value 1. Therefore, the estimate of p_1 is modified to $\hat{p}_1 = \min(\hat{p}_{MLE}, p_{ub})$.

As in the initial discussion of the GLR algorithm, a moving window is used to reduce the amount of calculation. For the remaining part of the dissertation, we take $m_2 = 0$ and use m for m_1. The window size m is chosen to be sufficiently large so that the performance of the GLR chart with a window is approximately equivalent to that without a window. The selection of the window size will be discussed in a later section. With an upper bound and a window, the Markov binary GLR statistic for monitoring the binary data with autocorrelation when $n = 1$ is defined as:

$$R_k = \max_{\max(0,k-m)\le\tau<k} \sum_{i=\tau+1}^{k} ln(\frac{f(x_i|x_{i-1},\hat{p}_1,\rho)}{f(x_i|x_{i-1},\ p_0,\rho)})$$

Then the above Markov binary GLR chart will be signal if $R_k > h$, where h is a pre-determined control limit which is determined by the required in-control performance. We call this GLR chart Markov binary GLR chart and will refer to it as the MBGLR chart in later sections.

When p_0 is very small, the ICANOS will usually be very large and simulating the binary sequence X_1, X_2, ...will be quite time consuming. Therefore, the geometric-type random variables are simulated instead, i.e. we simulated the number of observations between defectives. We store m' gemetric-type observations to calculate the MBGLR statistic. Here m' is the window size for the geometric-type variables the in simulation. The MBGLR statistic based on the geometric-type random variables is shown in Appendix A to be equivalent to the statistic based on the correlated binary observations if there is no window. The selection of the window size m' will be discussed in a later section. In this later section, the change point of the geometric-type variables is denoted by τ'.

3.3 Example Plot of the MBGLR Statistic with $n = 1$

As an example, Figure 3.1 shows 11000 simulated binary observations from a two state Markov process with $p_0 = 0.01$ and $\rho = 0.2$. The first 10000 observations are from an in-control process with $p = p_0 = 0.01$ and $\rho = 0.2$, and the last 1000 are out-of-control observations with $p = p_1 = 0.05$. A MBGLR control chart with upper bound $p_{ub} = 0.05$ is applied to monitor this process. The control limit was set to be $h = 3.8269$ to satisfy the required in-control performance ICANOS $= 16956.6$. This ICANOS value was selected to be the same as used by Mousavi and Reynolds (2009). In Figure 3.1, the MBGLR statistic values are smaller than h for the in-control observations and when the process proportion shifts to 0.05, the MBGLR statistic increases significantly. The MBGLR chart detects the change at the 371th binary observation after the shift occurred.

For the same stream of 11000 binary observations, a MBCUSUM chart with tuning parameter $p_t = 0.05$ was also used to monitor the process. To achieve the same in-control

performance of the MBGLR chart above, we set the control limit to be $h_C = 5.3102$. Figure 3.2 is a plot of this MBCUSUM chart. It is noted that the MBCUSUM chart will reset the statistic to 0 if it falls below 0 and Figure 3.2 shows the negative values of the statistic before the reset is applied.

The MBCUSUM chart with $p_t = 0.05$ detects the shift at the 319th binary observation. This MBCUSUM chart is designed to detect a shift equal to 0.05; therefore it is not surprising that the performance is better than the MBGLR chart at this particular shift.

Figure 3.1 The MBGLR Chart with $p_{ub} = 0.05$ for monitoring $p_1 = 0.05$ when $p_0 = 0.01$ and $\rho = 0.2$

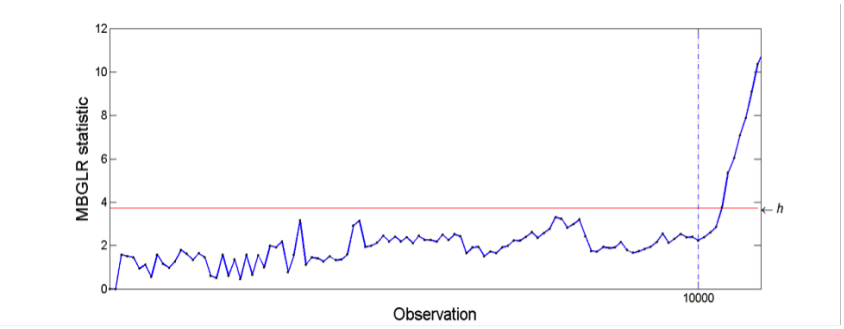

Figure 3.2 The MBCUSUM Chart with $p_t = 0.05$ for monitoring $p_1 = 0.05$ when $p_0 = 0.01$ and $\rho = 0.2$

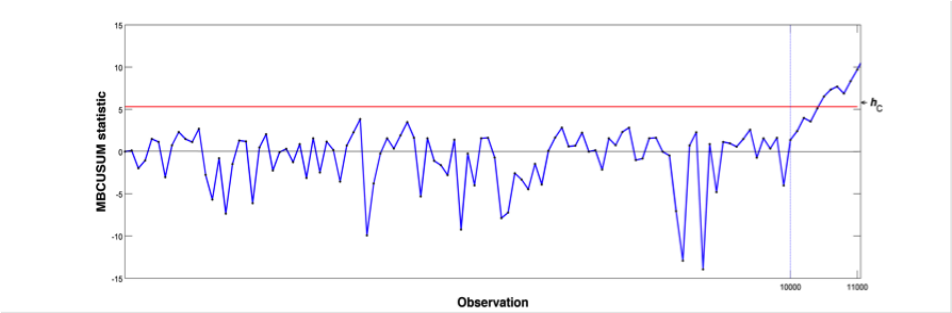

The MBCUSUM chart with some other pre-determined shift size may not work as well as the MBGLR chart. Figure 3.3 shows another MBCUSUM chart with $p_t = 0.13$. The control limit is set to be 6.4824 to achieve the desired ICANOS. This MBCUSUM chart detects the shift within 995 binary observations, which is much less effective than applying a MBGLR chart with upper bound 0.05. This MBCUSUM chart is also less effective than the first MBCUSUM chart with $p_t = 0.05$, which illustrate the fact that the performance of the MBCUSUM chart is

sensitive to the choice of p_t. More details on the selection of the tuning parameter for the MBCUSUM chart will be discussed in Section 3.5.3.

Figure 3.3 The MBCUSUM Chart with $p_t = 0.13$ for monitoring $p_1 = 0.05$ when $p_0 = 0.01$ and $\rho = 0.2$

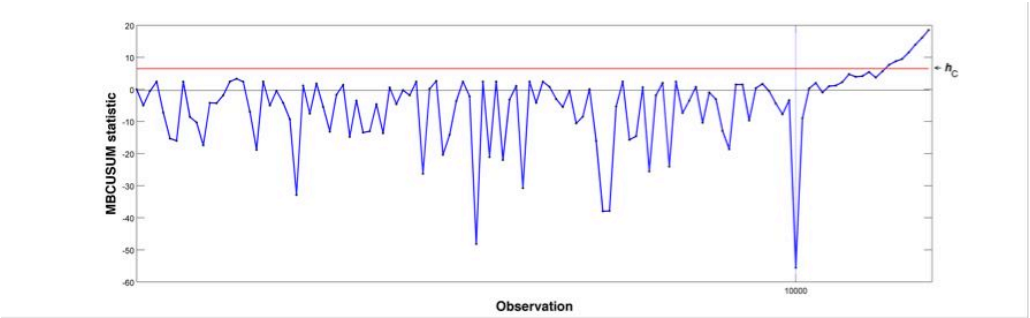

3.4 Performance of the MBGLR Chart

In this section, we look at the performance of the MBGLR chart to get an overall idea of how it performs, and then the design of this chart will be discussed in Section 3.5. The design of this chart involves the optimization of the upper bound and this issue will be discussed in detail in Subsection 3.5.3. We will compare the proposed MBGLR chart with the MBCUSUM chart, which is designed to detect a particular shift size equal to the tuning parameter p_t, and is expected to have good performance in detecting shift sizes equal to or close to p_t. We only consider the MBCUSUM chart as a competitor to the proposed MBGLR chart as the MBCUSUM chart has been shown by Mousavi and Reynolds (2009) to beat the traditional-type charts.

When there is correlation between the binary observation and we assume that the correlation remains constant in the monitoring process, it is hoped that the in-control chart performance is robust to the correlation. Mousavi and Reynolds (2009) showed that both the Shewhart chart and the Bernoulli CUSUM chart have an ICANOS that drops rapidly as the correlation increases from 0. The MBCUSUM chart can beat the traditional types of charts because it accounts for the correlation and it has a better overall performance in detecting shifts in p. Besides the traditional types of charts, another control chart for correlated data proposed by Shepherd et al. (2007) was beaten by MBCUSUM chart when the shift size is small. For relatively large shift sizes, the chart proposed by Shepherd et al. (2007) does not have

dramatically better performance than the MBCUSUM chart. Thus, based on the past literature, we will select the MBCUSUM chart as the competitor to the proposed MBGLR chart. When comparing chart performance, both the GLR chart and the MBCUSUM chart are set to have similar in-control performance, i.e. similar values of the ICANOS. Here, the ICANOS value used will be the same as used in Mousavi and Reynolds (2009), where the MBCUSUM chart was compared with Shewhart-type charts and the ICANOS was computed for Shewhart-type charts in their investigation.

We consider processes with in-control proportion $p_0 = 0.001, 0.01$ and 0.1 and correlation $\rho = 0.05, 0.1, 0.2$ and 0.4. It is noted that larger values of ρ will not be considered here as Mousavi and Reynolds (2009) showed that large correlation values of ρ combined with particular proportions are not possible for a binary sequence. For the first comparison, consider $p_0 = 0.01$, $\rho = 0.05$, $m' = 300$ and $\tau' = 100$. We compare MBGLR and MBCUSUM charts with p_{ub}, p_t, and control limits adjusted to values of ICANOS close to the desired value. Due to the discreteness of the binary observations, as the pre-determined shift size p_t increases, it becomes more difficult to find the control limits with the desired ICANOS value. Therefore, when p_t gets large the in-control performance is not as close to the target value as in the case of relatively small p_t. To make the comparisons as fair as possible, we will consider small values for the tuning parameters that can provide ICANOS values very close to the target value. The upper bound of the MBGLR chart is selected to be as small as 0.03, which is the 3 times larger than p_0 and as large as 0.17, which is 17 times larger than p_0. An even larger value of p_{ub} can also be applied here depending on the size of the shift that needs to be detected. In practice, the chance of having a very large shift is usually small and more effort in the monitoring process will be put on detecting relatively small shifts. In Table 3.1, five MBGLR charts with $p_{ub} = 0.03, 0.05, 0.1, 0.15,$ and 0.17 are used to compare with MBCUSUM charts with pre-determined shift sizes $p_t = 0.02, 0.04, 0.08, 0.11,$ and 0.15. All the MBGLR charts and the MBCUSUM charts are set to have an ICANOS that is approximately equal to the value 16956.6 used by Mousavi and Reynolds (2009) when traditional charts were compared with the MBCUSUM chart. The column labeled [1]-[5] in Table 3.1 gives SSANOS values for MBGLR charts with different upper bounds, and the columns labeled [6]-[10] give the SSANOS values for MUCUSUM charts with different pre-determined shift sizes.

The out-of-control performance of the 10 charts is evaluated for shifts ranging from 0.013 to 0.8. In practice, relative small shifts are usually of more concern to practitioners, as very large shifts are unlikely to occur in production processes. However, we will consider a very wide range of shifts for completeness. The SSANOS values in Table 3.1 are shaded with different colors, where lighter colors represent relatively small SSANOS values and darker colors represent relatively large SSANOS values. The shading color represents the ratio of the SSANOS to the minimum SSANOS for the same shift, with the lightest grey representing ratios between 1 to 1.05, and the darkest grey representing ratios greater than 1.8.

Table 3.1 SSANOS Values of the MBGLR and MBCUSUM charts with different p_{ub} and p_t when $p_0 = 0.01$ and $\rho = 0.05$

	MBGLR					*MBCUSUM*				
p_1	p_{ub}=0.03 [1]	p_{ub}=0.05 [2]	p_{ub}=0.1 [3]	p_{ub}=0.15 [4]	p_{ub}=0.17 [5]	p_t=0.02 [6]	p_t=0.04 [7]	p_t=0.08 [8]	p_t=0.11 [9]	p_t=0.15 [10]
0.01	**16918.91**	**16848.61**	**16924.80**	**16731.58**	**16857.04**	**16955.58**	**16959.18**	**16951.96**	**16901.40**	**16950.25**
0.013	3800.82	4085.50	4332.80	4462.28	4506.30	3715.36	5192.07	6543.70	7138.70	7634.03
0.015	2026.31	2174.55	2314.12	2382.72	2394.36	1953.17	2861.43	3939.58	4475.48	4951.33
0.02	789.92	835.47	883.29	907.76	912.91	752.43	997.27	1484.88	1785.72	2085.63
0.025	455.04	473.78	495.04	509.77	510.92	444.97	511.84	740.93	906.26	1087.44
0.03	311.36	318.77	332.36	339.96	341.00	314.07	325.99	441.46	538.42	650.93
0.035	234.56	236.21	243.60	249.60	250.80	242.76	235.21	297.06	356.06	430.32
0.04	187.52	185.87	191.36	194.63	196.07	198.07	182.77	217.43	255.21	304.80
0.05	133.60	128.88	130.21	132.39	132.99	145.05	126.09	136.79	153.92	178.95
0.06	103.88	98.12	97.97	99.10	99.45	114.93	96.38	98.17	106.79	120.38
0.07	85.23	78.95	78.00	78.55	78.66	95.26	78.18	76.37	80.77	88.71
0.08	72.32	66.22	64.30	64.73	65.11	81.60	65.78	62.43	64.64	69.45
0.09	62.92	57.03	54.79	54.93	55.32	71.41	56.95	52.88	53.83	56.74
0.1	55.81	50.19	47.74	47.57	47.71	63.61	50.27	45.86	46.12	47.92
0.2	27.32	23.47	21.01	20.16	20.09	31.82	23.82	20.45	19.33	18.89
0.3	19.07	16.14	13.92	12.98	12.87	22.48	16.34	13.63	12.60	12.18
0.4	15.19	12.81	10.71	9.75	9.64	18.16	12.96	10.49	9.61	9.25
0.5	13.09	10.95	8.90	7.94	7.86	15.91	11.10	8.74	7.95	7.63
0.6	11.93	9.82	7.80	6.80	6.75	14.78	10.04	7.67	6.93	6.60
0.7	11.39	9.17	7.11	6.03	5.99	14.40	9.48	7.01	6.28	5.90
0.8	11.35	8.84	6.69	5.50	5.47	14.68	9.29	6.62	5.88	5.40
h	3.7264	4.1491	4.4878	4.6507	4.6994	3.7760	5.1531	6.0494	6.4355	6.7544

In Table 3.1, comparing the five MBGLR charts in columns [1]-[5], a MBGLR chart with a small upper bound performs well at small shifts. For instance, the MBGLR chart with upper bound $p_{ub} = 0.03$ has the best performance among the five MBGLR charts in detecting shifts between 0.013 to 0.035. The SSANOS values of the 5 MBGLR charts at $p = 0.02$ are 789.92, 835.47, 883.29, 907.76, and 912.91, respectively. The larger the upper bound of the MBGLR chart, the worse the performance in detecting a shift to $p = 0.02$. A similar pattern can be concluded from other small shifts in the range of 0.013 to 0.035. However, when the shift increases, the performance of the first MBGLR chart with $p_{ub} = 0.03$ gets worse. For moderate

shift sizes 0.06 to 0.09, the MBGLR chart with upper bound equal to 0.09 has relatively good performance compared with the other four charts, and the MBGLR chart with $p_{ub} = 0.15$ works well for relatively large shifts from 0.2 to 0.8. Comparing the two MBGLR charts with $p_{ub} = 0.1$ and $p_{ub} = 0.15$, it is noted that the latter one has a much better performance for shift ≥ 0.1, while the former one still performs well for shifts smaller than its own upper bound. The color shading indicates that an MBGLR chart has a relatively good performance in detecting the shifts up to its own upper bound. For example, columns [1] and [4] have a relatively light shading color for shifts smaller than 0.03 and 0.15, respectively. A relatively large upper bound does not have a very good performance for very small shifts. For instance, when $p_{ub} = 0.15$, the performance of the chart is not very good when shift is less than 0.05. However, the overall performance for chart with $p_{ub} = 0.15$ is still very good.

In Table 3.1, the simulation results for the 5 MBCUSUM charts confirm the fact that a MBCUSUM chart has fast detection at the shift equal to the pre-determined shift p_t. For example, when $p = 0.02$, the first MBCUSUM chart with $p_t = 0.03$ in column [6] has the smallest SSANOS, and the third MBCUSUM chart with $p_t = 0.08$ in column [8] has the best performance at $p = 0.08$. The overall performance of a MBCUSUM chart is not as good as at the particular shift size it is designed to detect. A MBCUSUM chart with $p_t = 0.03$ has relatively bad performance when the shift is greater than 0.2, while a `MBCUSUM chart with $p_t = 0.15$ cannot quickly detect very small shifts such as 0.035. Comparing the MBGLR charts with the MBCUSUM charts, even though the MBGLR chart has slightly worse performance in detecting shifts equal to p_t, the overall performance of the MBGLR charts over a wider range of shifts can beat the MBCUSUM charts. The MBGLR charts with $p_{ub} = 0.09, 0.12,$ and 0.15 have most of their SSANOS values within 5% of the minimum SSANOS in the comparisons, and do not have extremely bad performance at any of the shifts.

The comparisons of the MBGLR and MBCUSUM charts under the second combination with $p_0 = 0.01$ and $\rho = 0.2$ are shown in Table 3.2. The 10 control charts are set to have an ICANOS approximately equal to 16890.00 used by Mousavi and Reynolds (2009). The tuning parameters p_{ub} and p_t in Table 3.2 are slightly different from the values used in Table 3.1 because it was necessary to select values that could achieve an ICANOS close to the desired value.

In Table 3.2, conclusions similar to those obtained from Table 3.1 can be reached when comparing the MBCUSUM charts with MBGLR charts.

Table 3.2 SSANOS values of the MBGLR and MBCUSUM charts with different p_{ub} and p_t when $p_0 = 0.01$ and $\rho = 0.2$

	MBGLR					*MBCUSUM*				
	p_{ub}=0.03	p_{ub}=0.05	p_{ub}=0.09	p_{ub}=0.13	p_{ub}=0.15	p_t=0.02	p_t=0.03	p_t=0.05	p_t=0.10	p_t=0.13
p_1	[1]	[2]	[3]	[4]	[5]	[6]	[7]	[8]	[9]	[10]
0.01	**16814.15**	**16832.13**	**16812.76**	**16704.51**	**16763.32**	**16875.33**	**16886.72**	**16891.96**	**16858.28**	**16837.49**
0.013	4115.67	4405.24	4629.0	4749.4	4846.0	3979.9	4812.1	5848.9	7104.7	7493.8
0.015	2235.66	2401.79	2528.7	2601.6	2635.0	2145.2	2633.0	3386.1	4472.5	4848.4
0.02	889.28	942.25	987.74	1013.6	1026.2	847.92	962.63	1244.1	1808.0	2046.5
0.025	516.75	539.69	559.01	576.05	583.87	504.86	526.97	640.05	933.66	1076.9
0.03	354.73	364.28	378.32	387.31	391.60	357.45	353.07	400.58	563.74	652.95
0.035	268.31	270.70	278.09	283.96	285.86	276.80	263.76	283.30	379.11	437.39
0.04	214.69	213.61	217.80	222.88	224.07	225.96	210.29	216.87	275.74	314.70
0.05	153.53	148.71	150.31	152.65	153.08	165.91	149.89	146.29	170.43	189.88
0.06	119.75	113.52	113.13	114.59	115.50	131.47	116.68	110.28	120.36	130.77
0.07	98.42	91.70	90.25	91.01	91.16	109.17	95.90	88.58	92.31	98.17
0.08	83.69	77.06	75.00	75.34	75.79	93.60	81.59	74.18	74.65	78.07
0.09	73.01	66.51	64.41	64.12	64.39	82.05	71.22	63.94	62.68	64.62
0.1	64.87	58.56	56.30	55.77	55.81	73.22	63.36	56.32	54.03	55.15
0.2	32.74	28.02	25.73	24.50	24.27	37.66	32.07	27.29	23.53	23.01
0.3	23.57	19.95	17.46	16.38	16.17	27.33	22.81	19.42	15.88	15.43
0.4	19.37	16.45	13.82	12.94	12.74	22.69	18.56	15.82	12.70	12.25
0.5	17.29	14.67	12.03	11.26	11.00	20.51	16.54	13.92	11.16	10.58
0.6	16.61	13.88	11.26	10.43	10.07	19.99	15.98	13.06	10.39	9.66
0.7	17.23	13.95	11.13	10.09	9.65	21.12	16.67	13.11	10.14	9.22
0.8	19.49	15.09	11.60	10.22	9.67	24.49	18.86	14.22	10.41	9.27
h	3.5456	3.8269	4.2530	4.4275	4.4821	3.6112	4.5025	5.3102	6.1891	6.4824

Above discussion shows the comparisons of the MBGLR chart with the MBCUSUM chart when $p_0 = 0.01$ and $\rho = 0.05$ and 0.2, which are the parameters used by Mousavi and Reynolds (2009). To achieve more general conclusions about the performance comparisons, we consider combinations of $p_0 = 0.01$ and $\rho = 0.1$ in Table 3.3 and $p_0 = 0.01, \rho = 0.4$ in Table 3.4. In Tables 3.3 and 3.4, the p_t values are different from p_{ub} and from Table 3.1 and 3.2 due to the discreteness problem when we try to achieve ICANOS values very close to the desired value. Similar conclusions can be reached as those from Table 3.1 and Table 3.2.

Now we will compare the chart performance across Tables 3.1-3.4 for different correlations. Compare the first column in Table 3.1-3.4, where $p_{ub} = 0.03$, it is noted that as the correlation increases, a longer time is needed to detect the same shift. For instance, when $p_1 = 0.02$, the SSANOS values for the MBGLR chart with $p_{ub} = 0.03$ when the correlation is $\rho = 0.05, 0.1, 0.2,$ and 0.4 are 789.92, 845.12, 889.28 and 1108.66, respectively. The simulation

results show in general that the detection of a shift requires more time when the correlation is higher.

Table 3.3 SSANOS values of the MBGLR and MBCUSUM charts with different p_{ub} and p_t when $p_0 = 0.01$ and $\rho = 0.1$

	MBGLR					*MBCUSUM*				
p_1	p_{ub}=0.03 [1]	p_{ub}=0.05 [2]	p_{ub}=0.1 [3]	p_{ub}=0.2 [4]	p_{ub}=0.5 [5]	p_t=0.03 [6]	p_t=0.04 [7]	p_t=0.06 [8]	p_t=0.08 [9]	p_t=0.10 [10]
0.01	**16888.84**	**17018.08**	**17011.54**	**17120.99**	**17641.21**	**16886.28**	**16926.18**	**16898.26**	**17027.17**	**16851.92**
0.013	3987.44	4299.19	4556.69	4802.38	5066.65	4635.40	5232.51	6034.49	6608.68	7012.58
0.015	2149.68	2309.77	2454.62	2591.04	2721.57	2501.11	2914.65	3519.84	3992.95	4340.20
0.02	845.14	888.95	938.63	984.53	1031.19	887.19	1029.38	1296.60	1525.70	1731.29
0.025	482.35	503.64	528.58	549.06	572.55	481.96	532.84	650.37	767.09	880.13
0.03	328.63	337.80	352.31	364.07	379.47	322.26	340.07	396.41	459.80	524.55
0.035	247.35	250.43	258.57	267.71	277.38	240.46	245.66	274.30	310.76	350.24
0.04	197.11	195.88	201.42	208.25	215.82	191.64	191.05	205.81	228.58	253.31
0.05	141.14	136.10	137.42	141.84	146.05	136.27	132.38	134.99	143.79	155.46
0.06	109.47	103.26	103.11	105.37	108.76	105.98	101.51	100.09	103.68	109.17
0.07	90.04	83.36	82.13	83.68	85.90	86.94	82.17	79.47	80.67	83.24
0.08	76.40	69.72	68.30	68.97	70.66	73.87	69.29	66.00	66.03	67.37
0.09	66.40	60.11	58.29	58.35	59.86	64.51	59.99	56.58	55.92	56.41
0.1	58.79	52.82	50.67	50.61	51.76	57.09	53.03	49.57	48.52	48.54
0.2	29.23	24.85	22.63	21.50	21.42	28.56	25.35	23.32	21.81	20.90
0.3	20.65	17.37	15.13	14.01	13.59	20.15	17.72	16.06	14.66	13.95
0.4	16.70	14.02	11.79	10.65	10.05	16.33	14.43	12.71	11.53	10.98
0.5	14.72	12.22	10.01	8.89	8.16	14.40	12.71	10.96	9.92	9.41
0.6	13.93	11.30	8.97	7.78	6.96	13.58	11.83	10.07	9.03	8.52
0.7	13.93	10.95	8.38	7.05	6.19	13.54	11.59	9.73	8.60	8.04
0.8	14.72	11.16	8.12	6.54	5.65	14.30	11.98	9.82	8.50	7.85
h	3.6871	3.9015	4.4217	4.6856	4.9033	4.6703	5.0990	5.6110	6.0068	6.2897

Table 3.4 SSANOS values of the MBGLR and MBCUSUM charts with different p_{ub} and p_t when $p_0 = 0.01$ and $\rho = 0.4$

	MBGLR					*MBCUSUM*				
p_1	p_{ub}=0.03 [1]	p_{ub}=0.05 [2]	p_{ub}=0.1 [3]	p_{ub}=0.2 [4]	p_{ub}=0.3 [5]	p_t=0.03 [6]	p_t=0.04 [7]	p_t=0.06 [8]	p_t=0.08 [9]	p_t=0.1 [10]
0.01	**16958.84**	**17030.13**	**16969.67**	**16810.99**	**16912.80**	**16989.85**	**17005.28**	**17025.41**	**16993.28**	**16878.00**
0.013	4749.03	5105.93	5399.87	5541.39	5699.67	5289.90	5850.08	6576.17	7086.50	7419.22
0.015	2695.38	2887.93	3072.48	3182.65	3255.64	3013.98	3431.40	4016.30	4475.61	4775.60
0.02	1108.66	1167.86	1239.57	1282.90	1319.59	1163.89	1317.11	1586.77	1833.94	2026.48
0.025	643.76	669.82	711.65	729.73	745.01	649.43	709.87	838.24	972.98	1084.09
0.03	445.00	454.68	476.57	490.99	501.10	438.99	463.14	526.76	602.80	670.97
0.035	335.83	337.83	353.30	362.82	368.56	329.06	338.29	370.94	415.37	459.32
0.04	269.18	268.22	276.29	284.46	288.97	262.33	263.36	281.33	309.66	337.59
0.05	191.88	185.84	191.02	194.01	197.29	187.74	182.93	186.72	197.98	211.42
0.06	149.59	142.67	143.57	145.86	148.69	146.68	140.85	139.46	144.39	150.96
0.07	123.34	115.12	114.70	115.88	117.60	120.88	114.42	111.54	113.26	116.33
0.08	105.72	96.90	95.30	96.22	97.00	103.10	96.49	93.21	93.11	94.45
0.09	92.18	83.48	81.64	81.83	82.86	90.19	83.57	79.94	78.94	79.48
0.1	82.12	73.54	71.36	70.82	71.81	80.06	73.97	70.35	68.68	68.73
0.2	42.48	35.46	32.16	31.21	31.04	39.75	36.35	33.51	31.10	30.33
0.3	30.05	25.18	21.76	20.86	20.50	27.84	26.25	23.01	21.24	20.80
0.4	24.11	20.80	17.37	16.48	15.85	22.93	21.98	18.36	17.24	17.00
0.5	21.31	18.84	15.58	14.26	13.44	20.92	20.08	16.22	15.54	15.27
0.6	20.65	18.15	15.03	13.16	12.14	20.79	19.60	15.72	15.14	14.65
0.7	22.09	18.80	15.49	12.73	11.52	22.48	20.42	16.56	15.71	14.85
0.8	26.72	21.46	17.06	13.16	11.54	26.82	23.24	19.16	17.42	15.99
h	3.2494	3.6636	4.0117	4.2121	4.3390	4.2271	4.7132	5.2470	5.6447	5.9127

Table 3.5 shows the transition probability p_{01} when $\rho = 0.05, 0.1, 0.2, 0.4$ and p takes values between 0.01 and 0.8. For each p, as the correlation increases from 0.05 to 0.4, $p_{01} = p(1-\rho)$ decreases. This indicates that, once a non-defective is observed, the probability of observing a defective in the next observation gets smaller as the correlation increases. However, once a defective is observed, the probability of observing a defective in the next observation gets larger because $p_{11} = 1-(1-p)(1-\rho)$ increases as the correlation increases. When p_0 is very small, it is easier to observe a non-defective item and therefore, detecting the same shift requires more observations when the correlation is relatively large.

Table 3.5 The Transition probability p_{01} for different values of p and ρ

p/ρ	0.05	0.1	0.2	0.4
0.01	0.0095	0.009	0.008	0.006
0.013	0.01235	0.0117	0.0104	0.0078
0.015	0.01425	0.0135	0.012	0.009
0.02	0.019	0.018	0.016	0.012
0.025	0.02375	0.0225	0.02	0.015
0.03	0.0285	0.027	0.024	0.018
0.035	0.03325	0.0315	0.028	0.021
0.04	0.038	0.036	0.032	0.024
0.05	0.0475	0.045	0.04	0.03
0.06	0.057	0.054	0.048	0.036
0.07	0.0665	0.063	0.056	0.042
0.08	0.076	0.072	0.064	0.048
0.09	0.0855	0.081	0.072	0.054
0.1	0.095	0.09	0.08	0.06
0.2	0.19	0.18	0.16	0.12
0.3	0.285	0.27	0.24	0.18
0.4	0.38	0.36	0.32	0.24
0.5	0.475	0.45	0.4	0.3
0.6	0.57	0.54	0.48	0.36
0.7	0.665	0.63	0.56	0.42
0.8	0.76	0.72	0.64	0.48

Previously we discussed the chart performance of MBGLR chart when $p_0 = 0.01$ with different correlations. Now we consider Tables 3.6 and 3.7 with $p_0 = 0.001$ and $\rho = 0.05$ and 0.2, repectively. The ICANOS is set to be the same as in the cases with $p_0 = 0.01$. In Table 3.6, the ICANOS $= 16956.6$ and the window size is selected to be $m' = 30$. In Table 3.7, same window size is used and the ICANOS $= 16890.0$. Both tables show that the most satisfactory

performance of the MBCUSUM chart is around its tuned shift. The MBGLR charts with relatively large upper bounds have fairly good overall performance.

Table 3.6 SSANOS values of the MBGLR and MBCUSUM charts with different p_{ub} and p_t when $p_0 = 0.001$ and $\rho = 0.05$

	MBGLR				*MBCUSUM*			
p_1	p_{ub}=0.0025 [1]	p_{ub}=0.005 [2]	p_{ub}=0.01 [3]	p_{ub}=0.015 [4]	p_t=0.003 [5]	p_t=0.005 [6]	p_t=0.008 [7]	p_t=0.01 [8]
0.001	**16983.35**	**17269.15**	**16918.41**	**16520.82**	**16828.13**	**16884.65**	**16981.36**	**16989.47**
0.0013	8153.47	8447.41	8691.74	8690.16	10183.96	8904.43	9561.89	9787.86
0.0015	5650.24	5871.10	6110.57	6155.17	7768.50	6427.38	7061.45	7280.47
0.002	2912.76	2994.69	3136.64	3195.37	4541.55	3457.36	3891.62	4074.02
0.0025	1861.34	1892.19	1987.58	2020.20	3016.06	2222.50	2507.43	2638.59
0.003	1334.81	1335.84	1388.28	1420.86	2175.51	1589.93	1780.67	1872.75
0.0035	1025.36	1014.77	1056.78	1072.18	1657.03	1220.59	1349.99	1418.13
0.004	827.25	808.83	840.04	847.92	1317.11	983.46	1073.83	1123.40
0.005	596.10	568.90	582.67	585.70	903.79	701.92	747.95	776.53
0.006	458.64	435.02	439.33	439.03	670.95	544.28	567.38	584.36
0.007	373.86	351.68	348.95	348.59	525.42	444.60	455.01	465.11
0.008	314.71	293.11	289.65	282.91	427.51	375.66	378.66	384.79
0.009	271.36	255.21	245.54	241.06	358.28	325.93	324.00	327.36
0.01	237.86	224.90	213.26	209.14	306.71	287.68	282.76	284.40
0.02	107.46	106.40	89.25	83.92	120.55	133.44	123.03	121.12
0.03	71.15	70.84	55.04	50.23	74.39	86.30	77.35	75.96
0.04	53.57	53.55	38.71	34.96	54.06	63.21	56.06	55.15
0.05	42.93	43.16	29.36	26.24	42.73	49.67	43.93	43.36
0.06	36.24	36.07	23.28	20.80	35.46	40.75	36.20	35.83
0.07	31.00	31.10	18.93	17.10	30.45	34.46	30.84	30.62
0.08	27.25	27.29	16.11	14.47	26.70	29.83	26.96	26.81
h	1.4184	1.7310	2.0539	2.1949	2.5575	3.1751	3.8696	4.1505

We finally consider monitoring a process with a higher in-control defective rate of $p_0 = 0.1$. Two cases with correlation $\rho = 0.05$ and ICANOS $= 16956.6$, and $\rho = 0.2$ and ICANOS $= 16890.0$ were investigated. The conclusions obtained for $p_0 = 0.1$ are similar to the conclusions obtained for $p_0 = 0.01$ and 0.001, and therefore the numerical values will not be given here.

In this section, MBGLR charts with different upper bounds have been compared with MBCUSUM charts with different pre-determined shifts. The comparisons show that the MBGLR charts with large upper bounds have better overall performance than the MBCUSUM charts. An upper bound around 0.15 for $p_0 = 0.01$ would be large enough to beat the MBCUSUM charts with reasonable pre-determined shift values. Here the reasonable p_t refers to the pre-determined shift size, which can provide a value of the control limit that is not significantly affected by the discreteness problems. In Section 3.5.3, more comparisons of the MBGLR and the MBCUSUM will given based on the loss function END. Over all the MBGLR charts, the upper bound is related to the performance in the sense that the MBGLR chart can very quickly detect shifts less

than or equal to the upper bound. The MBCUSUM chart can beat the MBGLR chart when detecting a shift equal to p_t, however, this must be considered along with the fact that the shift size is usually unknown in reality. The MBGLR chart has good detection over most of the possible shifts and thus can be recommended as a better overall chart than the MBCUSUM chart. Selecting the upper bound depends on the shifts of interest; a relatively small upper bound is recommended if the practitioners are only interested in relative small shifts while a larger upper bound may be used when a wider range of shifts is being considered.

Table 3.7 SSANOS values of the MBGLR and MBCUSUM charts with different p_{ub} and p_t with $p_0 = 0.001$ and $\rho = 0.2$

	MBGLR				*MBCUSUM*			
p_1	p_{ub}=0.0025 [1]	p_{ub}=0.005 [2]	p_{ub}=0.01 [3]	p_{ub}=0.015 [4]	p_t=0.003 [5]	p_t=0.005 [6]	p_t=0.007 [7]	p_t=0.02 [8]
0.001	**16893.71**	**17138.15**	**16446.70**	**16370.13**	**16987.84**	**16889.55**	**16940.81**	**16880.04**
0.0013	8397.65	8773.86	8800.22	8806.78	8710.79	9257.63	9672.11	10217.06
0.0015	5933.66	6184.38	6293.91	6341.99	6294.89	6797.82	7196.64	7804.14
0.002	3142.75	3237.48	3361.37	3376.84	3444.91	3764.33	4046.02	4583.62
0.0025	2005.83	2066.95	2130.28	2146.19	2269.96	2457.83	2645.37	3060.14
0.003	1444.37	1476.19	1515.01	1522.40	1661.68	1777.13	1901.93	2218.58
0.0035	1116.57	1130.43	1150.94	1160.10	1302.13	1373.04	1457.77	1700.29
0.004	906.43	913.69	908.45	917.26	1066.51	1110.03	1169.22	1356.60
0.005	650.77	642.99	635.53	635.16	781.57	795.62	825.07	940.32
0.006	505.06	495.81	475.87	474.77	617.15	616.58	630.77	704.89
0.007	411.98	403.30	379.61	376.89	510.77	503.18	509.17	557.21
0.008	348.84	339.65	312.75	312.83	435.98	424.76	425.87	457.27
0.009	301.57	292.81	265.64	264.03	380.90	367.72	365.12	385.79
0.01	266.17	259.19	230.17	227.91	338.62	323.88	320.00	332.85
0.02	125.61	123.30	93.30	89.86	163.19	146.48	140.15	136.66
0.03	84.44	81.83	55.76	53.46	108.53	93.08	88.52	85.89
0.04	63.64	61.12	38.80	36.95	81.49	67.60	64.53	63.02
0.05	50.98	48.93	29.20	27.99	65.44	52.91	50.89	50.10
0.06	42.86	40.34	23.34	22.40	54.78	43.47	42.14	41.73
0.07	37.04	34.51	19.29	18.77	47.20	36.93	36.06	35.86
0.08	32.48	30.08	16.51	16.13	41.54	32.16	31.58	31.49
h	1.2826	1.5762	1.9105	2.0107	2.3859	3.0927	3.5700	4.4700

3.5 Design of the MBGLR Chart

3.5.1 The Window Size

The calculation of the MBGLR statistic requires the storage of the all the past observations and thus usually will result in calculation intensity when using simulation. Therefore a moving window of size m can be used to reduce the calculation intensity. However, in practice the window may not necessarily be needed when the calculation capacity is very high.

In the study here, we still discuss the selection of the window size due to the calculation intensities from one million simulation runs. We want to select the window size to be reasonably large to accumulate enough information to achieve essentially the same chart performance as when there is no window. In most cases, the MBGLR chart provides the best performance when there is no window, however, a relatively small window size gives better performance for very large shifts but a large window is better otherwise. With the same control limits, the chart performance is uniformly better using a large window rather than a small window. Using different windows and adjusting the control limits to give the same ICANOS, we find that a small window is better for very large shifts. In general, we find from simulation results that a relatively large window size is preferred to give the best overall performance in the proposed MBGLR chart.

To reduce the number of observations stored in a window, we use the geometric-type random variables instead of the correlated binary variables in simulation. In this section, we discuss the selection of m' for the MBGLR chart, where m' refers to the number of geometric-type random variables Y in the window.

Table 3.8 ICANOSS and SSANOS values for different values of m for the MBGLR chart with $p_0 = 0.01, \rho = 0.05$ and $p_{ub} = 0.05$

p_1	10	50	100	200	300	400	1000	10000	30000	80000
0.01	**20653.39**	**17101.90**	**16999.70**	**16825.90**	**16832.13**	**16867.93**	**16832.44**	**16828.87**	**16782.54**	**16829.88**
0.013	6700.92	4709.14	4552.10	4404.23	4405.24	4407.86	4401.78	4400.95	4398.01	4402.46
0.015	3757.27	2539.23	2479.89	2401.49	2401.79	2401.99	2399.64	2404.71	2398.15	2401.40
0.02	1327.75	969.00	965.36	943.69	942.25	945.30	943.21	943.11	943.51	942.29
0.025	671.59	548.39	548.75	538.92	539.69	538.57	539.21	538.20	538.79	539.05
0.03	418.08	369.34	369.02	364.40	364.28	369.05	364.28	364.28	364.68	364.44
0.04	225.56	215.48	215.26	213.89	213.61	215.17	213.64	213.81	213.59	213.89
0.05	151.92	149.43	149.41	148.79	148.71	149.59	148.95	148.83	148.84	148.79
0.07	92.05	91.78	91.87	91.86	91.70	91.94	91.78	91.81	91.74	91.81
0.1	58.48	58.43	58.48	58.52	58.56	58.50	58.52	58.50	58.54	58.58
0.2	27.99	27.96	27.95	28.03	28.02	27.97	28.05	28.02	28.01	28.03
0.3	20.00	19.96	19.96	19.96	19.95	19.96	19.97	19.95	19.94	19.94
0.4	16.56	16.49	16.50	16.46	16.45	16.48	16.45	16.45	16.45	16.45
0.5	14.85	14.72	14.72	14.67	14.67	14.72	14.68	14.68	14.67	14.68
0.6	14.23	13.90	13.90	13.89	13.88	13.90	13.89	13.88	13.88	13.88
0.7	14.90	13.92	13.91	13.94	13.95	13.92	13.94	13.93	13.94	13.94
0.8	18.68	15.01	15.01	15.10	15.09	15.01	15.09	15.09	15.10	15.09

We first consider the case with $p_0 = 0.01, \rho = 0.05,$ and $p_{ub} = 0.05.$ Table 3.8 gives ICANOS values and out-of-control SSANOS values for various shifts in p with window size m' ranging from 10 to 80000. The control limits for all the MBGLR charts with different window sizes are set to be the same here at $h = 4.1511$, which leads to slightly different ICANOS values for each MBGLR chart. It is noted in Table 3.8 that a large window size is required for good

overall performance. A large window size is needed to detect small shifts, for example, when $p_1 = 0.013$, SSANOS $= 6144.37$ when $m' = 10$, while SSANOS $= 4088.50$ when $m' = 80{,}000$. It appears that a window of size $m' = 300$ is sufficiently large for detecting shifts as small as 0.013.

Results in Table 3.9 below show the in-control and out-of-control performance of MBGLR charts with $p_{ub} = 0.05$ when $p_0 = 0.01$, and $\rho = 0.2$. With different window sizes, the MBGLR charts are set to have the same control limit $h = 3.9675$. Again, we expect to see slightly different ICANOS values from different window sizes. This control limit is obtained to match the results in Mousavi and Reynolds (2009), where the Shewhart control limit was set to be 5 which provides ICANOS $= 16980.0$. In Table 3.9, again, we find that $m' = 300$ would be sufficiently large for shift sizes as small as 0.013.

Tables 3.8 and 3.9 show that the selection of m' has no effect for large shifts when h is the same for all values of m', but a relatively large m' is needed for small shifts. Now we consider effect of m' on the performances of the MBGLR charts when shift is small with $p_{ub} = 0.025$, 0.05 and 0.1. Table 3.10 presents the ICANOS and the SSANOS values for a shift to $p_1 = 0.013$ with $p_0 = 0.01, \rho = 0.05$ and 0.2, and the window size m' ranging from 10 to 80000. The results from Table 3.10 indicate that the window size required is not affected by the change of the upper bounds. We obtain the same result as from Table 3.8 and 3.9; $m' = 300$ would be large enough in this case. It is noted that the smallest shift being considered here is 0.013, a 30% increase from the in-control proportion $p_0 = 0.01$. A 30% increase in p_0 would usually be considered to be a very small shift in practice because it is not possible to detect shifts smaller than this in a short enough time to be of much use. If an even smaller shift is actually of interest, such as 0.012 or 0.011, a larger window size will be required.

In some situations the window size can be considered to be a tuning parameter for a GLR chart. The idea of using the window size as a tuning parameter is that with a particular window size, the MBGLR chart can provide relatively good performance at some shift sizes. However, for the current problem there is no big difference in detecting large shift sizes with different windows, and a relatively small window size, say $m' = 10$ or 50, does not provide better

performance in detecting a small shifts. Thus here we will not consider the window size as a tuning parameter.

Table 3.9 Window size selection for the MBGLR chart with $p_0 = 0.01, \rho = 0.2$, and $p_{ub} = 0.05$

p_1 /m	10	50	100	200	300	400	1000	10000	30000	80000
0.01	20117.85	16659.14	17057.80	16893.36	16848.61	16521.05	16891.58	16921.18	16910.47	16907.87
0.013	6144.37	4274.00	4235.33	4083.09	4085.50	4035.75	4089.54	4083.56	4087.23	4088.50
0.015	3353.24	2241.98	2246.74	2174.68	2174.55	2141.18	2177.12	2175.68	2174.92	2180.11
0.02	1134.01	851.76	856.05	837.13	835.47	830.86	835.93	836.05	836.40	837.70
0.025	566.92	485.09	483.45	474.19	473.78	469.58	473.63	474.97	474.00	473.90
0.03	352.65	328.36	324.05	318.98	318.77	316.81	318.67	318.80	319.14	319.14
0.04	191.96	191.98	187.69	185.70	185.87	184.80	185.71	186.15	185.86	186.33
0.05	130.33	133.81	129.66	129.05	128.88	128.63	128.76	128.86	128.78	128.87
0.07	79.41	82.55	79.26	79.13	78.95	78.47	79.06	79.17	79.11	79.06
0.1	50.23	52.53	50.21	50.18	50.19	49.98	50.15	50.14	50.07	50.15
0.2	23.44	24.88	23.45	23.49	23.47	23.35	23.48	23.48	23.47	23.48
0.3	16.09	17.19	16.08	16.14	16.14	16.04	16.14	16.14	16.14	16.14
0.4	12.75	13.61	12.75	12.80	12.81	12.71	12.80	12.80	12.80	12.80
0.5	10.90	11.66	10.91	10.94	10.95	10.81	10.94	10.94	10.95	10.95
0.6	9.79	9.80	9.79	9.83	9.82	9.83	9.83	9.83	9.82	9.83
0.7	9.14	9.81	9.14	9.17	9.17	9.06	9.17	9.17	9.16	9.17
0.8	8.80	8.80	8.80	8.83	8.84	8.84	8.84	8.83	8.83	8.83

As shown in Appendix B, with geometric-type random variables and m' as the window size, it is expected that the number of correlated binary observations stored in the window is $m'E(Y)$. Wandi, Wang, Reynolds (2012) argued that the window selected to be close to the ICANOS is sufficiently large. In the simulations, $m'E(Y)$ can be set to be equal to the desired ICANOS and then m' can be determined by $m' = \frac{\text{ICANOS}}{E(Y)}$. When $p_0 = 0.01, \rho = 0.05$ and $\text{ICANOS} = 16956.6$, we get $m' = \frac{\text{ICANOS}}{E(Y)} = \text{ICANOS} * \frac{p_0}{1-p_0} \approx 170$. It is noted that in Table 3.8, $m' = 200$ also provides a good enough in-control and out-of-control performance as in the case of no window. Here $m' = 200$ corresponds to 19800 correlated binary observations, which is close to $\text{ICANOS} = 16956.6$.

For other in-control proportion values, such as $p_0 = 0.001$ and 0.1, we find setting the window size m' to satisfy $m'E(Y) \approx$ ICANOSS would be large enough to achieve in and out-of-control performance close to the case in which there is no window (results not shown here). An even larger m' could be used in this example if there is no problem with calculation intensity. In this proposal, a relatively large window is used, i.e. $m' = 30, 300, 3000$ are used for the cases

with $p_0 = 0.001, 0.01, 0.1$, respectively. In practice, a window size approximately equal to the ICANOS, i.e. $m'E(Y)$would be sufficiently large to get satisfactory control chart performance.

Table 3.10 Window size selection for MBGLR charts with different p_{ub} and ρ for the in-control case and smallest shift size 0.013 with $p_0 = 0.01$

p_1/m	*10*	*50*	*100*	*300*	*400*	*1000*	*5000*	*10000*	*30000*	*80000*
	$p_0 = 0.01,\ \rho = 0.2,\ \text{ICANOSS} = 16890,\ h = 3.3303,\ p_{ub} = 0.025$									
0.01	26467.07	17052.27	17069.85	16828.64	16817.38	16813.19	16842.06	16860.64	16838.22	16839.24
0.013	7169.57	4174.62	4116.44	3972.46	3975.45	3974.22	3974.16	3974.93	3977.46	3977.81
	$p_0 = 0.01,\ \rho = 0.05,\ \text{ICANOSS} = 16956.6,\ h = 3.5073,\ p_{ub} = 0.025$									
0.01	23686.72	17079.31	17115.68	16871.38	16905.93	16883.03	16888.65	16873.45	16878.20	16869.28
0.013	6061.12	3847.15	3812.77	3664.38	3673.36	3673.50	3669.66	3670.68	3673.84	3672.74
	$p_0 = 0.01,\ \rho = 0.2,\ \text{ICANOSS} = 16890,\ h = 3.9675,\ p_{ub} = 0.05$									
0.01	20653.39	17101.90	16999.70	16832.13	16967.93	16832.44	16825.90	16828.87	16782.54	16829.88
0.013	6700.92	4709.14	4552.10	4405.24	4507.86	4401.78	4404.23	4400.95	4398.01	4402.46
	$p_0 = 0.01,\ \rho = 0.05,\ \text{ICANOSS} = 16956.6,\ h = 4.1511,\ p_{ub} = 0.05$									
0.01	20117.85	16659.14	17057.80	16848.61	16521.05	16891.58	16893.36	16921.18	16910.47	16907.87
0.013	6144.37	4274.00	4235.33	4085.50	4035.75	4089.54	4083.09	4083.56	4087.23	4088.50
	$p_0 = 0.01,\ \rho = 0.2,\ \text{ICANOSS} = 16890,\ h = 4.3036,\ p_{ub} = 0.1$									
0.01	19754.79	17017.26	16990.07	16766.36	16854.05	16888.22	16840.84	16876.46	16840.63	16854.43
0.013	7021.04	5000.24	4850.37	4658.87	4678.66	4677.79	4677.32	4678.27	4680.13	4672.36
	$p_0 = 0.01,\ \rho = 0.05,\ \text{ICANOSS} = 16956.6,\ h = 4.4898,\ p_{ub} = 0.1$									
0.01	19430.66	17078.72	17049.62	16924.80	16937.69	16924.20	16914.09	16944.10	16935.40	16942.83
0.013	6505.37	4648.65	4503.30	4332.80	4343.59	4345.81	4349.76	4344.25	4346.49	4337.93

3.5.2 The Control Limit

The value that should be used for the control limit h of the MBGLR chart depends on p_0, ρ, the desired ICANOS value, as well as p_{ub}. In this section, the impact of p_0, ρ_0, the desired ICANOS value, and p_{ub} will be discussed; a procedure that explains how to find the control limit will be provided.

First, the effect of the desired ICANOS will be discussed. For the case of $p_0 = 0.01$, $\rho = 0.2$, and $p_{ub} = 0.05$, the ICANOS was evaluated for h taking the values from 1 to 5.5 with an increment of 0.01. Instead of plotting the ICANOS values vs. h, we consider the plot of the logarithm of ICANOS with base 10, log(ICANOS) vs. h. In Figure 3.4, the solid line is the

simulation values of log(ICANOS) vs. h, which shows that there is a linear trend between the two values. The dashed line is the linear regression line fitted from the simulated data. The regression line $\hat{y} = -5.8830 + 1.0112 * \log(\text{ICANOS})$ fits the data well with $R^2 = 0.9981$.

Figure 3.4 The Relationship between the control limit of the MBGLR chart and log (ICANOS) for $p_0 = 0.01, \rho = 0.05$ and $p_{ub} = 0.05$

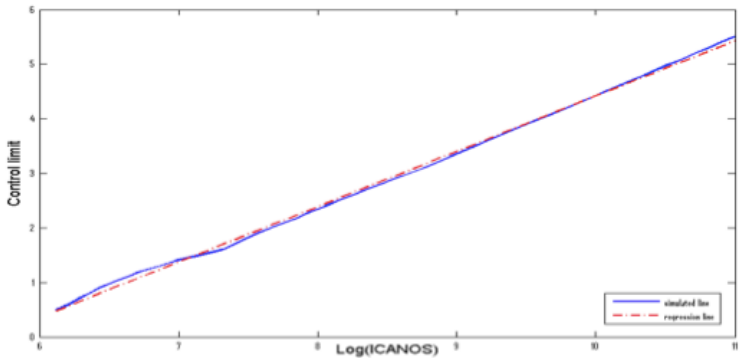

For any MBGLR chart with a given desired ICANOS value, the control limit h can be obtained from the fitted regression line. The linear relationship between the control limit and the logarithm of desired ICANOS has been shown in a GLR chart for monitoring a normal process mean by Reynolds and Lou (2011) and a GLR chart for monitoring a proportion in Bernoulli observations by Huang, Reynolds and Wang (2012). Figure 3.5 shows the linear relationship between h and $\log(\text{ICANOS} * p_0)$ with $p_0 = 0.001, 0.01$, and 0.1, and $p_{ub}/p_0 = 2.5, 5, 10$, and 15, when $\rho = 0.05$. It is apparent from these plots that the linear relationship holds for different p_0 and p_{ub}. The linear relationship shown in Figure 3.5 also holds for other values of ρ, but the plots are not shown here. We use $\log(\text{ICANOS} * p_0)$ instead of log(ICANOS) in Figure 3.5 as we found the fitted regressions lines using $\log(\text{ICANOS} * p_0)$ have similar slope values.

The above discussion indicates the linear relationship between h and $\log(\text{ICANOS} * p_0)$, and once p_0, ρ, and p_{ub} are fixed, the control limit can be calculated from a linear regression equation of $\log(\text{ICANOS} * p_0)$. In another words, to find the relation of control limit and the ICANOS, one need to specify the relation of p_0, ρ_0 and p_{ub} with the linear regression equation. To solve this problem, we consider 60 different combinations of p_0, ρ and p_{ub}, with $p_0 = 0.001, 0.01$, and 0.1, $\rho = 0.01, 0.05, 0.1, 0.2$, and 0.4, and $p_{ub} = 2.5 * p_0$, $5{*}p_0$, $10{*}\ p_0$, and $15{*}\ p_0$. For each of the combinations, the control limits were set to be from 1 to 5.5 with 0.01 increments. Then the ICANOS was obtained from simulation and a regression line between h and

log(ICANOS $* p_0$) was fitted. The following Table 3.11 lists the intercepts and the slopes for the 60 regression lines.

Figure 3.5 The Relationship between the control limit of the MBGLR chart and log(ICANOS $* p_0$) for $p_{ub}/p_0 = 2.5, 5, 10$ and 15

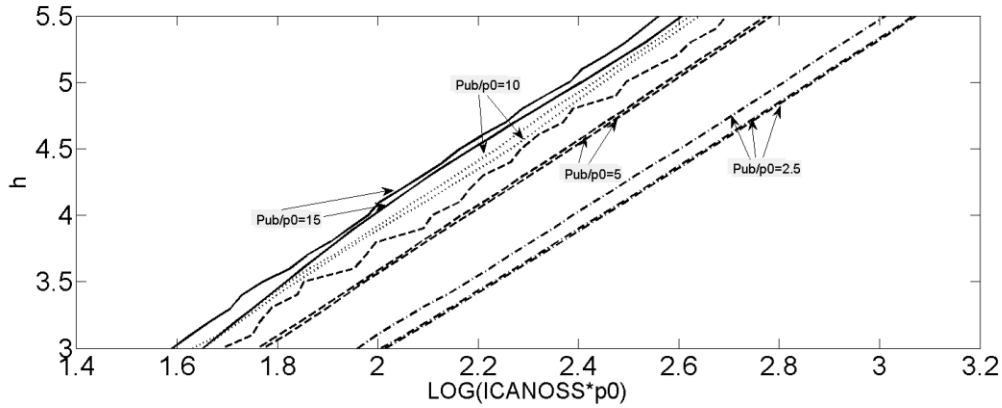

From Table 3.11, the regression lines have similar values for the intercept and the slope when ρ and p_{ub} are fixed. For the slope, once p_{ub} is fixed, there is no big change in the slope as ρ changes. For instance, the values for the slope are all approximately equal to 2.37 when $p_{ub} = 2.5 * p_0$. The intercept seems to be related to ρ and p_{ub}. The following regression lines were fitted from the 60 groups of data including intercept, slope, p_0, ρ, and p_{ub}:

$$Intercept=-2.0928-1.3104*\rho+0.2002*(p_{ub}/p_0)-0.0088(p_{ub}/p_0)^2 \quad (3.3)$$

$$Slope=2.151+0.1139*(p_{ub}/p_0)-0.0124*(p_{ub}/p_0)^2+0.0004*(p_{ub}/p_0)^3 \quad (3.4)$$

Both of the above equations have $R^2 \approx 0.94$. From the above two equations, once p_0, ρ, and p_{ub} are given, the regression line between h and $log(\text{ICANOS} * p_0)$ can be determined, and thus with a given ICANOS, the corresponding control limit can be obtained by

$$h = Intercept + slope * \log(ICANOS * p_0) \quad (3.5)$$

The equations resulted from scanning control limits from 1 to 5, which corresponds approximately to ICANOS $* p_0 \in [10, 1000]$. Therefore, the regression equations can be applied to cases with ICANOS $* p_0 \in [10, 1000]$ and correlation $\rho \in [0.05, 0.4]$.

Table 3.11 The intercept and slope of regression lines for the control limit and $\log(\text{ICANOSS} * p_0)$ with $p_0 = 0.001, 0.01$, and 0.1, $\rho = 0.01, 0.05, 0.1, 0.2$ and 0.4, and $p_{ub}/p_0 = 2.5, 5, 10$ and 15

ρ	p_0	p_{ub}/p_0	2.5	5.0	10.0	15.0
0.01	0.001	intercept	-1.76	-1.34	-1.05	-1.10
		slope	2.37	2.47	2.49	2.56
	0.01	intercept	-1.73	-1.32	-1.04	-0.97
		slope	2.37	2.47	2.50	2.52
	0.1	intercept	-1.64	-1.29	N/A	N/A
		slope	2.38	2.52	N/A	N/A
0.05	0.001	intercept	-1.80	-1.38	-1.09	-1.16
		slope	2.37	2.47	2.48	2.57
	0.01	intercept	-1.77	-1.35	-1.10	-1.03
		slope	2.37	2.47	2.51	2.54
	0.1	intercept	-1.66	-1.14	N/A	N/A
		slope	2.37	2.45	N/A	N/A
0.1	0.001	intercept	-1.85	-1.44	-1.15	-1.22
		slope	2.37	2.47	2.48	2.57
	0.01	intercept	-1.82	-1.41	-1.15	-1.14
		slope	2.36	2.47	2.51	2.57
	0.1	intercept	-1.70	-1.08	N/A	N/A
		slope	2.37	2.42	N/A	N/A
0.2	0.001	intercept	-1.97	-1.56	-1.27	-1.34
		slope	2.37	2.47	2.48	2.56
	0.01	intercept	-1.94	-1.46	-1.27	-1.33
		slope	2.36	2.43	2.51	2.60
	0.1	intercept	-1.80	-1.213	N/A	N/A
		slope	2.36	2.445	N/A	N/A
0.4	0.001	intercept	-2.26	-1.87	-1.57	-1.66
		slope	2.36	2.47	2.48	2.56
	0.01	intercept	-2.24	-1.85	-1.57	-1.68
		slope	2.36	2.47	2.50	2.61
	0.1	intercept	-2.09	-1.49	N/A	N/A
		slope	2.35	2.44	N/A	N/A

Table 3.12 The error rate of the ICANOS from control limits using the regression equations $p_0 = 0.001, 0.01$, and $0.1, \rho = 0.01, 0.05, 0.1, 0.2$ and 0.4, and $p_{ub}/p_0 = 2.5, 5, 10$ and 15

p_0	ρ	p_{ub}	Intercept	Slope	h_e	$ICANOS_e$	E_r
0.001	0.05	0.0025	-1.71	2.36	1.19	16686.75	2%
0.001	0.05	0.005	-1.38	2.46	1.65	16168.59	5%
0.001	0.05	0.01	-1.04	2.45	1.98	13353.03	21%
0.001	0.05	0.015	-1.14	2.42	1.84	12430.33	27%
0.001	0.1	0.0025	-1.78	2.36	1.13	15841.13	7%
0.001	0.1	0.005	-1.44	2.46	1.58	15592.64	8%
0.001	0.1	0.01	-1.10	2.45	1.91	13778.47	19%
0.001	0.1	0.015	-1.20	2.42	1.77	12443.63	27%
0.001	0.2	0.0025	-1.67	2.36	1.23	21112.95	25%
0.001	0.2	0.005	-1.34	2.46	1.69	19897.33	17%
0.001	0.2	0.01	-1.00	2.45	2.01	19320.61	14%
0.001	0.2	0.015	-1.10	2.42	1.88	15209.33	10%
0.001	0.4	0.0025	-2.17	2.36	0.74	13132.14	23%
0.001	0.4	0.005	-1.84	2.46	1.19	12477.96	26%
0.001	0.4	0.01	-1.49	2.45	1.52	15233.73	10%
0.001	0.4	0.015	-1.59	2.42	1.38	13565.51	20%
0.01	0.05	0.025	-1.71	2.36	3.56	17980.44	6%
0.01	0.05	0.05	-1.38	2.46	4.11	16325.49	4%
0.01	0.05	0.1	-1.04	2.45	4.43	16202.09	4%
0.01	0.05	0.15	-1.14	2.42	4.26	11894.63	30%
0.01	0.1	0.025	-1.78	2.36	3.49	17814.95	5%
0.01	0.1	0.05	-1.44	2.46	4.04	16212.43	4%
0.01	0.1	0.1	-1.10	2.45	4.36	15906.53	6%
0.01	0.1	0.15	-1.20	2.42	4.19	11822.77	30%
0.01	0.2	0.025	-1.67	2.36	3.60	22220.88	31%
0.01	0.2	0.05	-1.34	2.46	4.15	20104.58	19%
0.01	0.2	0.1	-1.00	2.45	4.46	19678.22	16%
0.01	0.2	0.15	-1.10	2.42	4.30	14505.12	14%
0.01	0.4	0.025	-2.17	2.36	3.10	17970.50	6%
0.01	0.4	0.05	-1.84	2.46	3.65	16773.85	1%
0.01	0.4	0.1	-1.49	2.45	3.97	16190.74	5%
0.01	0.4	0.15	-1.59	2.42	3.80	12619.43	26%
0.1	0.05	0.25	-1.71	2.36	5.92	16433.95	3%
0.1	0.05	0.5	-1.38	2.46	6.57	13310.61	22%
0.1	0.1	0.25	-1.78	2.36	5.86	15535.76	8%
0.1	0.1	0.5	-1.44	2.46	6.50	13529.36	20%
0.1	0.2	0.25	-1.67	2.36	5.96	15441.19	9%
0.1	0.2	0.5	-1.34	2.46	6.61	16432.21	3%
0.1	0.4	0.25	-2.17	2.36	5.46	15652.23	8%
0.1	0.4	0.5	-1.84	2.46	6.11	12720.70	25%

Now we consider the performance obtained from using the equations to find h. Table 3.12 shows the control limits h_e obtained using the equations when the desired ICANOS $= 16956.6$ and the error rate of the actual ICANOS, ICANOS_e using h_e with p_0, ρ, and p_{ub} taking different values. The error rate E_r is defined as $\frac{|\text{ICANOS}_e - \text{ICANOS}|}{\text{ICANOS}} * 100\%$, which defines the

percent derivation from the desired ICANOS using the control limit obtained from the equations. Table 3.12 shows that when using the equations to estimate control limits, the actual ICANOS values differ from the desired ICANOS values by 1% to 31%. In most of the cases, the actual ICANOS values are within 10% of the desired ICANOS. Considering the discreteness of the binary observations and the difficulty of finding a control limit to get very close to the desired ICANOS, this range of error rates should be acceptable for application. We also considered cases with ICANOS $* p_0 = 50$ and 5000 with $p_0 = 0.001, 0.01,$ and 0.1, the error rate are all within 40%.

3.5.3 The Upper Bound

In designing the MBGLR chart, there are a lot of possible values for the upper bound, and an upper bound with the best overall out-of-control performance is preferred. In Section 3.4, we saw that the performance of the MBGLR chart depends on the upper bound and the performance of MBCUSUM chart depends on the pre-determined shift size. It was concluded that the MBCUSUM chart has the best out-of-control performance when the shift size is exactly equal to the pre-determined shift size. The MBGLR chart works well for a wider range of shift sizes and the range depends on the upper bound. To make more complete comparisons between the two types of charts, in this section we will discuss the problem of selecting the upper bound of the MBGLR chart and compare the optimized MBGLR chart with the optimized MBCUSUM chart using the extra number of defectives (END) produced while the process is out of control.

3.5.3.1.1 The Extra Number of Defectives (END)

In the binary process case, if the process proportion shifts from p_0 to p_1, $p_1 > p_0$, we can consider the increased number of defectives due to the shift as the loss for the process. The loss depends on how long the process remains out of control at p_1 so define the expected loss when the process proportion shifts to p_1 as

$$l(p_1) = \text{SSANOS}(p_1) * (p_1 - p_0)$$

where SSANOS(p_1) is the SSANOS at p_1. Then the END can be defined as

$$\text{END} = \int_{p_0}^{p_{max}} l(p_1) * \pi(p_1) dp_1$$

where p_{max} is the maximum shift size that might reasonably occur, and $\pi(p_1)$ is the prior density function of the shift. The END is the expected loss due to an increase in p that can range from p_0 to p_{max}, and a small value of the END indicates good performance. The prior distribution used in the END specifies the distribution of the shift, and may be difficult to select in practice.

It is noted that the END also depends on the largest shift p_{max}, and thus we will consider optimizing the upper bound of the MBGLR chart under different combinations of p_0, ρ, and p_{max}. Similarly, the END can be applied to optimize the MBCUSUM chart over different values of the pre-determined shift size p_t. In this section, we optimize the MBGLR charts and the MBCUSUM charts over p_{ub} and p_t, respectively. The optimized MBCUSUM chart will be compared with the optimized MBGLR chart under different combinations of p_0, ρ, and p_{max}. The comparisons are aimed at showing that the MBGLR chart can beat the MBCUSUM chart when both of them are optimized. The END ratio of MBCUSUM chart to MBGLR chart in the optimized cases will be used to measure and quantify the advantage of the MBGLR chart.

The END is based on a prior distribution for p_1. We considered three types of beta prior distributions with parameters α and β, where the beta distributions were transformed to the interval $[p_0, p_{max}]$. The first beta prior has $\alpha = \beta = 1$, which is, of course, a uniform distribution. The second type of beta prior has parameter $\alpha \leq 1$ and $\beta > 1$, which provides a strictly decreasing density, which is appropriate if shifts close to p_0 have a larger probability of occurring while extremely large shifts can only occur with a very small probability. The third type of beta prior has $\beta \geq \alpha > 1$. This prior has a concave shape and assumes some particular shift in (p_0, p_{max}) occurs with the highest probability. In the simulation results, we found that the results from the three types of beta priors are very close, so here we only show the results for the uniform prior.

Figure 3.6 shows the truncated densities of the beta(0.5, 1), beta(0.5, 2), beta(2,5) and beta(2,10) prior distributions when p is takes values between 0.01 and 0.5. As in the figure, the densities of the beta(0.5, 1) and beta(0.5, 2) distributions decrease rapidly as p increases. As β

increases, the probability of a relatively small shift increases. The beta(2,5) and beta(2,10) distributions both have a density that increases to a maximum at some value of p and then decrease. As β increases, the value of p at the maximum gets smaller.

Figure 3.6 Beta prior distributions with different parameters

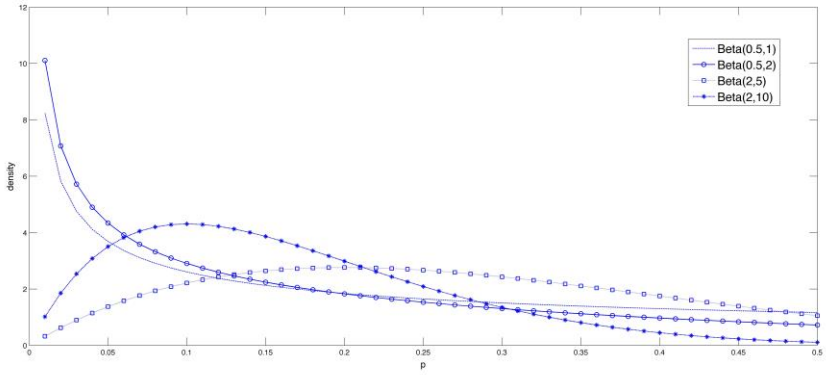

3.5.3.2 Optimization of the MBGLR and MBCUSUM charts

In this section, we use END to optimize the upper bound of the MBGLR chart and the pre-determined shift size of the MBCUSUM chart under different priors for p and different values of p_0, ρ, and p_{max}. The prior distributions used here are the uniform distribution and 6 beta prior distributions: beta(0.5, 1), beta(0.5, 2), beta(1, 3), beta(1, 5), beta(2, 5), and beta(2, 10).

First we consider $p_0 = 0.01$ combined with correlation $\rho = 0.05$ and $p_{max} = 0.2, 0.5,$ and 0.8. Tables 3.13-15 show the END values under each of the p_0, ρ and p_{max} combinations. The MBGLR charts are set to have ICANOS close to 16956.6 and the END values have been rounded to 4 decimal places. Figure 3.7 shows the END as a function of p_{ub} under the uniform prior. Figure 3.8 shows the END of MBGLR chart as a function of p_{ub} with $p = 0.01, \rho = 0.05,$ and $p_{max} = 0.2, 0.5,$ and 0.8 under the $\text{beta}(0.5, 1)$ and $\text{beta}(2,5)$ priors.

From Tables 3.13-3.15, under the uniform prior, the END values are relatively large when the upper bound is small. Figure 3.7 shows that END values decrease rapidly as the upper bound increases and the END lines become flatter as p_{ub} reaches 0.15. The END values reach the minimum at different upper bounds depending on p_{max}. When $p_{max} = 0.2, 0.5,$ and 0.8, the minimum END is achieved at $p_{ub} = 0.10, 0.4,$ and 0.4, respectively.

Figure 3.7 The END values of the MBGLR chart as a function of p_{ub} with $p_0 = 0.01, \rho = 0.05$, and $p_{max} = 0.2, 0.5$, and 0.8 under the uniform prior

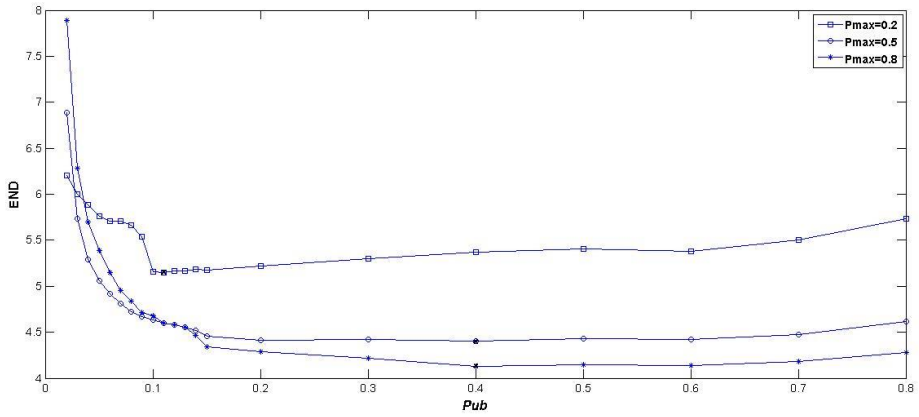

Figure 3.8 The END values of the MBGLR chart as a function of p_{ub} with $p_0 = 0.01, \rho = 0.05$, and $p_{max} = 0.2, 0.5$, and 0.8 under the beta(1, 3) and beta(2,5)

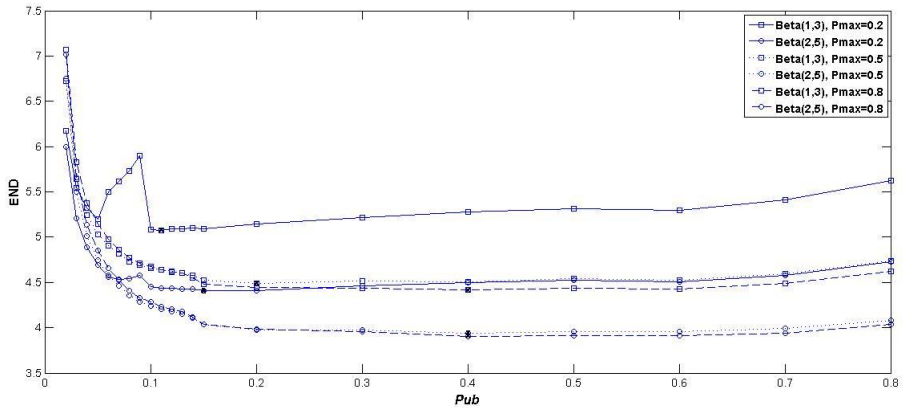

Comparing the END values from different p_{max} values in Table 3.13-3.15, we notice that the loss is much larger with small upper bound when p_{max} is relatively large under the uniform prior. For instance, the MBGLR chart with $p_{ub} = 0.02$ has END $= 6.0235, 6.8981$, and 8.0922, respectively for $p_{max} = 0.2, 0.5$, and 0.8. When using a larger upper bound of $p_{ub} = 0.2$, the loss is larger when p_{max} is small, such as END $= 5.2228, 4.2017, 4.1499$, respectively, for $p_{max} = 0.2, 0.5$, and 0.8. It is apparent that when p_{max} is large, it is safer to use an MBGLR chart with a relatively large upper bound while with a smaller p_{max}, it is reasonable to apply a MBGLR chart with small upper bound to avoid a large loss.

Table 3.13 The END values of MBGLR charts with $p_0 = 0.01, \rho = 0.05$, and $p_{max} = 0.2$ under different priors

p_{ub}	Uniform	beta(0.5,	beta(0.5,	beta(1,3)	beta(1,5)	beta(2,5	beta(2,10)
0.02	6.2035	6.4869	6.5235	6.1733	6.2139	5.9960	6.0181
0.03	5.9967	6.0782	6.1413	5.5461	5.6270	5.2048	5.2829
0.04	5.8829	5.9642	6.0408	5.3232	5.4267	4.8912	5.0036
0.05	5.7602	5.9101	5.9961	5.1953	5.3160	4.6952	4.8366
0.06	5.7086	6.8378	6.9993	5.5011	5.7276	4.5588	4.8143
0.07	5.7084	7.1006	7.2816	5.6116	5.8714	4.5339	4.8362
0.08	5.6674	7.3462	7.5432	5.7343	6.0224	4.5416	4.8842
0.09	5.5389	7.6497	7.8649	5.8980	6.2177	4.5769	4.9649
0.1	5.1580	5.9355	6.0392	5.0833	5.2369	4.4528	4.6521
0.11	5.1506	5.9359	6.0407	5.0759	5.2322	4.4351	4.6393
0.12	5.1657	5.9665	6.0733	5.0887	5.2479	4.4363	4.6452
0.13	5.1693	5.9818	6.0902	5.0918	5.2545	4.4257	4.6409
0.14	5.1806	6.0005	6.1100	5.1023	5.2670	4.4286	4.6476
0.15	5.1737	6.0035	6.1144	5.0955	5.2639	4.4073	4.6336
0.2	5.2228	6.0971	6.2140	5.1413	5.3200	4.4115	4.6535
0.3	5.3028	6.2132	6.3350	5.2168	5.4025	4.4589	4.7104
0.4	5.3665	6.2986	6.4234	5.2795	5.4711	4.4981	4.7599
0.5	5.4054	6.3542	6.4811	5.3163	5.5107	4.5234	4.7884
0.6	5.3814	6.3212	6.4469	5.2931	5.4855	4.5082	4.7697
0.7	5.5042	6.5061	6.6400	5.4082	5.6119	4.5772	4.8539
0.8	5.7303	6.8288	6.9752	5.6205	5.8391	4.7271	5.0206

Table 3.14 The END values of MBGLR charts with $p_0 = 0.01, \rho = 0.05$, and $p_{max} = 0.5$ under different priors

p_{ub}	Uniform	beta(0.5,	beta(0.5,	beta(1,3)	beta(1,5)	beta(2,5	beta(2,10)
0.02	6.8981	6.8577	6.8154	6.7259	6.6278	6.7512	6.4370
0.03	5.6675	5.8555	5.8998	5.6382	5.6666	5.5017	5.3846
0.04	5.1981	5.5017	5.5895	5.2389	5.3337	5.0128	5.0020
0.05	4.9476	5.3193	5.4320	5.0257	5.1583	4.7439	4.7889
0.06	4.7837	5.2134	5.3489	4.9025	5.0703	4.5778	4.6834
0.07	4.6674	5.1347	5.2850	4.8130	5.0033	4.4614	4.6053
0.08	4.5644	5.0649	5.2281	4.7320	4.9433	4.3528	4.5342
0.09	4.5015	5.0360	5.2126	4.6933	4.9255	4.2886	4.5071
0.1	4.4589	5.0093	5.1920	4.6607	4.9026	4.2429	4.4777
0.11	4.4227	4.9886	5.1775	4.6364	4.8888	4.2057	4.4606
0.12	4.3976	4.9785	5.1729	4.6193	4.8796	4.1774	4.4439
0.13	4.3721	4.9676	5.1676	4.6033	4.8732	4.1479	4.4318
0.14	4.3287	4.9465	5.1557	4.5779	4.8618	4.1079	4.4178
0.15	4.2580	4.8977	5.1162	4.5263	4.8258	4.0392	4.3806
0.2	4.2017	4.8711	5.1009	4.4888	4.8064	3.9771	4.3498
0.3	4.1990	4.9094	5.1549	4.5127	4.8536	3.9722	4.3833
0.4	4.1657	4.9137	5.1746	4.5089	4.8740	3.9414	4.3973
0.5	4.1885	4.9522	5.2187	4.5396	4.9125	3.9605	4.4272
0.6	4.1807	4.9339	5.1966	4.5266	4.8942	3.9556	4.4145
0.7	4.2259	5.0233	5.3015	4.5922	4.9810	3.9888	4.4749
0.8	4.3383	5.2082	5.5113	4.7366	5.1583	4.0832	4.6090

For the beta priors, the change in END is also small when the upper bound is relatively large. We find similar conclusions to those obtained from the uniform prior. In Figure 3.8, under $\text{beta}(1,3)$ and $\text{beta}(2,5)$ priors, the change in END has a pattern similar to that under the uniform prior. In some of the cases, the END value first increases at relatively small values of p_{ub} and then decreases and become flatter as p_{ub} increases. Different beta priors provide similar values of the END and the optimized upper bounds are close under different priors. For example,

when $p_{max} = 0.2$ in Table 3.14, the MBGLR chart is optimized at p_{ub} =0.11, 0.11, 0.11, 0.11, 0.11, 0.15, and 0.15 under the uniform prior and 6 beta priors, respectively.

Table 3.15 The END values of MBGLR charts with $p_0 = 0.01, \rho = 0.05$, and $p_{max} = 0.8$ under different priors

p_{ub}	Uniform	beta(0.5,	beta(0.5,	beta(1, 3)	beta(1, 5)	beta(2, 5	beta(2, 10)
0.02	8.0922	7.6104	7.1899	7.0729	6.7278	7.0176	6.4543
0.03	6.3611	6.2498	6.0937	5.8311	5.7238	5.6601	5.3935
0.04	5.7172	5.7640	5.7173	5.3790	5.3771	5.1398	5.0102
0.05	5.3806	5.5182	5.5322	5.1419	5.1999	4.8558	4.7990
0.06	5.1102	5.3318	5.4050	4.9800	5.0979	4.6612	4.6879
0.07	4.8945	5.1850	5.3086	4.8616	5.0255	4.5236	4.6104
0.08	4.7697	5.0985	5.2467	4.7745	4.9672	4.4110	4.5414
0.09	4.6307	5.0111	5.1972	4.7088	4.9385	4.3287	4.5123
0.1	4.5840	4.9808	5.1768	4.6748	4.9169	4.2821	4.4821
0.11	4.5009	4.9268	5.1446	4.6354	4.8967	4.2348	4.4612
0.12	4.4733	4.9118	5.1367	4.6159	4.8872	4.2038	4.4453
0.13	4.4514	4.8992	5.1297	4.6005	4.8807	4.1781	4.4351
0.14	4.3437	4.8328	5.0934	4.5519	4.8614	4.1185	4.4167
0.15	4.2033	4.7370	5.0314	4.4806	4.8210	4.0368	4.3796
0.2	4.1499	4.7096	5.0198	4.4484	4.8117	3.9818	4.3621
0.3	4.0467	4.6759	5.0363	4.4394	4.8470	3.9525	4.3892
0.4	3.9455	4.6317	5.0325	4.4139	4.8654	3.9050	4.4085
0.5	3.9551	4.6559	5.0650	4.4329	4.8924	3.9150	4.4248
0.6	3.9506	4.6433	5.0477	4.4225	4.8771	3.9100	4.4150
0.7	3.9829	4.7204	5.1513	4.4866	4.9697	3.9429	4.4788
0.8	4.0613	4.8698	5.3432	4.6189	5.1449	4.0328	4.6136

We also find that the END of MBGLR charts with different upper bounds does not change significantly when $p_{ub} \geq 0.15$. Numerically, under the uniform prior, with $\rho = 0.05$ and $p_{max} = 0.5$, the END $= 5.40$ when $p_{ub} = 0.15$ and the END $= 5.56$ when $p_{ub} = 0.8$. The change in END is within 3% for the moderately large shift size $p_{max} = 0.5$, and with the relatively large $p_{max} = 0.8$, the END change in this range of p_{ub} is within 1%. When $p_{max} = 0.2$, the change in the END is more significant than for the other two cases but still within 10%.

Figure 3.9 The END values of the MBCUSUM chart as a function of p_t with $p_0 = 0.01, \rho = 0.05$, and $p_{max} = 0.2, 0.5$, and 0.8 under the uniform prior

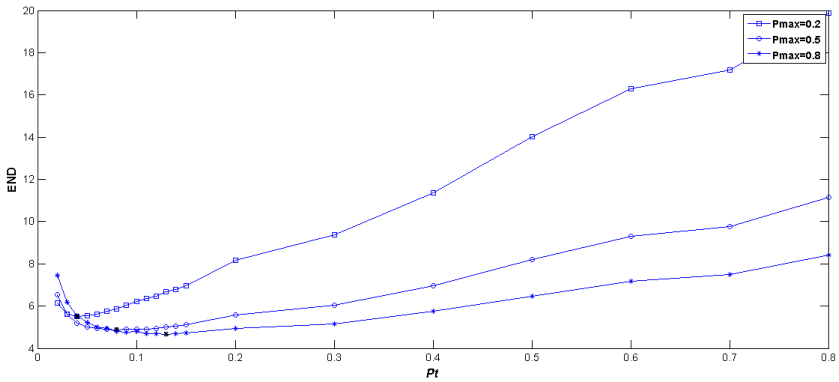

Tables 3.16-3.18 present the END values of the MBCUSUM chart when p_t is in the interval $[0.02, 0.8]$ with $p_0 = 0.01, \rho = 0.05$, and $p_{max} = 0.02, 0.05$, and 0.08. To make fair comparisons, the ICANOS values of those MBCUSUM charts are set to be close to 16956.6 as was done for the GLR charts in Table 3.13-3.15. When p_t is relatively small, say less than 0.3, the MBCUSUM charts can reach a ICANOS very close to 16956.6, however, due to the discreteness problem of CUSUM-type charts, as p_t increase, the ICANOS is not very close to 16956.6. Figure 3.9 shows the END of the MBCUSUM chart with $p_{max} = 0.02, 0.05,$ and 0.08 under the uniform prior.

Figure 3.10 The END values of MBCUSUM chart with $p_0 = 0.01, \rho = 0.05$ and $p_{max} = 0.2, 0.5, 0.8$ under beta(1,3) and beta(2,5)

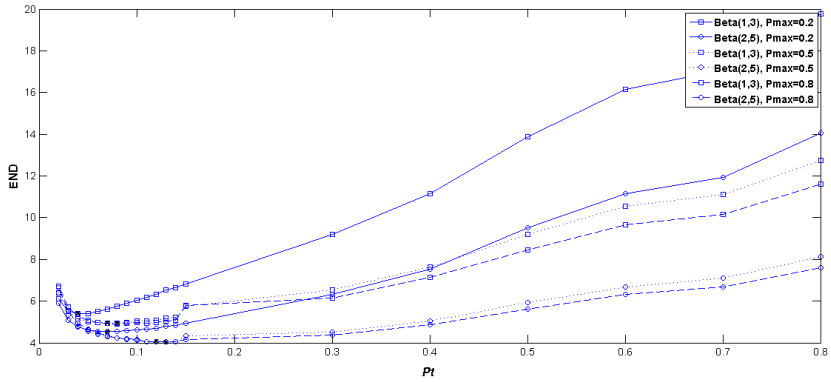

Table 3.16 The END values of MBCUSUM charts with $p_0 = 0.01, \rho = 0.05$, and $p_{max} = 0.2$ under different priors

p_{ub}	Uniform	beta(0.5,	beta(0.5,	beta(1, 3)	beta(1, 5)	beta(2, 5	beta(2, 10)
0.02	6.0574	6.3191	6.3549	6.0988	6.1459	5.8940	5.9203
0.03	5.4449	5.9654	6.0391	5.5410	5.6461	5.0967	5.1932
0.04	5.2635	5.9889	6.0932	5.4058	5.5595	4.7624	4.9230
0.05	5.2382	6.1324	6.2620	5.4187	5.6130	4.6087	4.8214
0.06	5.2963	6.3287	6.4790	5.5086	5.7367	4.5600	4.8165
0.07	5.3754	6.5387	6.7090	5.6195	5.8808	4.5351	4.8385
0.08	5.4713	6.7433	6.9303	5.7424	6.0320	4.5429	4.8866
0.09	5.6051	6.9991	7.2049	5.9064	6.2277	4.5783	4.9674
0.1	5.7257	7.2209	7.4425	6.0536	6.4025	4.6140	5.0453
0.11	5.8435	7.4255	7.6609	6.1952	6.5687	4.6567	5.1272
0.12	5.9520	7.6034	7.8501	6.3241	6.7187	4.7018	5.2079
0.13	6.1280	7.8880	8.1514	6.5271	6.9498	4.7902	5.3370
0.14	6.2281	8.0366	8.3082	6.6432	7.0823	4.8423	5.4193
0.15	6.3735	8.2602	8.5440	6.8089	7.2690	4.9227	5.5317
0.3	8.5316	11.2157	11.6308	9.2122	9.9217	6.3406	7.3969
0.4	10.3014	13.6365	14.1556	11.1655	12.0630	7.5445	8.9168
0.5	12.8241	16.6375	17.2444	13.8842	14.9749	9.5244	11.3194
0.6	14.9327	19.2354	19.9257	16.1593	17.4162	11.1537	13.2791
0.7	15.8036	20.1802	20.8852	17.0671	18.3589	11.9331	14.1485
0.8	18.3510	23.1414	23.9197	19.7718	21.2182	14.0476	16.5985

Table 3.17 The END values of MBCUSUM charts with $p_0 = 0.01$, $\rho = 0.05$, and $p_{max} = 0.5$ under different priors

p_{ub}	Uniform	beta(0.5,	beta(0.5,	beta(1,3)	beta(1,5)	beta(2,5)	beta(2,10
0.02	6.5318	6.5191	6.4872	6.3770	6.2922	6.3877	6.0932
0.03	5.5302	5.7880	5.8543	5.5206	5.5736	5.3395	5.2362
0.04	5.0516	5.5184	5.6600	5.1507	5.3113	4.8140	4.8581
0.05	4.8396	5.4612	5.6573	5.0129	5.2490	4.5614	4.6960
0.06	4.7210	5.4774	5.7217	4.9625	5.2671	4.4096	4.6319
0.07	4.6502	5.5258	5.8117	4.9459	5.3105	4.2972	4.5931
0.08	4.5933	5.5792	5.9051	4.9476	5.3705	4.2134	4.5878
0.09	4.5806	5.6799	6.0458	4.9888	5.4696	4.1640	4.6108
0.1	4.5838	5.7759	6.1743	5.0351	5.5640	4.1324	4.6394
0.11	4.5427	5.8346	6.2702	5.0526	5.6384	4.0696	4.6613
0.12	4.5507	5.9116	6.3723	5.0967	5.7213	4.0532	4.6983
0.13	4.5882	6.0543	6.5525	5.1864	5.8655	4.0598	4.7753
0.14	4.6109	6.1265	6.6428	5.2359	5.9444	4.0630	4.8206
0.15	4.8200	6.8928	7.7130	5.6893	6.8697	4.1900	5.7424
0.3	5.3520	7.8468	8.7260	6.5340	7.8145	4.5133	6.1268
0.4	6.0973	9.2751	10.4031	7.6448	9.3071	5.0481	7.2096
0.5	7.1599	11.0571	12.4681	9.2027	11.3519	5.9277	8.9344
0.6	8.0978	12.6349	14.2898	10.5412	13.0910	6.6951	10.3622
0.7	8.5152	13.2374	14.9684	11.1047	13.7885	7.0891	11.0200
0.8	9.7137	15.0876	17.0743	12.7508	15.8669	8.1469	12.8450

Table 3.18 The END values of MBCUSUM charts with $p_0 = 0.01$, $\rho = 0.05$, and $p_{max} = 0.8$ under different priors

p_{ub}	Uniform	beta(0.5,	beta(0.5,	beta(1,3)	beta(1,5)	beta(2,5)	beta(2,10
0.02	7.6329	7.2093	6.8320	6.6987	6.3868	6.6363	6.1111
0.03	6.2306	6.1721	6.0428	5.7161	5.6332	5.5058	5.2491
0.04	5.5187	5.7097	5.7449	5.2664	5.3453	4.9311	4.8651
0.05	5.1410	5.5133	5.6669	5.0735	5.2659	4.6470	4.7022
0.06	4.8978	5.4204	5.6711	4.9785	5.2698	4.4689	4.6365
0.07	4.7926	5.4174	5.7282	4.9441	5.3037	4.3527	4.5951
0.08	4.6360	5.3830	5.7727	4.9085	5.3521	4.2462	4.5882
0.09	4.5639	5.4202	5.8771	4.9265	5.4434	4.1871	4.6110
0.1	4.5564	5.4870	5.9861	4.9634	5.5332	4.1557	4.6390
0.11	4.4235	5.4644	6.0358	4.9449	5.5955	4.0705	4.6589
0.12	4.4135	5.5135	6.1200	4.9785	5.6745	4.0512	4.6960
0.13	4.3661	5.5801	6.2594	5.0391	5.8102	4.0426	4.7724
0.14	4.3768	5.6325	6.3369	5.0811	5.8859	4.0440	4.8175
0.15	4.4901	6.1810	7.6927	5.4090	6.6488	4.1334	5.5780
0.3	4.6082	6.8025	8.0948	6.1506	7.6744	4.3863	6.1127
0.4	5.0764	7.8984	9.5739	7.1291	9.1199	4.8657	7.1903
0.5	5.6036	9.1803	11.3550	8.4644	11.0937	5.6228	8.9067
0.6	6.1933	10.3913	12.9616	9.6439	12.7777	6.3111	10.3273
0.7	6.4543	10.8525	13.5586	10.1390	13.4516	6.6633	10.9803
0.8	7.2142	12.2785	15.4207	11.5936	15.4672	7.6148	12.7974

Tables 3.16-3.18 show that the MBCUSUM charts have similar END values when p_t is relatively small, while when p_t is relatively large, the END values are relatively large and can be about 3 times as large compared to relatively small p_t. As shown in Figure 3.9, the END first decreases and then increases rapidly when p_t increases (Figure 3.10 shows the END of the MBCUSUM chart under the beta priors and we see a similar pattern as in the case under the uniform prior). The simulation results show that the MBCUSUM charts are optimized at relatively small values of p_t compared to p_{ub} for MBGLR charts. The optimized values of p_t are similar and all are around 0.05 under different priors when p_{max} is 0.2 in Table 3.16. As

p_{max} gets larger, then optimization happens at different values for different priors: with some priors the optimized p_t is at 0.13 and for others at 0.05.

Table 3.19 The END comparisons of the optimized MBGLR and MBCUSUM charts with $p_0 = 0.01, \rho = 0.05$, and $p_{max} = 0.2, 0.5$, and 0.8 under different priors

	Uniform	beta(0.5,	beta(0.5,	beta(1, 3)	beta(1, 5)	beta(2, 5)	beta(2, 10
				$p_{max} = 0.2$			
END_G	4.9280	5.5925	5.6913	5.0759	5.2322	4.4073	4.6336
$p_{ub_{opt}}$	0.11	0.11	0.11	0.11	0.11	0.15	0.15
END_M	5.2382	5.9654	6.0391	5.4058	5.5595	4.5351	4.8165
$p_{t_{opt}}$	0.05	0.03	0.03	0.04	0.04	0.07	0.06
$R_{M/G}$	1.06	1.07	1.06	1.06	1.06	1.03	1.04
				$p_{max} = 0.5$			
END_G	4.1657	4.8711	5.1009	4.4888	4.8064	3.9414	4.3498
$p_{ub_{opt}}$	0.4	0.2	0.2	0.2	0.2	0.4	0.2
END_M	4.5427	5.4612	5.6573	4.9459	5.2490	4.0532	4.5878
$p_{t_{opt}}$	0.11	0.05	0.05	0.07	0.05	0.12	0.08
$R_{M/G}$	1.09	1.12	1.11	1.10	1.09	1.03	1.05
				$p_{max} = 0.8$			
END_G	3.9455	4.6317	5.0198	4.4139	4.8117	3.9050	4.3621
$p_{ub_{opt}}$	0.4	0.4	0.2	0.4	0.2	0.4	0.2
END_M	4.3661	5.3830	5.6669	4.9085	5.2659	4.0426	4.5882
$p_{t_{opt}}$	0.13	0.08	0.05	0.08	0.05	0.13	0.08
$R_{M/G}$	1.11	1.16	1.13	1.11	1.09	1.04	1.05

Table 3.19 shows some results for optimized MBGLR and MBCUSUM charts. The notation END_G and END_M refers to the minimized END of the MBGLR and MBCUSUM charts, respectively. The notation $p_{ub_{opt}}$ and $p_{t_{opt}}$ refers to the upper bound of the GLR chart and the pre-determined shift size of the MBCUSUM chart when they reach the minimum END, respectively. The ratio $R_{M/G}$ is (END_M/ END_G), with a value greater than 1 representing the case in which the minimized loss of the GLR chart is less than that of the MBCUSUM chart. Table 3.19 shows that the $R_{M/G}$ values are all greater than 1 for different priors and values of p_{max}. When $p_{max} = 0.2$, the optimized MBCUSUM chart with $p_t = 0.05$ has 6% more loss than the optimized GLR chart with $p_{ub} = 0.11$ under the uniform prior. While for the beta(0.5, 1) prior, $R_{M/G} = 1.07$, which indicates the optimized MBCUSUM chart with $p_t = 0.03$ has 7% more loss than the optimized MBGLR chart with $p_{ub} = 0.11$. As p_{max} increases, the $R_{M/G}$ values increase for the same prior distribution. When $p_{max} = 0.8$, the optimized MBCUSUM chart has more than 10% loss than the optimized MBGLR chart for some of the priors. It is noted that under the $\text{beta}(2, 5)$ and $\text{beta}(2, 10)$ priors, the advantage of MBGLR chart is not as clear as

that under the other priors. These two priors have a concave shape and assume a particular shift p_s has the highest chance of occurring. Then the MBCUSUM chart with $p_t = p_s$ designed to detect this p_s has relatively good performance compared with the cases of a uniform prior or a beta prior with a strictly decreasing density.

Table 3.20 The END values of MBGLR charts with $p_0 = 0.01, \rho = 0.2$, and $p_{max} = 0.2$ under different priors

p_{ub}	Uniform	beta(0.5,	beta(0.5,	beta(1, 3)	beta(1, 5)	beta(2, 5	beta(2, 10)
0.02	7.0590	7.2615	7.2885	7.0866	7.1197	6.9365	6.9392
0.03	6.3463	6.7259	6.7795	6.4149	6.4910	6.0898	6.1519
0.04	6.0453	6.5319	6.6024	6.1432	6.2490	5.7010	5.8146
0.05	5.8941	6.4469	6.5277	6.0092	6.1328	5.4954	5.6371
0.06	5.8451	6.4345	6.5209	5.9694	6.1026	5.4170	5.5731
0.07	5.8129	6.4237	6.5136	5.9433	6.0827	5.3662	5.5332
0.08	5.7833	6.4173	6.5109	5.9207	6.0669	5.3171	5.4977
0.09	5.7666	6.4277	6.5257	5.9117	6.0656	5.2779	5.4723
0.1	5.7368	6.4155	6.5164	5.8877	6.0474	5.2319	5.4381
0.11	5.7378	6.4339	6.5375	5.8933	6.0577	5.2188	5.4330
0.12	5.7413	6.4527	6.5588	5.9013	6.0702	5.2092	5.4319
0.13	5.7319	6.4523	6.5598	5.8949	6.0668	5.1914	5.4199
0.14	5.7511	6.4832	6.5925	5.9167	6.0912	5.2022	5.4343
0.15	5.7428	6.4791	6.5891	5.9101	6.0864	5.1894	5.4258
0.2	5.8624	6.6732	6.7944	6.0465	6.2404	5.2538	5.5140
0.3	6.0723	6.9663	7.0996	6.2737	6.4860	5.4055	5.6882
0.4	6.1225	7.0332	7.1694	6.3299	6.5481	5.4391	5.7342
0.5	6.1475	7.0611	7.1979	6.3565	6.5761	5.4602	5.7588
0.6	6.1213	7.0262	7.1616	6.3279	6.5452	5.4410	5.7356
0.7	6.2347	7.1502	7.2876	6.4455	6.6668	5.5425	5.8449
0.8	6.3915	7.3654	7.5115	6.6152	6.8502	5.6566	5.9777

The second case considered is $p_0 = 0.01, \rho = 0.2$. We still use $p_{max} = 0.2, 0.5$, and 0.8. The results for the MBGLR chart when $p_{max} = 0.2$ will be discussed first in Table 3.20. It is noted that the conclusions obtained are similar to those obtained when $p_0 = 0.01, \rho = 0.05$. When correlation increases to 0.2, the END value increase for the same MBGLR chart under the same combination of p_0, ρ, p_{max}, and prior distribution. For instance, in Tables 3.13 and 3.20, the END values of the MBGLR chart with $p_{ub} = 0.15$ when $p_{max} = 0.2$ are 5.1737 and 5.7428 for $\rho = 0.05$ and 0.2, respectively, under the uniform prior. Under the beta(0.5,1) prior, the END values are 6.0035 and 6.4791, respectively. As we discussed in the previous section, for the same size of shift the control charts take a longer time to detect shifts when the correlation is higher. The END is the integral of the product SSANOS $*$ $(p - p_0)$, and therefore will result in the same trend as the SSANO*S* when the correlation increases. Table 3.21 presents END values of MBCUSUM chart with $p_0 = 0.01, \rho = 0.2$ and $p_{max} = 0.2$. It is noted that the conclusion that the END increases as the correlation increases also applied to the MBCUSUM charts. For example, in Table 3.16, the END of the MBCUSUM chart with $p_t = 0.05$ is 6.0530 under the

uniform prior, and for the same settings of p_0, p_{max}, and p_{ub} in Table 3.16, the END of the MBCUSUM chart is 5.2382 under uniform prior. The END values of MBGLR and MBCUSUM charts for $p_{max} = 0.5$, and 0.8 reflect similar results and will not be discussed here.

Table 3.21 The END values of MBCUSUM charts with $p_0 = 0.01, \rho = 0.2$, and $p_{max} = 0.2$ under different priors

p_{ub}	Uniform	beta(0.5,	beta(0.5,	beta(1,3)	beta(1,5)	beta(2,5	beta(2,10)
0.02	6.9741	7.2079	7.2391	7.0057	7.0435	6.8347	6.8383
0.03	6.3217	6.8245	6.8951	6.4108	6.5097	5.9886	6.0675
0.04	6.0547	6.7878	6.8935	6.1992	6.3557	5.5440	5.7069
0.05	6.0530	6.9471	7.0767	6.2327	6.4269	5.4209	5.6287
0.06	6.1095	7.1404	7.2907	6.3215	6.5498	5.3704	5.6240
0.07	6.1627	7.3262	7.4970	6.4086	6.6721	5.3156	5.6221
0.08	6.2636	7.5606	7.7520	6.5436	6.8424	5.3075	5.6673
0.09	6.3797	7.7908	8.0001	6.6895	7.0193	5.3281	5.7351
0.1	6.5077	8.0192	8.2442	6.8441	7.2015	5.3715	5.8209
0.11	6.6413	8.2439	8.4833	7.0021	7.3849	5.4273	5.9164
0.12	7.0000	8.8245	9.0971	7.4113	7.8476	5.6169	6.1758
0.13	6.9027	8.6586	8.9225	7.3063	7.7332	5.5545	6.1153
0.14	7.0433	8.8760	9.1519	7.4676	7.9159	5.6299	6.2244
0.15	7.1594	9.0470	9.3319	7.6001	8.0653	5.6955	6.3194
0.3	9.3725	12.0835	12.5030	10.0615	10.7795	7.1560	8.2276
0.4	17.2202	21.3805	22.0556	18.4496	19.7013	13.4955	15.6993
0.5	13.8182	17.6720	18.2839	14.8821	15.9768	10.5049	12.3002
0.6	15.2410	19.1164	19.7404	16.3590	17.5018	11.8183	13.7798
0.7	17.2202	21.3805	22.0556	18.4496	19.7013	13.4955	15.6993
0.8	17.4727	20.2843	20.7644	18.4358	19.3951	14.7189	16.6450

Table 3.22 The END comparisons of optimized MBGLR and MBCUSUM chart with $p_0 = 0.01, \rho = 0.2$, and $p_{max} = 0.2, 0.5$, and 0.8 under different priors

	Uniform	beta(0.5	beta(0.5	beta(1,3	beta(1,5	beta(2,	beta(2,1
				$p_{max} = 0.2$			
END_G	5.7319	6.4155	6.5109	5.8877	6.0474	5.1894	5.4199
$p_{ub_{opt}}$	0.13	0.1	0.08	0.1	0.1	0.15	0.13
END_M	6.0530	6.7878	6.8935	6.1992	6.3557	5.3075	5.6221
$p_{t_{opt}}$	0.05	0.04	0.04	0.04	0.04	0.08	0.07
$\text{R}_\text{M/G}$	1.06	1.06	1.06	1.05	1.05	1.02	1.04
				$p_{max} = 0.5$			
END_G	5.1648	5.8272	6.0179	5.4345	5.6949	4.8978	5.2131
$p_{ub_{opt}}$	0.6	0.15	0.13	0.15	0.13	0.6	0.15
END_M	5.4719	6.3966	6.6045	5.8013	6.1467	4.9657	5.3852
$p_{t_{opt}}$	0.09	0.07	0.04	0.08	0.07	0.13	0.08
$\text{R}_\text{M/G}$	1.06	1.10	1.10	1.07	1.08	1.01	1.03
				$p_{max} = 0.8$			
END_G	5.0083	5.7562	6.0857	5.4523	5.7310	4.8856	5.2227
$p_{ub_{opt}}$	0.7	0.7	0.15	0.6	0.15	0.6	0.15
END_M	5.6983	6.5977	6.7373	5.9104	6.1753	5.0321	5.3918
$p_{t_{opt}}$	0.14	0.08	0.07	0.08	0.07	0.14	0.08
$\text{R}_\text{M/G}$	1.14	1.15	1.11	1.08	1.08	1.03	1.03

Now, we compare the optimized MBGLR and MBCUSUM charts when $p_0 = 0.01, \rho = 0.2$, and $p_{max} = 0.2, 0.5$, and 0.8. Table 3.22 presents the END_G, END_M, $p_{ub_{opt}}$, $p_{t_{opt}}$, and $R_{M/G}$ values under different prior distributions. Similar to the results from Table 3.19, the $R_{M/G}$ values

show that the optimized MBCUSUM chart is beaten by the optimized MBGLR chart for some of the cases with up to 15% more loss for the MBCUSUM chart. The optimized MBGLR chart is always at least as good as the optimized MBCUSUM chart. For the $\text{beta}(2,5)$ and $\text{beta}(2,10)$ priors, the difference is relatively small.

Table 3.23 The END comparisons of optimized MBGLR and MBCUSUM charts with $p_0 = 0.01, \rho = 0.1, p_{max} = 0.2, 0.5$, and 0.8 under different priors

	Uniform	beta(0.5,	beta(0.5,	beta(1, 3)	beta(1, 5)	beta(2, 5	beta(2, 10)
				$p_{max} = 0.2$			
END_G	5.0198	5.5249	5.5994	5.1289	5.2453	4.6478	4.7895
$p_{ub_{opt}}$	0.06	0.06	0.06	0.06	0.06	0.06	0.06
END_M	5.5223	6.2415	6.3133	5.6635	5.8163	4.7957	5.0772
$p_{t_{opt}}$	0.04	0.03	0.03	0.04	0.04	0.07	0.06
$\text{R}_{\text{M/G}}$	1.10	1.13	1.13	1.10	1.11	1.03	1.06
				$p_{max} = 0.5$			
END_G	4.4891	5.2080	5.3186	4.8053	5.0767	4.2565	4.6706
$p_{ub_{opt}}$	0.3	0.3	0.06	0.3	0.06	0.3	0.3
END_M	4.8804	5.8204	5.9896	5.2481	5.5789	4.4189	4.8594
$p_{t_{opt}}$	0.09	0.06	0.04	0.08	0.06	0.1	0.08
$\text{R}_{\text{M/G}}$	1.09	1.12	1.13	1.09	1.10	1.04	1.04
				$p_{max} = 0.8$			
END_G	4.3237	4.9990	5.3449	4.7369	5.1157	4.2391	4.6670
$p_{ub_{opt}}$	0.6	0.3	0.3	0.3	0.06	0.3	0.3
END_M	5.0513	5.8271	6.0859	5.2600	5.6001	4.4823	4.8631
$p_{t_{opt}}$	0.1	0.09	0.06	0.09	0.06	0.1	0.08
$\text{R}_{\text{M/G}}$	1.17	1.17	1.14	1.11	1.09	1.06	1.04

Table 3.24 The END comparisons of optimized MBGLR and MBCUSUM chart with $p_0 = 0.01, \rho = 0.4, p_{max} = 0.2, 0.5$, and 0.8 under different priors

	Uniform	beta(0.5,	beta(0.5,	beta(1, 3)	beta(1, 5)	beta(2, 5	beta(2, 10)
				$p_{max} = 0.2$			
END_G	7.2220	7.9768	8.0723	7.3982	7.5824	6.5998	6.8818
$p_{ub_{opt}}$	0.1	0.07	0.06	0.1	0.09	0.2	0.1
END_M	7.5413	8.3039	8.4141	7.6931	7.8578	6.6692	7.0328
$p_{t_{opt}}$	0.04	0.04	0.04	0.04	0.04	0.08	0.07
$\text{R}_{\text{M/G}}$	1.04	1.04	1.04	1.04	1.04	1.01	1.02
				$p_{max} = 0.5$			
END_G	6.5314	7.3059	7.5210	6.8532	7.1623	6.2405	6.6145
$p_{ub_{opt}}$	0.4	0.4	0.2	0.4	0.2	0.4	0.2
END_M	6.9743	7.8775	8.1201	7.2566	7.6007	6.4513	6.7802
$p_{t_{opt}}$	0.08	0.07	0.06	0.07	0.07	0.1	0.08
$\text{R}_{\text{M/G}}$	1.07	1.08	1.08	1.06	1.06	1.03	1.03
				$p_{max} = 0.8$			
END_G	6.7079	7.2875	7.5506	6.8752	7.2021	6.2979	6.6259
$p_{ub_{opt}}$	0.7	0.4	0.4	0.4	0.2	0.4	0.2
END_M	7.9903	8.4362	8.3632	7.5148	7.6542	6.6865	6.7921
$p_{t_{opt}}$	0.1	0.08	0.07	0.08	0.07	0.1	0.08
$\text{R}_{\text{M/G}}$	1.19	1.16	1.11	1.09	1.06	1.06	1.03

The third and forth cases considered are $p_0 = 0.01$ and $\rho = 0.1$ and 0.4. Tables 3.23 and 3.24 show the comparisons of the optimized MBGLR and MBCUSUM charts. When $\rho = 0.1$,

the optimized MBCUSUM charts has up to 17% more loss than the corresponding optimized MBGLR charts for the same p_{max} and prior distribution. When $\rho = 0.4$, the largest $R_{M/G}$ is 0.19, which is 19% more loss for the optimized MBCUSUM chart compared with the optimized MBGLR chart. Except for the $\text{beta}(2,5)$ and $\text{beta}(2,10)$ priors, almost all $R_{M/G}$ values are between 4%-20%.

The above discussion shows the results for the optimized MBGLR and MBCUSUM charts when $p_0 = 0.01$, and $\rho = 0.05, 0.1, 0.2, 0.4$. Now we consider two more combinations with $p_0 = 0.001$ and $\rho = 0.05$ and 0.2. The largest shift sizes are set to be $p_{max} = 0.02, 0.05,$ and 0.08, which are 20, 50, and 80 times of the in-control p_0, respectively. The upper bound of the MBGLR charts and the pre-determined shift size of the MBCUSUM charts take values between 0.002 and 0.08. In each of the combinations, the MBGLR and MBCUSUM chart are set to have ICANOS $= 16956.6$, which is the same as in the combination of $p_0 = 0.01,$ and $\rho = 0.05$. The optimized MBGLR chart is compared with the optimized MBCUSUM chart in Tables 3.25 and 3.26.

Table 3.25 The END comparisons of optimized MBGLR and MBCUSUM charts with $p_0 = 0.001, \rho = 0.05,$ and $p_{max} = 0.002, 0.005,$ and 0.008 under different priors

	Uniform	beta(0.5,	beta(0.5,	beta(1,3)	beta(1,5)	beta(2,5	beta(2,10)
				$p_{max} = 0.02$			
END_G	2.0235	2.1863	2.1888	2.0279	2.0324	1.8190	1.8255
$p_{ub_{opt}}$	0.03	0.03	0.03	0.03	0.03	0.03	0.03
END_M	2.6600	2.7181	2.7188	2.6624	2.6648	2.5190	2.5241
$p_{t_{opt}}$	0.006	0.005	0.005	0.006	0.006	0.008	0.008
$\text{R}_{\text{M/G}}$	1.31	1.24	1.24	1.31	1.31	1.38	1.38
				$p_{max} = 0.05$			
END_G	1.6356	1.8503	1.8570	1.6459	1.6564	1.4479	1.4603
$p_{ub_{opt}}$	0.08	0.08	0.08	0.08	0.08	0.08	0.08
END_M	2.3904	2.5480	2.5522	2.3990	2.4076	2.2183	2.2299
$p_{t_{opt}}$	0.01	0.007	0.007	0.01	0.01	0.02	0.02
$\text{R}_{\text{M/G}}$	1.46	1.38	1.37	1.46	1.45	1.53	1.53
				$p_{max} = 0.08$			
END_G	1.4624	1.6929	1.7038	1.4780	1.4939	1.2920	1.3103
$p_{ub_{opt}}$	0.04	0.04	0.04	0.04	0.04	0.04	0.04
END_M	2.2888	2.4643	2.4718	2.2997	2.3111	2.1501	2.1606
$p_{t_{opt}}$	0.01	0.008	0.008	0.01	0.01	0.02	0.02
$\text{R}_{\text{M/G}}$	1.57	1.46	1.45	1.56	1.55	1.66	1.65

In Table 3.25 with $\rho = 0.05$, the MBCUSUM chart is optimized at relatively small values of p_t compared with the optimized value of p_{ub} for the MBGLR chart. For instance, in the first part of Table 3.25 with $p_{max} = 0.02$, $p_{t_{opt}} = 0.006$ and $p_{ub_{opt}} = 0.03$ under the

uniform prior; and $p_{t_{opt}} = 0.005$ and $p_{ub_{opt}} = 0.03$ under the beta$(0.5, 1)$ prior. It is noted that when $p_0 = 0.001$, the optimized MBCUSUM chart is far and away worse than the optimized MBGLR chart in Table 3.25. As p_{max} increases, the optimized MBGLR chart can beat the optimized MBCUSUM chart dramatically. When $p_{max} = 0.05$, $R_{M/G}$ is between 1.37 and 1.53 for different priors. When $p_{max} = 0.08$, the END of the optimized MBCUSUM chart is 57% more than that of the MBGLR chart under the uniform prior and 45% to 66% more under the beta priors. The advantage of the MBGLR chart over MBCUSUM chart is clear when p_{max} is large. Compared with the cases with $p_0 = 0.01$, the MBGLR chart are significantly better than the MBCUSUM chart when $p_0 = 0.001$.

Table 3.26 presents the results when $\rho = 0.2$. Table 3.26 shows that the optimized MBCUSUM chart has about 30% to 70% more loss than that of the MBGLR charts and similar conclusions can be reached as in Table 3.25. The p_{max} values considered here for $p_0 = 0.001$ are much smaller than those for the case of $p_0 = 0.01$. If relatively large p_{max} values such as $0.2, 0.5,$ or 0.8 were used when $p_0 = 0.001$, the advantage of the MBGLR chart over the MBCUSUM chart would be even larger.

Table 3.26 The END comparisons of optimized MBGLR and MBCUSUM charts with $p_0 = 0.001, \rho = 0.2$, and $p_{max} = 0.002, 0.005$, and 0.008 under different priors

	Uniform	beta(0.5,	beta(0.5,	beta(1, 3)	beta(1, 5)	beta(2, 5	beta(2, 10)
				$p_{max} = 0.02$			
END_G	2.2055	2.3668	2.3690	2.2101	2.2147	1.9949	2.0018
$p_{ub_{opt}}$	0.02	0.01	0.01	0.02	0.02	0.02	0.02
END_M	2.9761	3.0256	3.0264	2.9786	2.9812	2.8375	2.8435
$p_{t_{opt}}$	0.006	0.005	0.005	0.006	0.006	0.009	0.009
$R_{M/G}$	1.35	1.28	1.28	1.35	1.35	1.42	1.42
				$p_{max} = 0.05$			
END_G	1.7814	2.0063	2.0134	1.7924	1.8036	1.5808	1.5942
$p_{ub_{opt}}$	0.02	0.02	0.02	0.02	0.02	0.02	0.02
END_M	2.7060	2.8513	2.8556	2.7138	2.7217	2.5548	2.5654
$p_{t_{opt}}$	0.009	0.007	0.007	0.009	0.009	0.02	0.02
$R_{M/G}$	1.52	1.42	1.42	1.51	1.51	1.62	1.61
				$p_{max} = 0.08$			
END_G	1.6049	1.8455	1.8569	1.6211	1.6378	1.4266	1.4451
$p_{ub_{opt}}$	0.02	0.02	0.02	0.02	0.02	0.02	0.02
END_M	2.6214	2.7776	2.7843	2.6310	2.6410	2.5060	2.5145
$p_{t_{opt}}$	0.009	0.007	0.007	0.009	0.009	0.02	0.02
$R_{M/G}$	1.63	1.51	1.50	1.62	1.61	1.76	1.74

In the end, we consider $p_0 = 0.1$ and $\rho = 0.05, 0.2$. The largest shift sizes are set to be $p_{max} = 0.5,$ and 0.8, which are 5 and 8 times the value of the in-control p_0. The upper bound of the MBGLR charts and the pre-determined shift size of the MBCUSUM chart take values

between 0.2 and 0.8. In each of the combinations, the MBGLR and MBCUSUM charts are set to have ICANOS $= 16956.6$. Simulation results (not shown here) show the optimized MBGLR chart can beat the optimized MBCUSUM chart with END ratios close to the cases with $p_0 = 0.01$.

3.5.4 Conclusions

In this section, the design of the MBGLR chart was discussed. First, the choice of the window size for the geometric-type variable was investigated by simulation based on the idea that the window size should be large enough to achieve essentially the same in and out-of control performance as in the case in which as there is no window. The rule that the window size can be set to be equal to the ICANOS was confirmed by simulation. The window sizes $m' = 30, 300,$ and 3000 were selected for the cases with $p_0 = 0.001, 0.01,$ and 0.1, respectively. The control limit can be selected by using a fitted regression line once $p_0, \rho,$ and p_{ub} are given. The END was proposed for use in optimizing the upper bound of the MBGLR chart and the pre-determined shift size of the MBCUSUM chart. The optimized MBGLR and MBCUSUM charts were then compared under several different assumptions about the shift sizes. It was concluded that the optimized MBGLR chart has overall performance at least equal to the optimized MBCUSUM chart. For most of the cases considered, the optimized MBCUSUM chart has 5% to 60% more loss than the optimized GLR chart depending on the values of p_0, ρ and p_{max}. We found that setting $p_{ub} = p_{max}$, gives an END value that is almost equal to the case using the optimized upper bound. It is best not to set p_{ub} and p_{max} to be 1, as 1 will result in a discreteness problem when estimating p_1. In practice, p_{max} is the largest value of p that might reasonably occur and it will be unrealistic to be equal to 1 in practice.

3.6 A Real Data Example

3.6.1 Process and Data Description

In this section, we will discuss using an MBGLR chart to monitor a real data set concerned with the quality of silicon wafers. The binary data set is from a production process, where the quality of the wafers is measured and then classified into the defective (represent by 1)

and non-defective categories (represent by 0). We obtained the dataset from Dr. Ran Jin, assistant professor from Department of Industrial and Systems Engineering at Virginia Tech. More information about the data set can be found from Zhao et al. (2011). It is believed by the manufacturer that the quality of the current inspected wafer depends on the previous one as they share one slicing wire. There are 480 binary observations in the data set and the binary sequence corresponds to the time order when the wafers were produced. Figure 3.11 shows the plot of the binary data set, where 1 represents defective and 0 represents non-defective.

Figure 3.11 Quality of the wafers with 0=non-defective and 1=defective

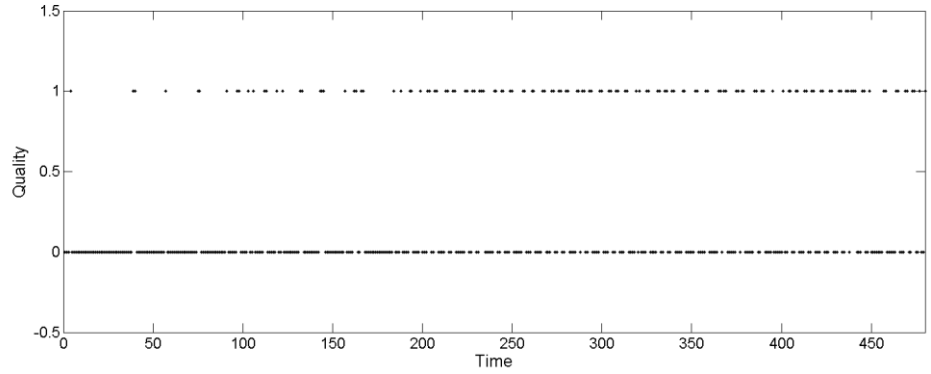

3.6.2 Phase I Analysis

There are 480 binary observations in the data set and the binary sequence corresponds to a time order. It is noted that there are fewer defectives in the first 180 binary observations, compared with the rest of the observations. Therefore, we use the first 180 binary observations as the Phase I data to estimate the in-control parameters. In a real application, using 180 observations for Phase I estimation is far from what would be desirable for accuracy and precision in parameter estimation. A much larger Phase I data set would preferred, however, in this example, due to the limitations of the data set, we will use the first 180 observations for Phase I estimation. It is noted that a two-state Markov chain model to fit the data. To confirm this idea, the Bernoulli model and the first-order Markov chain model will be considered here.

In the Bernoulli model, the in-control proportion p_0 can be estimated by $\hat{p}_0 = \frac{N_1}{180} = \frac{25}{180} = 0.14$, where N_1 is the number of defectives from Phase I. In a two-state Markov chain model, the maximum likelihood estimator of the transition probability p_{ij} is:

$$\hat{p}_{ij} = \frac{N_{ij}}{N_{i0} + N_{i1}}$$

where N_{ij} is the number of transitions from state i to state j for $i, j = 0, 1$. Then the estimators for p_0 and ρ are:

$$\hat{p}_0 = \frac{\hat{p}_{01}}{\hat{p}_{01} + \hat{p}_{10}}$$

$$\hat{\rho} = 1 - (\hat{p}_{01} + \hat{p}_{10})$$

The estimators for the transition probabilities of Markov chain model were proposed by Bhat and Lal (1990) and more details can be found in Mousavi and Reynolds (2009). Using the above estimators, we get $\hat{p}_{01} = 0.1039, \hat{p}_{10} = 0.64, \hat{p}_0 = 0.14$, and $\hat{\rho} = 0.26$.

MacDonald and Zucchini (1997, p. 144) suggested that the fit of different Markov chain models can be compared based on the unconditional log likelihoods (denoted by L), and the model selection criteria AIC and BIC. If K is the number of parameters estimated in order to fit a model, and T represents the length of the observation sequence, then the AIC and BIC are defined as

$$AIC = -2L + 2K$$

$$BIC = -2L + KlogT$$

Table 3.27 Comparisons likelihood, AIC, and BIC of the fitted Bernoulli and First-order Markov Chain models for the real data set

Model	K	-L	AIC	BIC
Bernoulli	1	72.53	145.06	155.44
First-order MC	**2**	**67.7**	**135.41**	**145.79**

Table 3.27 shows the comparisons of the two models. It is noted that the first order Markov chain model achieves the smaller $-L, AIC$, and BIC. The results confirm the nature of

the process as explained by the manufacturer. Therefore we conclude that a first order Markov chain model is more appropriate than the independent Bernoulli model.

3.6.3 Phase II monitoring

After the Phase I parameter estimation, we start the monitoring process for Phase II (consisting of remaining 280 observations) using the proposed MBGLR chart. We apply a MBGLR chart with $p_{ub} = 0.42$, which is about 3 times the value of p_0 and provides relatively good performance for shifts smaller than 0.42. As in the discussion of the upper bound selection, we found that a relatively large upper bound is preferred in the detection process. With $\hat{p}_0 = 0.14$, $\hat{\rho} = 0.26$ and $p_{ub} = 0.42$, the control limit h can be estimated from the Equation (3.5). From Equations (3.3) and (3.4), the intercept and slope are -1.9121 and 2.3919, respectively. Taking the desired ICANOS to be 1000, the control limit is $h = 3.2212$.

Figure 3.12 The MBGLR chart with $p_{ub} = 0.42$ chart for monitoring the Phase II data

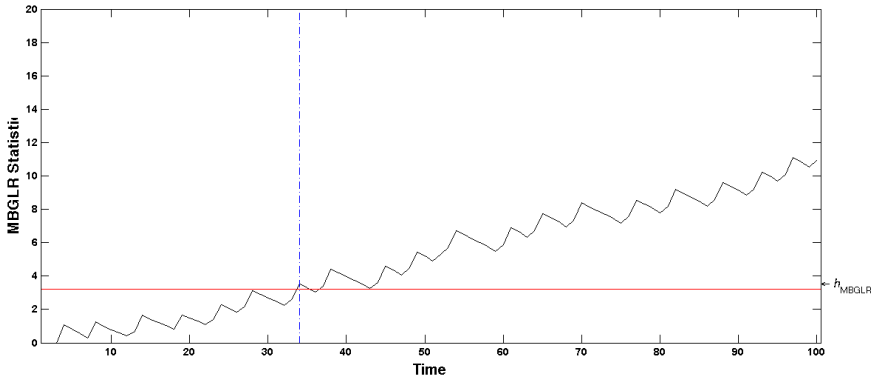

The MBGLR chart was applied to monitor the Phase II data set with 280 binary observations and Figure 3.12 shows the monitoring processes for the first 100 observations in the Phase II data. The MBGLR statistic increases as the monitoring process starts and the shift is detected at the 34th binary observation. Figure 3.13 shows the estimated shift and estimated change-point with the vertical dashed line indicating the time of the signal. In both of the two estimation plots, the estimated values become stable after a period of time. The estimated shift is stable after about 30 observations with $\hat{p}_1 \approx 0.39$. The estimated change-point plot becomes stable after only 4 observations with $\hat{\tau} = 3$, which indicates that the shift occurred very soon after the start of monitoring in Phase II.

In this example, the estimated out-of-control proportion is 0.39, which is less than the upper bound. However, if the estimated proportion is equal to the upper bound, it indicates that the estimated proportion may be incorrect due to restriction from the upper bound. In that case, there is no problem with the detection on the process change, however a larger upper bound is needed to re-estimate the shift in the diagnostic process.

An advantage of the MBGLR is that it provides estimates of the change point and the shifted value of p when a signal is given. Lou and Reynolds (2012) discussed diagnostics for the EWMA chart for the mean and variance of the normal distribution and used the maximum-likelihood estimates for the change point and current process parameters. The diagnostics procedure is applied when the EWMA chart signals. Using a similar idea, the GLR control chart can provide maximum-likelihood estimates for the change point and the current process parameters after each observation is inspected. In the example, we provide the estimates for both the shift size and change point from the MBGLR chart and the estimates become stable at the time the shift was detected. Note that an MBCUSUM chart designed for detecting a shift size equal to p_t will not directly provide an estimate of the actual shift size.

Figure 3.13 Estimated shift in proportion and change point from the MBGLR chart

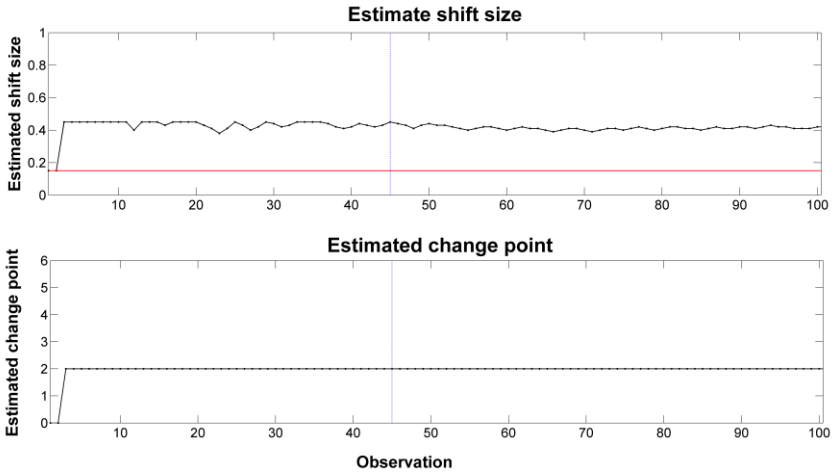

In this example, the MBGLR chart detected a change in p at the 45th binary observation, and the MBGLR chart can provide an estimate of shift as the monitoring process goes on. The estimates for both shift size and change point become stable at the time the shift is detected. Note that an MBCUSUM chart designed for detecting a shift size equal to p_t will not directly provide an estimate of the actual shift size.

3.7 Conclusion and Discussion

This chapter considered the situation in which there is a continuous stream of binary data from a process that follows the two-state Markov chain model. The binary observations are assumed to be available immediately for inspection with the inspected sample size equal to 1. The Markov binary GLR chart was proposed to monitoring the proportion of defectives. This MBGLR chart has been shown to have overall better performance than the existing MBCUSUM chart, which has previously been proved to be a better control chart than the traditional types of charts. The MBGLR chart with an upper bound can quickly detect shifts at or smaller than the upper bound. An upper bound equal to the largest shift size being considered is suggested to practitioners for applications when assuming all the sizes of shift have an equal chance to occur. Besides the proposed MBGLR chart, a loss function based on the extra number of defectives (END) has been developed. An optimization based on END has been conducted over MBGLR charts with different upper bounds and MBCUSUM charts with different pre-determined shift sizes. The optimization shows that the optimized MBGLR chart has less loss than the optimized MBCUSUM charts under various parameter combinations.

Chapter 4. Control Charts for Monitoring the Proportion and Correlation

4.1 Summary of Previous Work

In Chapter 3, we focused on monitoring the proportion in the correlated binary process where the data can be modeled as a two-state Markov chain model. The binary observations are assumed to come from a continuous stream and will be available for inspection immediately. The sample size is considered to be $n = 1$. Binary processes can be well monitored by the traditional types of charts when the observations are independent. The Shewhart-type charts can detect large shifts very well, while the CUSUM-type charts can be designed to detect shifts according to the tuning parameter selected. However, when correlation is present, the in-control performance of these traditional charts is not robust. In this situation, the MBCUSUM chart has been shown to be a better choice because it takes the correlation into account and has better performance in detecting changes in the proportion.

In Chapter 3, we proposed the Markov binary GLR chart with an upper bound as a tuning parameter. The MBGLR chart was shown to quickly detect shifts closer to or less than the upper bound. The design of the MBGLR chart requires the specification of the window size, control limit, and the upper bound. The calculation of MBGLR statistic requires maximization over all the past samples, and a moving window can be used to relieve part of the computational burden. The window size is required to be large enough to include a sufficiently large number of observations to achieve in and out-of-control performance similar to the case of no window. It was found that the control limit of the MBGLR chart and the log of in-control ANOS have a linear relationship for many combinations of p_0, ρ and p_{ub}. Fitted linear regression equations were provided for practitioners to use in finding the control limit for given values of p_0, ρ, p_{ub}, and the desired ICANOS. The upper bound of the MBGLR chart was optimized using a loss function END, which counts the overall extra number of defectives produced when the process proportion shifts. It was shown that the upper bound selection depends on the possible maximum shift that can occur as well as the prior distribution of the possible shift. When all shifts have an equal chance to occur, it was suggested that the upper bound be selected to be equal to the

maximum shift. The MBGLR chart and the MBCUSUM chart were optimized with respect to the upper bound and the pre-determined shift size, respectively, using the END under different combinations of $p_0, \rho,$ maximum shift, and the prior distribution. It was concluded that the optimized MBGLR chart is better than the optimized MBCUSUM chart with less loss in terms of END. The optimized MBGLR chart can be much better than the optimized MBCUSUM chart when there is a wide range of possible shifts, and especially for high quality processes with small values of p_0.

4.2 Introduction to Monitoring the Proportion and Correlation

In the previous work on monitoring the binary process, it is assumed that the correlation remains unchanged in the process while the proportion shifts upward. An assumption that may be more realistic in some situations is that both the proportion and correlation can change simultaneously. In the literature, it has been shown that a change in correlation is difficult to detect, especially a decrease in correlation. When monitoring the correlated binary process, the main concern is monitoring the proportion, but we would like to see how correlation changes would affect the monitoring process. In this chapter we propose several control charts for monitoring the proportion and correlation simultaneously and investigate the performance of these charts.

Let p_0 and ρ_0 be the in-control proportion and correlation, respectively. Then let p_1 and ρ_1 be the shifted values of the proportion and correlation, respectively. In the monitoring process, it is assumed that the proportion will shift upward, i.e. $p_1 > p_0,$ as an increase represents worse quality for the process and is more important to be detected in the production processes. We assume that the correlation can shift upward and downward, i.e. both increases and decreases will be considered. Through out the work in this chapter, we will assume that the correlation is non-negative. Therefore, the shifted value ρ_1 satisfies $0 \leq \rho_1 < \rho_0$ or $\rho_1 > \rho_0 \geq 0$.

When monitoring one parameter, the shift is defined as the value to which the in-control parameter changes. When there are two parameters being monitored by a control chart, we have two potential shifts with one for each parameter. Then the shifts occur in a two-dimension coordinate system. Figure 4.1 shows the area in which the shifts in p and ρ could occur. In

Figure 4.1, the point (p_0, ρ_0) represents the in-control parameters for p and ρ. The shifts in the horizontal direction (line with slope equal to 0) represent the situation in which ρ remains at the target value ρ_0 and just p increases. This direction assumes there is only a shift in p. The changes in the vertical direction (line with slope equal to $\pm\infty$) represent the situation in which p remains at the target p_0 value and ρ either decreases or increases. The directions with a positive slope correspond to increases in both p and ρ. The directions with a negative slope correspond to an increase in p and a decrease in ρ. To compare chart performance in later sections, we will look at different directions for the shifts in the coordinate system. In each direction, as the shifts point gets farther away from the in-control parameters, the larger the shifts in the two parameters.

Figure 4.1 Directions of shifts in proportion and correlation when slope $s = 5, 10, -2.5, 0$, and $\pm\infty$

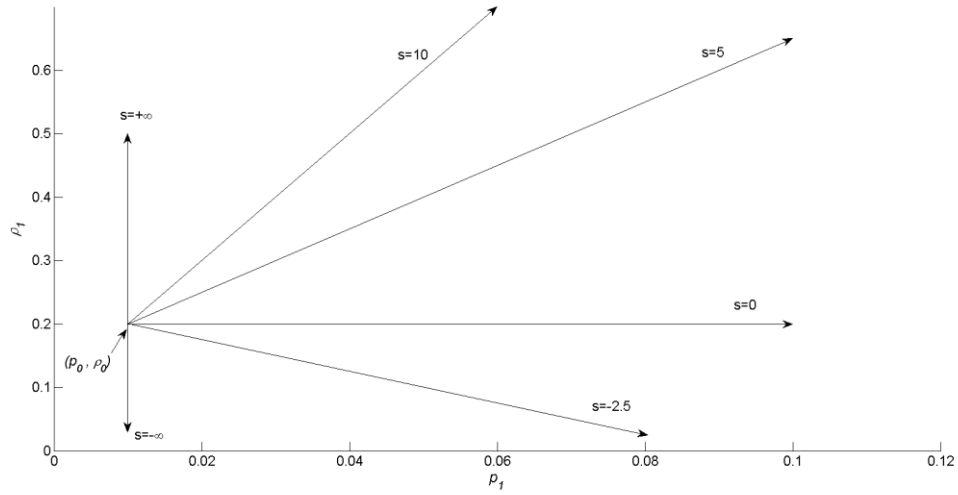

When monitoring two parameters, one can use two control charts with each chart monitoring one parameter. For instance, when simultaneously monitoring the mean and variance of a normal process, the traditional standard practice is to use two Shewhart charts. The Shewhart-$\bar{X}$ chart is used to monitor the process mean and a Shewhart-R or Shewhart-S chart is used to monitor the process variance. Gan (1999) used a two-sided CUSUM chart for monitoring the mean and another two-sided CUSUM chart for monitoring the variance. The Shewhart, CUSUM and EWMA charts can be combined when monitoring two parameters, for more reference see McCracken and Chakraborti (2013). Reynolds and Stoumbos (1999) compared a variety of combinations of charts, including Shewhart, EWMA, and CUSUM charts. They

recommended a combination consisting of two EWMA (or CUSUM) charts for monitoring the two parameters.

In this chapter, we will first introduce a CUSUM-$p\rho$ chart with two tuning parameters for monitoring the proportion and correlation simultaneously. Based on this CUSUM-$p\rho$ chart, we develop a CUSUM-$p\rho$ combination of two charts with one CUSUM-$p\rho$ chart for detecting increases in both p and ρ, and the other CUSUM-$p\rho$ chart for detecting an increase in p and a decrease in ρ. The CUSUM-$p\rho$ and the CUSUM-$p\rho$ chart combination will be compared with a three-CUSUM chart combination. This chart combination has three CUSUM charts with one monitoring p, one monitoring the increase shift in ρ, and the third one monitoring the decrease shift in ρ. In the end, we propose a GLR-$p\rho$ chart for monitoring p and ρ, and compare the GLR-$p\rho$ chart performance with that of the CUSUM-type charts.

4.3 CUSUM-Type Charts for Monitoring Proportion and Correlation

4.3.1 The CUSUM-$p\rho$ Chart

A CUSUM-type chart is traditionally designed for monitoring the process to detect a particular shift, and the pre-determined shift is used as a tuning parameter for the chart. It has been shown that the CUSUM-type chart has very good performance in detecting a shift equal to the tuning parameter value. When monitoring the correlated binary process proportion, the MBCUSUM chart with pre-determined shifted value p_t has been has been shown to work well when the actual shift is at or close to p_t. In this section, we extend the idea of the MBCUSUM chart and define a CUSUM- $p\rho$ chart with two tuning parameters to monitor p and ρ simultaneously.

Let $X_1, X_2, \ldots$ be the correlated binary observations where the process can be modeled as a two-state Markov chain model with joint density function:

$$f(x_1, x_2, \ldots x_k|p, \rho) = \prod_{i=1}^{k} f(x_i|x_{i-1}, p, \rho)$$

where $f(x_i|x_{i-1}, p, \rho)$ is the conditional probability mass function of the i^{th} binary observation and $f(x_i|x_{i-1}, p, \rho) = f(x_1|p, \rho)$ when $i = 1$. Then the CUSUM-$p\rho$ control statistic is defined as

$$C_{p\rho,k} = max\{0, C_{p\rho,k-1}\} + Q_{p\rho,k}, \quad k = 1,2,3, \ldots \text{ and } C_{p\rho,0} = 0$$

where

$$Q_{p\rho,k} = ln\frac{f(x_k|x_{k-1}, p_t, \rho_t)}{f(x_k|x_{k-1}, p_0, \rho_0)}, \quad k = 1, 2, 3, \ldots$$

where p_t and ρ_t are the pre-determined shifted value of p and ρ that the CUSUM-$p\rho$ chart is tuned to detect, respectively. A signal is given if $C_{p\rho,k} > h_{p\rho,C}$, where $h_{p\rho,C}$ is the control limit of the CUSUM-$p\rho$ chart.

The CUSUM-$p\rho$ chart proposed here has two tuning parameters p_t and ρ_t, and is tuned to detect the shift to $p_1 = p_t$ and $\rho_1 = \rho_t$. The CUSUM-$p\rho$ statistic looks very similar to the MBCUSUM statistic designed for detecting shifts in p. Here, we add one more tuning parameter to tune the chart to detect shifts in both p and ρ.

4.3.2 The CUSUM-$p\rho$ chart Combination

As the shifts in proportion considered here are all increases, the pre-determined shifted value $p_t > p_0$. The shift in correlation can be either an increase or a decrease; therefore, the pre-determined shifted value ρ_t can be either larger than ρ_0 or smaller than ρ_0. When $\rho_t > \rho_0$, the CUSUM-$p\rho$ chart is designed to detect increases in both proportion and correlation, and this means that the tuning parameter ρ_t is mis-specified in direction if the actual shift in correlation is a decrease. Similarly, when $\rho_t < \rho_0$, the pre-determined shifted value ρ_t is mis-specified in direction if the actual shift in correlation is an increase.

The CUSUM-$p\rho$ chart is designed to detect shifts with $p_1 = p_t$ and $\rho_1 = \rho_t$, and is expected to provide good performance when the actual shifts are close to p_t and ρ_t. However, when ρ_t is mis-specified in direction, the performance would not be expected to be very good. In practice, it is difficult to know how the correlation will change, therefore, one intuitive idea is to combine two CUSUM-$p\rho$ charts, where one chart has $\rho_t > \rho_0$ and the other one has $\rho_t < \rho_0$.

The idea of using a chart combination to obtain good performance in monitoring a process has been studied for the traditional CUSUM chart in literature. One example is using two CUSUM charts to monitor the normal process mean, with one chart for detecting increases in the mean and the other for detecting decreases in the mean. Another example is using multiple CUSUM charts and setting the tuning parameters of the CUSUM charts to be different values so that the combination of charts can be tuned to detect a wider range of shifts. This idea has been used in monitoring the parameters in a normal process (see, for example, Han (2007), Reynolds and Lou (2010)). Huang, Reynolds and Wang (2012) discussed using combination of multiple CUSUM charts to monitoring the proportion in a binomial distribution. They also showed that when the number of CUSUM charts in a combination increases, the performance of the chart combinations is quite similar to the binomial GLR chart proposed in their paper.

To design a CUSUM-$p\rho$ chart combination from two CUSUM-$p\rho$ charts $C_{p\rho}^1$ and $C_{p\rho}^2$, first the tuning parameters need to be specified. The tuning parameters p_t for $C_{p\rho}^1$ and $C_{p\rho}^2$ can be different values satisfying $p_t > p_0$. The tuning parameters ρ_t^1 and ρ_t^2 for $C_{p\rho}^1$ and $C_{p\rho}^2$ seperately are selected to satisfy that $0 < \rho_t^2 < \rho_0 < \rho_t^1$.

Then we need to specify the control limits of the two CUSUM-$p\rho$ charts $h_{p\rho,C1}$ and $h_{p\rho,C2}$. Huang, Reynolds and Wang (2012) used the same control limits for the individual CUSUM chart in a combination, in which case individually the CUSUM charts have different in-control performance, but as a combination the ICANOS value matches that of the corresponding Shewhart chart. Here we use different control limits for the two CUSUM-$p\rho$ charts in the combination, where the different control limits can provide similar in-control performance for the individual CUSUM-$p\rho$ charts. The selection of control limits for each chart is adjusted so that the chart combination has an ICANOS close to a pre-specified value. The CUSUM-$p\rho$ chart combination signals if $C_{p\rho,k}^1 > h_{p\rho,C1}$ or $C_{p\rho,k}^2 > h_{p\rho,C2}$, where $h_{p\rho,C1}$ and $h_{p\rho,C2}$ are the control limits for the two individual CUSUM-$p\rho$ charts.

4.3.3 The Three-CUSUM Chart Combination

In Section 4.3.2, we proposed using two CUSUM-$p\rho$ charts as a combination to achieve good performance for both increases and decreases in the correlation. The most common use of two charts in a combination is actually to monitor two parameters, for example, to monitor the

normal process mean and variance. To detect both increases and decreases in ρ and increases in p, another option is to use three traditional CUSUM charts, with one for the increases in p, one for increases in ρ, and one for decreases in ρ. Here the CUSUM chart for monitoring p is a MBCUSUM chart. To make more consistent notation, we redefine the MBCUSUM chart control statistic as

$$C_{p,k} = max\{0, C_{p,k-1}\} + Q_{p,k}, \quad k = 1,2,3, \ldots$$

and $C_{p,0} = 0$, where

$$Q_{p,k} = ln\frac{f(x_k|x_{k-1}, p_t, \rho_0)}{f(x_k|x_{k-1}, p_0, \rho_0)}, \quad k = 1, 2, 3, \ldots$$

where p_t is the pre-determined shift for p.

The CUSUM chart for monitoring ρ, CUSUM-ρ chart, is defined in a similar manner. For correlated binary process with observations $X_1, X_2, \ldots$, the control statistic for the CUSUM-ρ chart is

$$C_{\rho,k} = max\{0, C_{\rho,k-1}\} + Q_{\rho,k}, \quad k = 1,2,3, \ldots$$

and $C_{\rho,0} = 0$, where

$$Q_{\rho,k} = ln\frac{f(x_k|x_{k-1}, p_0, \rho_t)}{f(x_k|x_{k-1}, p_0, \rho_0)}, \quad k = 1, 2, 3, \ldots$$

where ρ_t is the pre-determined shift for ρ. We use two CUSUM-ρ charts, C_ρ^1 and C_ρ^2 to monitor ρ. Here the pre-determined shift for C_ρ^1 satisfies $\rho_t^1 > \rho_0$ and pre-determined shift for C_ρ^1 satisfies $\rho_t^2 < \rho_0$. When using the combination of one MBCUSUM chart and two CUSUM-ρ charts, the combination provides a signal if $C_{p,k} > h_{p,MBCUSUM}$ or $C_{\rho,k}^1 > h_{\rho,C1}$ or $C_{\rho,k}^2 > h_{\rho,C2}$, where $h_{p,MBCUSUM}$, $h_{\rho,C1}$, and $h_{\rho,C2}$ are the control limits for the MBCUSUM chart, the CUSUM-ρ chart for detecting increases in ρ, and the CUSUM-ρ chart for detecting decreases in ρ, respectively. The values of $h_{p,MBCUSUM}$, $h_{\rho,C1}$, and $h_{\rho,C2}$ are adjusted to provide similar in-

control performance for each individual chart with the overall ICANOS of the chart combination equal to a pre-specified value.

4.4 Performance of the CUSUM-Type Charts

In this section, we will compare the performance of the Shewhart chart, the MBCUSUM chart, the CUSUM$-p\rho$ chart, the CUSUM$-p\rho$ chart combination, and the three-CUSUM chart combination. The Shewhart chart monitors the process by aggregating the observations from the continuous stream into samples with $n = 100$. The control statistic is the number of defectives in a sample and we assume that the shift can occur within a sample. The MBCUSUM chart is designed to detect a shift in p and may not work well when p and ρ change simultaneously. Four CUSUM $-p\rho$ charts, two CUSUM $-p\rho$ chart combinations, and three-CUSUM chart combinations were designed to detect shifts in both proportion and correlation, and these charts will be compared with the MBCUSUM chart to show that the charts accounting for the correlation change work better.

As discussed in Section 4.2, the shift occurs in a two dimensional space of p and ρ, and therefore we use a slope to define the direction of the shift from the in-control parameters (p_0, ρ_0) in the two-dimensional coordinate system. Let s be the slope and consider the values $s = -2.5, -5, 0, 2.5, 5, 10, 15$ and $\pm\infty$. When $s = -2.5$ and -5, the directions correspond to the increases in p and decreases in ρ. When $s = 2.5, 5, 10$ and 15, the directions correspond to increases in p and increases in ρ. With $s = 0$, the direction assumes that the shift only occurs in p, with ρ remaining unchanged. With $s = \pm\infty$, it is assumed that there is no shift in p and the shift only occurs to ρ. The slope $s = \pm\infty$ indicates that the shift in ρ can be either an increase or a decrease. For each of the value of s, we look at several values of p_1 and ρ_1 in the direction corresponding to s. For each specified value of s, p_1 and ρ_1 satisfy:

$$\rho_1 = s(p_1 - p_0) + \rho_0$$

It is noted that when the shift in correlation equals to 0, the transition probabilities $p_{01} = p_{11} = p$ and the observations are independent and the binary process is a Bernoulli process. The values of correlation can be in the range [-1, 1]. In practice, a negative value in

correlation corresponds to the case when the previous observation is defective, it is likely to get a non-defective observation currently. Especially when $\rho_1 = -1$, the extreme case indicates that once a defective is observed, the next observation is non-defective. The cases discussed for negative correlations seem to be very unusual in practice. Therefore, we will only consider the non-negative correlation in the discussion in the later sections. When $\rho_1 = 1$, once a defective is observed, the next observation is a defective. This situation is also not that common in practice and we will not look at the case with $\rho_1 = 1$ neither.

In Chapter 3, when the proportion increases and the correlation remains at the target value, the transition probabilities p_{01} and p_{11} both increase. When the proportion and correlation shift simultaneously, the transition probabilities p_{01} and p_{11} will not necessarily increase as p and ρ increase. From Equation (3.1), $p_{01} = p(1-\rho)$ and $p_{11} = 1-(1-p)*(1-\rho) = \rho + p_{01}$. Table 4.1 shows the values of the transition probabilities p_{01} and p_{11} when shifts occurs in both the proportion and the correlation with $p_0 = 0.01$ and $\rho_0 = 0.2$.

In the cases with $s > 0$, when p_1 and ρ_1 increase, the transition probability p_{01} first increases and then decreases, and p_{11} increases. With $s < 0$, when p_1 and ρ_1 increase, p_{01} decreases while p_{11} increases. When the proportion and the correlation shift simultaneously, as the shifts in the two parameters get large, the probability of observing a defective is large and therefore with a large p_{11}, it is easy to detect the increases in the two parameters. When $s = 0$, the shift only occurs in the proportion and p_{01} and p_{11} both increase when p_1 gets large. When $s = \pm\infty$, the shift only occurs to the correlation and as ρ_1 increases, p_{01}decreases and p_{11} increases. In this case, there is no shift in the proportion and with a small in-control proportion p_0, most of the observations would be non-defectives. With a small p_{01}, once a non-defective is observed, the chance of getting a defective in the next observation is small and therefore the shift in the correlation may be difficult to detect.

In this section, we will first compare the charts' performance when p and ρ shift simultaneously, i.e. in the directions with $s = 2.5, 5, 10, 15, -2.5$ and -5. Then we will look at the performance when the shift occurs to only one of the two parameters, i.e. in the directions with $s = 0$ and $\pm\infty$.

Table 4.1 Transition probabilities p_{01} and p_{11} with $p_0 = 0.01$ and $\rho_0 = 0.2$ when $s = 2.5, 5, 10, 15, -2, 5, -5, 0$ and $\pm\infty$

s	p_1	ρ_1	p_{01}	p_{11}	s	p_1	ρ_1	p_{01}	p_{11}
	0.01	0.2	0.008	0.208		0.01	0.2	0.008	0.208
	0.03	0.25	0.023	0.273		0.03	0.3	0.021	0.321
2.5	0.05	0.3	0.035	0.335	5	0.05	0.4	0.030	0.430
	0.1	0.425	0.058	0.483		0.08	0.55	0.036	0.586
	0.2	0.675	0.065	0.740		0.1	0.65	0.035	0.685
	0.3	0.925	0.023	0.948		0.2	0.85	0.030	0.880
	0.01	0.2	0.008	0.208		0.01	0.2	0.008	0.208
	0.02	0.3	0.014	0.314		0.02	0.35	0.013	0.363
10	0.03	0.4	0.018	0.418	15	0.025	0.425	0.014	0.439
	0.04	0.5	0.020	0.520		0.03	0.5	0.015	0.515
	0.05	0.6	0.020	0.620		0.04	0.65	0.014	0.664
	0.07	0.8	0.014	0.814		0.05	0.8	0.010	0.810
	0.01	0.2	0.008	0.208		0.01	0.2	0.008	0.208
	0.02	0.175	0.017	0.192		0.015	0.175	0.012	0.187
-2.5	0.03	0.15	0.026	0.176	-5	0.02	0.15	0.017	0.167
	0.05	0.1	0.045	0.145		0.025	0.125	0.022	0.147
	0.07	0.05	0.067	0.117		0.03	0.1	0.027	0.127
	0.08	0.025	0.078	0.103		0.05	0	0.050	0.050
	0.01	0.2	0.008	0.208		0.01	0.05	0.010	0.060
	0.03	0.2	0.024	0.224		0.01	0.1	0.009	0.109
0	0.05	0.2	0.040	0.240	$\pm\infty$	0.01	0.2	0.008	0.208
	0.1	0.2	0.080	0.280		0.01	0.3	0.007	0.307
	0.2	0.2	0.160	0.360		0.01	0.4	0.006	0.406
	0.3	0.2	0.240	0.440		0.01	0.5	0.005	0.505

4.4.1 Comparisons of Chart Performance when the Proportion and Correlation Shift Simultaneously

In this subsection, we will look at the charts' performance when $s = 2.5, 10, 15, -2.5$ and -5. When s is positive and as s increases, for the same value of p_1, ρ_1 increases. For instance, when $p_1 = 0.015$, $\rho_1 = 0.2125, 0.3000, 0.2500,$ and 0.2750 for $s = 2.5, 5, 10,$ and

15, respectively. Therefore, the shifts in the two parameters get larger as s increases even when the shift in p is the same for the different values of s. While for negative values of s, as s increases, for the same value of p_1, ρ_1 increases. For instance, when $p_1 = 0.015, \rho_1 = 0.175$ and 0.185 for $s = -5$ and -2.5, respectively, i.e. larger value of s corresponds to the shift in correlation closer to ρ_0.

4.4.1.1 Comparisons of Chart Performance with $p_0 = 0.01$ and $\rho_0 = 0.2$

First we consider the case with $p_0 = 0.01$ and $\rho_0 = 0.2$. Table 4.2 shows the SSANOS of the Shewhart chart, the MBCUSUM chart, the CUSUM-$p\rho$ chart, the CUSUM-$p\rho$ chart combination, and the three-CUSUM chart combination when $s = 2.5, 5, 10, 15, -2.5$ and -5, respectively. In Table 4.2, the Shewhart chart in column [1] has $n = 100$ and ICANOS = 16890.0 when the control limit is 5. We will use this ICANOS values as the specification for the in-control performance of the control charts, i.e. the control limits of the other charts are adjusted to have similar ICANOS values as the Shewahrt chart. We consider two MBCUSUM charts in columns [2] and [3] with pre-determined shift p_t equal to 0.02 and 0.05, respectively. Both of the two MBCUSUM charts are designed to detect increases in p, with ρ remaining unchanged. It is noted that the MBCUSUM chart works well for detecting shifts in p assuming that ρ remain unchanged. Here in the comparisons, we want to include this chart to see how it works when the two parameters shift simultaneously. We look at four CUSUM-$p\rho$ charts, with pre-determined shifts specified for both p and ρ. Here we use $(p_t, \rho_t) = (0.02, 0.1), (0.02, 0.4), (0.05, 0.1)$, and $(0.05, 0.4)$ for the four CUSUM-$p\rho$ chart in columns [4]-[7], respectively. The CUSUM-$p\rho$ charts with $(p_t, \rho_t) = (0.02, 0.1)$, and $(p_t, \rho_t) = (0.05, 0.1)$ are designed to detect increases in p and decreases in ρ, while the other two cases with $(p_t, \rho_t) = (0.02, 0.4)$ and $(0.05, 0.4)$ are designed to detect increases in both p and ρ. The CUSUM-$p\rho$ charts used here are all one-sided for ρ and are designed to detect either an increase or a decrease in ρ. We look at these one-sided charts to see the performance when the actual shift in ρ is on the other side compared with ρ_t, i.e. the actual shift is less than ρ_0 when ρ_t is greater than ρ_0.

We combine the two CUSUM- $p\rho$ charts in columns [4] and [5] to form the first CUSUM- $p\rho$ chart combination in column [8] and the two CUSUM- $p\rho$ charts in columns [6] and [7] to form the second CUSUM- $p\rho$ chart combination in column [9]. Columns [10]-[11] list

the SSANOS values of the three-CUSUM chart combinations. In column [10], the pre-determined shifts for p and ρ are $p_t = 0.02$, $\rho_t^1 = 0.4$, and $\rho_t^2 = 0.1$. The SSANOS of three-CUSUM chart combination with $p_t = 0.05$, $\rho_t^1 = 0.4$, and $\rho_t^2 = 0.1$ is listed in column [11]. It is noted that the pre-determined shift for p and ρ in the CUSUM- $p\rho$ chart combination in columns [8] and [9] are the same as for the three-CUSUM chart combination in columns [10] and [11], separately. This setting allows a fair comparison for the CUSUM- $p\rho$ chart combination and the three-CUSUM chart combination.

In Tables 4.2, color shadings are used to compare the performance of the 11 control charts, with dark grey representing large SSANOS values and light grey representing small SSANOS values, as was done for the comparisons in Chapter 3. In Table 4.2, the first 4 positive directions correspond to increases in both p and ρ. In these 4 directions, we look at the shifts combinations (p_1, ρ_1) where the largest ρ_1 is between 0.65 to 0.7. We found that the case of ρ_1 larger than 0.7 would be difficult to detect for some charts we consider here, because we consider the one-sided CUSUM-$p\rho$ chart and it is difficult to detect large increases in correlation when the chart is designed to detect decreases in correlation. For instance, with $s = 15$, the CUSUM-$p\rho$ chart in column [5] has SSANOS values 38889.22 when $\rho_1 = 0.65$. The SSANOS value is more than twice as large as the ICANOS=16890.0 and thus this shift cannot be detected. Similar situations occur when $s = 10$. Therefore, we will not consider very large values for ρ_1 and the corresponding largest values of p_1 are 0.2, 0.1, 0.06 and 0.04 for $s = 15, 10, 5$ and 2.5, respectively. In the two negative directions with $s = -2.5$ and -5, we look at the shift combination with p_1 increasing and ρ_1 decreasing. The extreme shift combinations are when the ρ_1 is equal or very close to 0.

Mousavi and Reynolds (2009) showed that the traditional Shewhart chart for monitoring p is not robust to correlation and will not detect shifts in p as well as the MBCUSUM chart. In Table 4.2, it is not surprising to see that the performance of the Shewhart chart in column [1] is not very good, especially for small positive values and negative values of s, as this chart does not take account of the correlation structure of the data. In the comparisons in this section, we will not explicitly discuss the performance of the Shewhart but will still shows results for the Shewhart chart here because it is the standard chart traditionally used to monitor p and serves as a reference point.

Table 4.2 SSANOS values of some CUSUM control charts when $p_0 = 0.01, \rho_0 = 0.2$ and $s = 2.5, 5, 10$ and 15

			Shewhart	MBCUSUM		CUSUM-$p\rho$				CUSUM-$p\rho$		Three-CUSUM Combination	
			$n = 100$	$p_t = 0.02$	$p_t = 0.05$	p_t	$p_t = 0.02$	$p_t = 0.05$	p_t	$p_t = 0.02$ &	$p_t = 0.05$ &	$p_t = 0.02$	$p_t = 0.05$
						ρ_t	$\rho_t = 0.1$	ρ_t	ρ_t	$p_t = 0.02$ &	$p_t = 0.05$ &	$\rho_t^1 = 0.4$	$\rho_t^1 = 0.4$
s	p_1	ρ_1	[1]	[2]	[3]	[4]	[5]	[6]	[7]	[8]	[9]	[10]	[11]
	0.01	0.2	16815.14	16814.80	16849.12	17377.22	16762.02	17235.94	16849.18	16692.42	16931.82	16763.70	16828.76
	0.015	0.21	5231.7	2347.45	3554.01	4423.63	2864.11	3770.77	3873.69	2771.55	3544.66	2862.25	4701.35
	0.02	0.22	2272.8	953.45	1356.78	1840.90	1178.27	1405.74	1530.51	1118.46	1337.17	1117.74	1691.33
	0.025	0.23	1258.9	574.95	715.45	1046.34	709.95	728.40	819.17	664.80	704.58	668.80	850.96
	0.03	0.25	771.35	414.17	456.85	707.97	507.66	461.51	523.56	472.71	452.94	478.40	529.94
2.5	0.04	0.27	412.01	270.76	256.76	412.03	334.81	258.46	292.50	302.38	252.55	309.93	287.34
	0.05	0.3	271.27	205.10	178.15	281.62	262.81	177.86	203.63	224.62	175.19	233.39	197.71
	0.06	0.32	204.10	167.87	138.49	211.57	225.78	135.56	160.09	179.54	134.99	189.30	152.06
	0.08	0.37	144.60	128.68	99.71	137.09	193.39	94.03	118.17	128.89	95.05	141.05	107.80
	0.1	0.42	119.77	108.94	81.67	99.21	191.90	73.21	100.71	100.84	74.93	114.49	86.29
	0.2	0.67	86.90	93.81	63.93	43.76	1084.47	41.76	147.01	47.56	44.29	58.50	51.44
	0.015	0.22	4824.4	2357.62	2450.71	3912.68	2443.94	1878.86	4162.42	2826.87	3278.83	2951.06	2993.00
	0.02	0.25	2084.2	1019.11	1043.33	1596.18	1145.05	865.61	1750.59	1166.07	1263.50	1185.72	1267.30
	0.025	0.27	1140.8	635.85	628.24	900.31	739.46	506.36	987.10	705.35	712.16	721.98	714.30
	0.03	0.3	736.26	466.69	444.93	604.74	566.12	347.77	661.91	504.86	481.94	524.39	477.37
5	0.04	0.35	388.97	317.38	283.57	348.68	419.69	207.05	403.26	323.69	286.90	348.55	284.47
	0.05	0.4	268.42	252.15	215.34	240.14	376.49	150.17	307.27	238.70	204.83	267.92	207.68
	0.06	0.45	209.12	217.84	179.96	179.89	380.83	118.57	267.80	188.54	161.32	220.44	168.80
	0.08	0.55	155.86	189.95	149.68	120.15	534.74	87.26	267.57	130.97	116.97	163.23	131.96
	0.1	0.65	134.74	191.69	145.85	92.31	1244.05	73.82	385.50	101.31	96.87	127.02	115.49
	0.015	0.25	4292.9	2802.47	4118.83	3201.37	4077.50	3409.53	4832.81	2832.15	3617.50	3175.34	4683.11
	0.017	0.27	2902.4	1896.57	2818.96	2065.14	2958.78	2180.05	3469.44	1875.62	2357.15	2105.15	3121.71
	0.02	0.3	1810.7	1246.19	1787.89	1248.79	2143.78	1308.63	2364.07	1191.76	1423.41	1346.92	1891.21
10	0.025	0.35	975.61	808.20	1058.40	710.50	1619.90	716.05	1532.22	719.94	783.50	839.29	1032.84
	0.03	0.4	644.45	626.73	753.90	481.58	1508.68	477.70	1202.92	509.32	521.21	613.40	682.47
	0.04	0.5	369.42	487.39	514.23	284.18	2041.05	288.88	1057.69	314.51	316.08	401.41	394.83
	0.05	0.6	270.93	467.84	454.46	202.15	5101.24	215.21	1434.10	226.03	235.64	287.47	274.42
	0.06	0.7	224.24	527.00	472.76	165.24	28270.4	182.87	3384.65	180.71	196.74	215.66	210.06
	0.015	0.27	3833.3	3206.39	4541.40	2693.66	5325.95	3187.74	5638.62	2751.93	3603.29	3253.90	4375.40
	0.017	0.30	2600.2	2251.20	3224.54	1709.80	4262.93	2062.91	4357.99	1798.76	2340.14	2194.45	2916.10
15	0.02	0.35	1569.5	1552.41	2183.00	1043.32	3629.29	1243.10	3323.11	1128.23	1413.40	1416.50	1753.08
	0.025	0.42	862.75	1090.57	1424.64	594.67	3815.52	699.24	2651.59	674.23	789.80	869.16	951.48
	0.03	0.5	568.85	936.30	1118.35	410.31	5687.49	477.69	2741.44	465.55	538.19	606.73	615.45
	0.04	0.65	354.94	987.00	1004.02	260.00	38889.2	305.63	6183.53	287.58	334.73	346.41	339.26
	0.015	0.18	5681.4	2091.28	3237.08	5747.58	2332.25	3984.69	3351.13	2567.60	3429.66	2607.62	4484.79
	0.02	0.17	2751.1	818.31	1144.35	2698.78	870.15	1453.01	1195.14	964.48	1236.62	963.60	1450.01
	0.025	0.16	1474.9	479.76	572.86	1603.16	491.93	724.39	594.55	552.14	613.90	561.94	686.53
-2.5	0.03	0.15	919.81	337.80	351.87	1105.97	337.29	447.32	358.90	382.03	375.72	392.65	408.98
	0.05	0.1	271.97	148.62	122.40	505.12	142.01	158.06	120.18	162.87	128.19	172.72	137.14
	0.07	0.05	154.19	93.25	71.20	341.55	86.42	93.78	68.50	100.33	73.51	108.16	79.03
	0.08	0.02	131.64	77.79	58.25	297.70	71.61	77.46	56.09	83.41	60.13	90.27	64.90
	0.015	0.17	6280.9	1979.23	3086.49	6699.57	2113.06	4120.07	3135.94	2424.18	3360.05	2480.61	4484.79
	0.02	0.15	2985.4	761.27	1056.48	3459.91	768.20	1482.54	1061.66	880.04	1158.37	898.17	1450.01
-5	0.025	0.12	1650.0	441.10	520.63	2177.12	427.21	722.37	516.04	493.97	563.11	520.02	686.53
	0.03	0.1	998.12	307.35	314.67	1587.16	288.40	436.15	309.37	334.74	335.33	358.18	408.98
	0.05	0	273.47	131.11	105.95	891.13	116.12	149.78	99.78	134.04	108.67	151.88	137.14
		h	5.0000	2.9314	3.7069	2.8227	3.2481	3.7571	3.7547	3.4154	4.2441	3.4580	4.2701
										3.8856	4.2556	3.4200	3.4200
												3.4200	3.4200

In column [2] in Table 4.2, the MBCUSUM chart works well for the shift ranges $0.015 \leq p_1 \leq 0.04$ and $0.2125 \leq \rho_1 \leq 0.275$ for $s = 2.5$, $0.015 \leq p_1 \leq 0.025$ and $0.225 \leq \rho_1 \leq 0.275$ for $s = 5$, $0.015 \leq p_1 \leq 0.02$ and $0.25 \leq \rho_1 \leq 0.3$ for $s = 10$, and $0.015 \leq p_1 \leq$

0.017 and $0.275 \leq \rho_1 \leq 0.305$ for $s = 15$, respectively. It is noted that the MBCUSUM chart designed to detect shifts equal to p_t still works well for the simultaneous shifts in p and ρ when the value of p_1 is close to p_t and the value of ρ_1 is not too far away from ρ_0. In column [3], the MBCUSUM chart works well for the shift ranges $0.04 \leq p_1 \leq 0.08$ and $0.275 \leq \rho_1 \leq 0.375$ for $s = 2.5$, and $0.017 \leq p_1 \leq 0.04$ and $0.235 \leq \rho_1 \leq 0.35$ for s =5. The values of p_1 here are close to $p_t = 0.05$ and ρ_1 is relatively small. But when $s = 10$, and 15, the MBCUSUM chart in column [3] has large SSANOS values for all of the shifts. It is noted that, in these two cases, when p_1 is close to $p_t = 0.05$, the corresponding shift in correlation is far away from ρ_0. For those shifts with p_1 far away from p_t, the MBCUSUM chart does not have good performance either. For the negative directions, both of the charts work well as the shifts in p are all close to p_0, where the largest values of p_1 are 0.08 and 0.05 for $s = -2.5$ and -5, respectively. In both of the two cases, the corresponding values of ρ_1 are less than ρ_0 but quite close to ρ_0.

In column [4], the CUSUM-$p\rho$ chart is designed to detect a shift to $p_1 = p_t = 0.02$ and $\rho_1 = \rho_t = 0.4$. This shift is in the direction with $s = 20$. For the positive directions, with relatively small value of s, the shift combinations of p and ρ can be far away from (p_t, ρ_t); even if the shift in p or ρ is close to the pre-determined shift. In column [4], we find that when $s = -2.5, -5, 2.5$ and 5, the CUSUM-$p\rho$ chart has large SSANOS values when the shifts are small. For example, when $0.015 \leq p_1 \leq 0.05$ and $0.2125 \leq \rho_1 \leq 0.3$ with $s = 2.5$, the chart performance is worse than most of the other charts. Similarly when $s = 5$, the chart does not work well for $0.015 \leq p_1 \leq 0.2$ and $0.225 \leq \rho_1 \leq 0.25$. In these two directions, the chart only works well at relatively large shifts where both p_1 and ρ_1 are close to $p_t = 0.02$ and $\rho_t = 0.4$, respectively. In the other two directions, $s = 10$ and 15, we find better performance than for small values of s for this CUSUM-$p\rho$ chart, as the shift combinations are close to the pre-determined shifts combinations. In column [6], the CUSUM-$p\rho$ chart is designed to detect the shift $p_1 = p_t = 0.05$ and $\rho_1 = \rho_t = 0.4$, which is in the direction with $s = 5$. We find similar conclusions to those from the CUSUM-$p\rho$ chart in column [4]. The chart works well when the shifts are close to the pre-determined shifts combination. In particular, the chart in column [6] is uniformly better than the chart in column [4] when $s = 5$.

In the negative directions, both of the charts in columns [4] and [6] show worse performance than in the positive directions as the two charts are designed to detect increases in

correlation. Especially for the CUSUM-$p\rho$ chart in column [4], the chart performance is uniformly worse than the other 10 charts in the negative shift directions. The CUSUM-$p\rho$ chart in column [6] has slightly better performance than the CUSUM-$p\rho$ chart in column [4] and the Shewhart chart in column [1]. Comparing the CUSUM-$p\rho$ charts in columns [4] and [6], even when ρ_t is mis-specified in both of the two charts, most of the actual shifts in proportion p_1 in the negative directions are closer to p_t =0.05 in column [6] than to p_t =0.02 in column [4]. Therefore, when ρ_t is mis-specified, if the actual shift in proportion is close to p_t, the SSANOS values are not very large.

For the CUSUM chart in column [5], for the positive directions, we find that the chart only works well when the shift in p is close to p_t =0.02 when $s = 2.5$ and 5. In these two directions, the corresponding shifts in ρ are close to ρ_0. For the other shifts with p_1 far away from p_t =0.02 or p_1 close to p_t =0.02 but ρ_1 is far away from ρ_0, the CUSUM$-p\rho$ chart cannot quickly detect the shifts. For some extreme cases, the chart cannot even detect the shift, because the SSANOS values much larger than the ICANOS value. For instance, when p_1 =0.06 and $\rho_1 = 0.7$ with $s = 10$, the SSANOS value is 28270.49. In the negative directions, the chart works very well as most of the shift combinations in the directions $s = -2.5$ and -5 are close to (p_t, ρ_t)=(0.02, 0.1). Similarly in column [7], in most of the cases, with the pre-determined shifts mis-specified in the positive direction, the CUSUM$-p\rho$ chart does not work well. However, in the negative direction, the chart is better than most of the other control charts.

It is noted that the performance both of the MBCUSUM and CUSUM$-p\rho$ charts depends on the pre-determined shifts in the proportion and correlation. The MBCUSUM chart works well when the shift in proportion is close to p_t and the corresponding shift in correlation is relatively small. The CUSUM$-p\rho$ chart with two tuning parameters can detect a wider range of shifts than the MBCUSUM chart if the tuning parameters are specified in the correct direction. The chart works very well when the pre-determined shifts is in the same direction as the actual shifts. But when the tuning parameters are mis-specified, the chart has very bad performance.

To avoid the mis-specification problem with the tuning parameters, columns [8]-[11] in Table 4.2 give SSANOS values for combinations of CUSUM-type charts. Columns [8] and [9] list the SSANOS values for the combination of two CUSUM$-p\rho$ charts. In column [8], one

CUSUM$-p\rho$ chart has p_t =0.02 and $\rho_t = 0.4$, and the other CUSUM$-p\rho$ chart has p_t =0.02 and $\rho_t = 0.1$. The CUSUM-$p\rho$ chart combination in column [8] is thus combined from the two CUSUM$-p\rho$ charts in columns [4] and [5] but with control limits adjusted to give the required in-control ANOS for the combination. The CUSUM-$p\rho$ chart combination in column [9] is combined from the two charts in columns [6] and [7]. In both of the two CUSUM-$p\rho$ combinations charts, the overall performance is better than the other control charts when considering both positive and negative directions. The two CUSUM-$p\rho$ chart combinations have the same pre-determined shift for ρ. Therefore the difference comes from the ability to detect the shift in p. The chart in column [8] has smaller SSANOS values than that of the chart in column [9] when p_1 is relatively small. When p_1 is relatively large, the chart in column [9] with larger p_t works well.

The last two columns [10] and [11] in Table 4.2 show the SSANOS values of three-CUSUM-chart combinations. In each combination, one MBCUSUM chart and two CUSUM-ρ charts are used. In column [10], $p_t = 0.02, \rho_{t1} = 0.4$, and $\rho_{t2} = 0.1$. It is noted that these pre-determined shifts for p and ρ are equal to the values in the CUSUM-$p\rho$ chart combination in column [8]. In column [11], $p_t = 0.05, \rho_{t1} = 0.4$, and $\rho_{t2} = 0.1$, which are equal to the pre-determined shifts in the CUSUM-$p\rho$ chart combination in column [9]. We found a similar pattern in columns [10] and [11] as in columns [8] and [9], respectively. The three-CUSUM-combination with larger p_t in column [11] works well at relatively large shifts and the combination with small p_t in column [10] works well at small shifts. It is also noted that, in most of the cases, the three-CUSUM chart combinations detect the shifts in p and ρ slower than the CUSUM-$p\rho$ chart combination when the pre-determined shifts are the same for the two types of chart combinations.

4.4.1.2 Comparisons of Chart Performance for Shifts in Both the Proportion and Correlation with $p_0 = 0.01$ and $\rho_0 = 0.05$

The second case being considered has $p_0 = 0.01$ and $\rho_0 = 0.05$. Table 4.3 shows the SSANOS values of the Shewhart chart, MBCUSUM chart, CUSUM-$p\rho$ chart, CUSUM-$p\rho$ chart combination, and three-CUSUM chart combination when $s = 2.5, 5, 10, 15, -2.5$ and -5, respectively as in Table 4.2 for $p_0 = 0.01$ and $\rho_0 = 0.2$. In Table 4.3, the Shewhart chart in column [1] has $n = 100$ and ICANOS $= 16956.6$ when the control limit is equal to 4. We

consider two MBCUSUM charts in column [2] and [3], four CUSUM-$p\rho$ charts in columns [4]-[7], two CUSUM-$p\rho$ chart combinations in columns [8] and [9], and two three-CUSUM chart

Table 4.3 SSANOS values some CUSUM control charts when $p_0 = 0.01, \rho_0 = 0.05$, and $s = 2.5, 5, 10, 15, -2.5$ and -5

			Shewhart	MBCUSUM		CUSUM-$p\rho$				CUSUM-$p\rho$		Three-CUSUM Combination	
			$n = 100$	$p_t = 0.02$	$p_t = 0.05$	$p_t = 0.02$ ρ_t	p_t ρ_t	$p_t = 0.05$ $\rho_t = 0.1$	$p_t = 0.05$ $\rho_t = 0.03$	$p_t = 0.02$ & $p_t = 0.02$	$p_t = 0.05$ & $p_t = 0.05$	$p_t = 0.02$ $\rho_t^1 = 0.1$	$p_t = 0.05$ $\rho_t^1 = 0.1$
s	p_1	ρ_1	[1]	[2]	[3]	[4]	[5]	[6]	[7]	[8]	[9]	[10]	[11]
	0.01	0.05	16935.59	16931.60	16912.25	16953.89	16993.17	16962.51	17049.21	17100.65	16739.36	16932.92	16690.86
	0.015	0.0625	3982.22	2089.61	3270.86	2093.56	2197.40	3184.73	3354.78	2140.93	3195.63	2538.15	4096.93
	0.02	0.075	1562.02	824.43	1183.09	817.56	864.21	1147.96	1225.57	836.05	1153.08	967.86	1444.46
	0.025	0.0875	817.23	492.60	607.03	491.85	519.53	585.04	629.48	493.21	590.18	574.34	708.51
	0.03	0.1	513.62	351.59	380.19	345.67	372.70	367.90	393.56	351.62	370.70	413.50	437.41
2.5	0.04	0.125	278.84	227.08	209.30	214.95	243.09	200.77	215.82	226.00	203.01	260.37	234.24
	0.05	0.15	192.93	170.11	142.48	157.58	186.17	136.65	148.63	165.59	138.66	192.71	158.59
	0.06	0.175	153.36	137.62	109.35	124.85	153.84	104.24	113.80	131.70	105.80	153.70	120.89
	0.08	0.225	116.99	102.48	76.19	87.38	120.32	72.01	80.44	93.97	73.36	112.37	83.52
	0.1	0.275	100.54	83.89	60.31	67.65	103.75	55.88	63.94	73.81	57.05	86.38	65.03
	0.2	0.525	76.48	55.97	36.51	34.51	117.53	30.94	41.56	37.48	31.91	39.89	35.07
	0.015	0.075	3739.13	2171.10	3344.22	2050.29	2358.16	3146.97	3483.10	2089.22	3192.12	2516.69	3774.36
	0.02	0.1	1453.99	871.79	1234.51	808.47	962.48	1138.59	1310.99	830.06	1166.10	988.34	1385.52
	0.025	0.125	777.01	528.15	643.66	482.66	587.52	590.02	686.87	501.38	604.67	596.98	713.24
5	0.03	0.15	488.82	381.19	413.50	342.14	430.75	376.26	440.97	358.53	388.58	426.43	450.27
	0.04	0.2	276.16	252.64	234.02	216.40	295.17	211.10	250.34	228.41	217.25	273.90	250.07
	0.05	0.25	196.03	194.36	163.45	158.94	237.86	148.10	177.13	168.96	151.58	203.70	173.47
	0.06	0.3	158.83	162.21	128.46	126.18	210.57	114.55	140.78	135.21	117.49	161.68	134.12
	0.08	0.4	124.02	129.16	95.72	91.12	195.03	82.56	106.79	97.75	85.04	114.08	95.71
	0.1	0.5	108.65	115.21	81.21	73.14	221.31	67.73	94.09	78.55	69.81	86.55	76.61
	0.015	0.1	3348.43	2355.50	3459.03	1920.43	2736.22	3021.39	3730.08	2073.19	3159.15	2369.10	3087.98
	0.02	0.15	1289.05	983.88	1344.76	784.91	1195.73	1122.86	1496.73	839.14	1180.39	987.16	1185.51
	0.025	0.2	699.77	613.07	735.59	480.68	779.36	602.73	834.09	514.93	634.28	598.53	648.19
10	0.03	0.25	458.98	457.43	488.60	341.24	621.69	395.54	560.20	367.63	413.46	436.80	429.84
	0.04	0.35	277.40	322.45	294.27	219.59	511.99	232.98	351.07	237.47	243.53	272.65	253.00
	0.05	0.45	205.48	272.53	222.76	164.75	544.81	172.14	276.05	175.94	178.59	194.36	180.41
	0.06	0.55	174.97	250.24	191.07	136.44	809.75	142.17	247.76	147.47	146.96	148.07	142.28
	0.015	0.1	3043.55	2560.31	3576.42	1832.90	3312.05	2913.12	3998.06	1993.07	3095.76	2106.45	2491.11
	0.02	0.15	1147.79	1115.93	1442.05	761.34	1593.06	1095.99	1709.40	818.70	1172.99	920.63	985.29
	0.025	0.2	633.66	732.35	824.92	458.93	1179.16	604.45	1018.48	502.79	641.81	559.72	560.04
15	0.03	0.25	426.12	567.31	569.85	339.35	1089.85	407.02	739.12	367.97	430.44	397.83	378.70
	0.04	0.35	273.18	447.82	375.35	225.58	1607.18	255.29	524.41	241.02	266.32	236.27	230.29
	0.05	0.45	241.16	432.03	331.73	199.72	3173.04	221.26	491.08	212.80	231.48	198.26	194.87
	0.06	0.55	221.59	438.29	305.25	186.28	11655.9	201.45	484.39	191.20	207.88	173.88	172.80
	0.013	0.0425	**7132.31**	3705.30	5629.31	4130.51	3700.10	5834.48	5571.75	3987.46	5639.61	4960.46	7968.51
	0.015	0.0375	**4549.16**	1931.02	3154.56	2203.28	1915.58	3295.48	3116.50	2071.56	3223.26	2457.45	4511.12
-2.5	0.017	0.0325	**3034.86**	1208.14	1939.49	1385.45	1198.38	2057.56	1929.61	1303.08	1979.28	1505.49	2680.19
	0.02	0.025	**1837.83**	736.80	1089.14	847.16	723.78	1148.59	1078.44	799.92	1103.17	886.42	1408.42
	0.025	0.0125	**930.04**	434.45	535.94	494.90	422.20	565.01	525.29	467.99	545.82	513.20	646.10
	0.013	0.035	**7576.21**	3596.62	5567.74	4254.95	3521.77	5902.26	5492.72	3976.56	5668.05	4979.49	8263.53
-5	0.015	0.025	**4828.69**	1867.45	3080.24	2279.92	1799.20	3358.89	3019.06	2027.19	3132.25	2397.74	4565.21
	0.017	0.015	**3257.27**	1153.67	1889.90	1420.70	1112.03	2082.13	1842.87	1246.08	1948.85	1426.04	2647.61
		h	**4.0000**	**3.0932**	**3.8792**	**3.0480**	**3.1293**	**3.8701**	**3.8714**	**3.3604**	**4.0678**	**3.6965**	**4.4943**
										3.4534	**4.0579**	**1.8816**	**1.8687**
												1.2132	**1.1421**

combinations in columns [10] and [11]. In these control charts, we use the same p_t values as in Table 4.2. In Table 4.3, the in-control correlation $\rho_0 = 0.05$ and we use $\rho_t = 0.05$ and $\rho_t = 0.3$, which are smaller than those used in Table 4.2. The control limits of the charts in column [2]-[11]

are selected so that the ICANOS values of the charts are all close to 16956.6. Here, we will look at relatively small shifts, which would be expected to occur with larger probability than the relatively large shifts.

Comparing the performance of the control charts in Table 4.3, we find conclusions similar to those obtained from Table 4.2. The chart performance in Table 4.3 confirms that it is important to select p_t to be close to the middle of the reasonable range of the shifts in proportion. Even though the two parameters shift simultaneously, the tuning parameter p_t is the main determinant of the performance of the chart.

4.4.1.3 Conclusions when the Proportion and Correlation Shift Simultaneously

From the simulation results presented above, we found that the MBCUSUM chart still works well if the shift in correlation is small and the shift is proportion is close to the pre-determined shift size. However, this chart does not work well for other cases. The performance of the CUSUM-$p\rho$ chart highly depends on the specification of the pre-determined shifts. When the pre-determined shifts are correctly specified, the chart will have very good performance. Comparing the pre-specified shifts in proportion and correlation, it is more important to correctly specify the pre-determined shift in proportion than correlation. The chart can still provide good performance if the pre-determined shift in proportion is correctly specified and the shift in correlation is small but the pre-determined shift in correlation is mis-specified.

The CUSUM-$p\rho$ chart combination has the best overall performance among the charts discussed in this section. We found that in the case of $p_0 = 0.01$ and $\rho_0 = 0.2$, the combination of one CUSUM-$p\rho$ chart with $p_t = 0.02$ and $\rho_t = 0.4$ with one CUSUM-$p\rho$ chart with $p_t = 0.02$ and $\rho_t = 0.1$ works well for both positive and negative directions when the shifts in proportion and correlation as in the ranges (0.01, 0.1] and [0, 0.7], respectively. When $p_0 = 0.01$ and $\rho_0 = 0.05$, and the shifts are in the ranges (0.01, 0.1] and [0.015, 0.55] in proportion and correlation, respectively, the CUSUM-$p\rho$ chart combination with $p_t = 0.02$ and $\rho_t = 0.3$ for one chart and $p_t = 0.02$ and $\rho_t = 0.03$ for the other chart can provide very good overall performance.

The overall performance of the three-CUSUM-chart combination is worse than that of the CUSUM-$p\rho$ chart combination. Also, the three-CUSUM-chart combination has three control limits that need to be specified, and the design of the chart will be more complicated than the design of the CUSUM-$p\rho$ chart combination.

4.4.2 Comparisons of Chart Performance when the Shift Only Occurs in the Proportion or Correlation

4.4.2.1 Comparisons with $p_0 = 0.01$ and $\rho_0 = 0.05$ and 0.2

In the previous subsection, the performance of the charts was compared when the proportion and correlation change simultaneously. Now in this subsection, we will look at the chart performance when the shift only occurs in the proportion or the correlation. When the shift is known to occur only in the proportion, the MBCUSUM and the MBGLR chart can be used to monitor the process. The MBCUSM chart is designed to detect a known shift and the MBGLR chart can effectively detect a range of shifts less than its upper bound. In the previous subsection, the CUSUM-$p\rho$ chart combination has been shown to have overall better performance than the other charts when the two parameters shift simultaneously.

When the shift only occurs in the correlation with $s = \pm\infty$, then this means that the proportion remains at the target value and correlation can either decrease or increase. In practice, it is more common to have a shift occur in the proportion or occur in both the proportion and correlation. When shift only occurs in the correlation but the proportion remains at the target value, the quality of the process in terms of the proportion defective is not affected. Therefore, practitioners may not be very interested in detecting the shift in the correlation alone. However, even though the process quality is not affected in this case, it may also important to detect the shift and therefore identify the cause of the shift. This case may not often happen in practice, and in addition it is not very easy to detect a shift in the correlation when it is small. Here, we will still look at shifts that occur in this direction to complete the comparisons of the charts.

In this subsection, we will look at the performance of the 11 control charts considered in Tables 4.4 and 4.5 in the two cases with in-control parameters $p_0 = 0.01$ and $\rho_0 = 0.2$ and 0.05, separately. In both of the two cases, in the direction $s = 0$, we will look at a shift in proportion with $p_1 \leq 0.5$, which is 50 times the in-control proportion. In the direction $s = \pm\infty$, in the first

case with $p_0 = 0.01$ and $\rho_0 = 0.2$, p_0 remains at the target value and ρ_1 varies from 0.03 to 0.17 when there is a decrease, and varies from 0.25 to 0.5 when there is an increase. In the second case with $p_0 = 0.01$ and $\rho_0 = 0.05$, the smallest and largest value for ρ_1 are 0.01 and 0.35, respectively. The ranges of the shifts in correlation are slightly different considering that the in-control correlation values are different in the two cases.

Table 4.4 SSANOS values some CUSUM control charts when $p_0 = 0.01, \rho_0 = 0.2$, and $s = \pm\infty$ and 0

			Shewhart	MBCUSUM		CUSUM-$p\rho$				CUSUM-$p\rho$ Combination		Three-CUSUM Combination	
						p_t	p_t	p_t	p_t	$p_t = 0.02$ &	$p_t = 0.05$ &	$p_t = 0.02$	$p_t = 0.05$
			$n = 100$	$p_t = 0.02$	$p_t = 0.05$	$= 0.02$	$= 0.02$	$= 0.05$	$= 0.05$	$\rho_t = 0.4$	$\rho_t = 0.4$		
						ρ_t	ρ_t	ρ_t	ρ_t	$p_t = 0.02$ &	$p_t = 0.05$ &	$\rho_t^1 = 0.4$	$\rho_t^1 = 0.4$
						$= 0.4$	$= 0.1$	$= 0.4$	$= 0.1$	$\rho_t = 0.1$	$\rho_t = 0.1$	$\rho_t^2 = 0.1$	$\rho_t^2 = 0.1$
s	p_1	ρ_1	[1]	[2]	[3]	[4]	[5]	[6]	[7]	[8]	[9]	[10]	[11]
0	0.01	0.2	**16815.14**	**16814.80**	**16849.12**	**17377.22**	**16762.02**	**17235.94**	**16849.18**	**16692.42**	**16931.82**	**16763.70**	**16828.76**
	0.02	0.2	2461.78	877.23	1240.83	2187.97	1005.72	1429.72	1347.28	1050.22	1294.25	1034.58	1566.20
	0.03	0.2	847.10	370.60	399.85	857.24	403.16	454.14	428.29	429.90	415.73	431.75	464.74
	0.04	0.2	425.00	235.05	215.86	510.39	251.92	247.67	227.11	269.32	224.52	272.49	243.62
	0.05	0.2	273.11	172.97	145.24	357.59	183.47	167.04	151.49	195.83	151.03	199.56	162.77
	0.08	0.2	137.43	97.14	73.71	183.97	104.85	84.42	75.54	110.49	76.46	112.29	81.95
	0.1	0.2	111.16	75.74	55.92	135.94	82.58	63.46	57.31	86.70	57.63	87.78	61.96
	0.2	0.2	77.08	39.16	27.21	54.52	46.19	29.00	28.40	43.46	26.96	45.41	29.03
	0.3	0.2	67.60	28.97	19.45	31.37	38.66	18.98	20.90	29.31	18.55	31.81	20.06
	0.4	0.2	63.35	24.22	15.81	21.00	40.45	14.25	18.17	21.75	14.50	24.47	16.12
	0.5	0.2	60.04	21.85	13.89	15.15	51.71	11.50	17.66	16.83	12.08	19.66	13.87
	0.6	0.2	57.77	21.08	13.00	11.54	86.29	9.69	19.46	13.29	10.38	16.04	12.24
$\pm\infty$	0.01	0.03	108464.62	6242.91	9017.49	10921208	3650.90	54947.30	6685.32	5177.94	9821.88	9269.30	14856.67
	0.01	0.05	78653.11	6912.75	9647.61	1991819	4214.78	47265.21	7369.97	6134.00	10887.61	10467.67	16160.43
	0.01	0.1	41600.49	9106.48	11576.94	170695.13	6294.38	33063.56	9494.13	9733.22	13684.10	14232.68	19515.63
	0.01	0.15	25340.76	12171.30	13967.46	42816.71	9962.01	23702.18	12559.05	14871.59	16037.43	18274.62	21322.19
	0.01	0.17	21374.05	13882.60	15015.53	28609.16	12203.47	20732.87	13961.34	16408.90	16700.82	18774.99	20462.59
	0.01	0.2	**16815.14**	**16814.80**	**16849.12**	**17377.22**	**16762.02**	**17235.94**	**16849.18**	**16692.42**	**16931.82**	**16763.70**	**16828.76**
	0.01	0.25	11717.69	24121.09	20543.79	9307.72	30645.60	12829.75	23274.70	12593.36	15599.48	9918.71	9520.65
	0.01	0.3	8647.83	35418.04	25245.24	5900.14	60206.34	9734.51	33069.37	8291.41	13035.62	5453.44	5288.93
	0.01	0.35	6405.44	53034.83	30867.89	4144.60	126934.8	7605.18	48963.45	5676.71	10339.57	3383.78	3332.11
	0.01	0.4	5124.16	82451.64	37967.54	3120.97	286093.3	6016.04	75545.08	4140.90	8029.92	2376.15	2342.48
	0.01	0.45	3966.93	132618.5	46286.88	2494.61	702583.2	4823.62	121364.4	3207.37	6200.12	1828.55	1813.59
	0.01	0.5	3285.67	220400.6	55799.78	2107.45	1866019.	3948.74	206946.8	2575.89	4887.97	1499.23	1491.89
		h	**5.0000**	**2.9314**	**3.7069**	**2.8227**	**3.2481**	**3.7571**	**3.7547**	**3.4154**	**4.2441**	**3.4580**	**4.2701**
										3.8856	**4.2556**	**3.4200**	**3.4200**
												3.4200	**3.4200**

The upper half of Table 4.4 lists the SSANOS values when $p_0 = 0.01$ and $\rho_0 = 0.2$ for the 11 control charts when $s = 0$, i.e. shift only occurs in the proportion. The MBCUSUM chart has been shown to have good performance when p_1 equals or is close to p_t, and from Table 4.4, we find a similar conclusion. When $p_1 = 0.02$ or 0.03, the MBCUSUM chart with $p_t = 0.02$ in

column [2] is better than the other 10 charts. While when $p_1 = 0.04, 0.05, 0.08,$ or 0.1, the MBCUSUM chart with $p_t = 0.05$ in column [3] works better.

When $s = 0$, it is noticed that the CUSUM-$p\rho$ chart with a relatively large p_t still works well. Comparing the CUSUM-$p\rho$ chart with the MBCUSUM chart with the same the same value of p_t. we found that the MBCUSUM chart is uniformly better than the CUSUM-$p\rho$ chart if $\rho_t < \rho_0$. For instance, in Table 4.4, the performance of the MBCUSUM charts in columns [2] and [3] are uniformly better than that of the CUSUM-$p\rho$ charts in columns [5] and [7]. When $\rho_t > \rho_0$, the MBCUSUM chart is better than the CUSUM-$p\rho$ for most of the shifts when p_t for the two charts is the same. With relatively large values of p_t, the performance of the CUSUM-$p\rho$ chart is very similar to MBCUSUM chart, but with small values of p_t, using a MBCUSUM chart can detect the shift in the proportion much faster than the CUSUM-$p\rho$ chart.

The performance of the two types of chart combinations in columns [8]-[11] shows a pattern similar to the MBCUSUM chart, i.e. the performance is good when p_1 equals or is close to p_t. The CUSUM-$p\rho$ chart combination is uniformly better than that of the three-CUSUM chart combination when the pre-determined shifts are the same. When they have the same values of p_t, the CUSUM-$p\rho$ chart combination has slightly worse performance than the MBCUSUM chart when p_1 is small or moderate. However, the SSANOS value of the CUSUM-$p\rho$ chart combination is smaller than that of the MBCUSUM chart when p_1 is large. For example, comparing the MBCUSUM chart in column [2] with the CUSUM-$p\rho$ chart combination in column [8], the later one is better when $p_1 = 0.4$ or 0.5. The MBCUSUM chart in column [3] has smaller SSANOS values than the CUSUM-$p\rho$ chart combination in column [9] when $p_1 = 0.2, 0.3, 0.4,$ or 0.5.

The discussion of the chart performance in the upper half of Table 4.4 shows that the MBCUSUM chart is a good choice when it is known that the shift only occur in the proportion. With the same values of p_t, the CUSUM-$p\rho$ chart combination has better performance than the MBCUSUM chart when the shift in proportion is large. Similar conclusions can be reached from the results in Table 4.5 where $\rho_0 = 0.05$ and we will omit the discussion of this table here.

When $s = \pm\infty$, the shift only occurs to the correlation and the proportion remains at p_0.From the lower half of Table 4.4, it is noticed that a small shift (both increase and decrease) in

correlation is very difficult to detect for all the charts. For instance, when $p_1 = 0.01$ and $\rho_1 = 0.17$, there is 15% decrease in correlation and the SSANOS values for all the charts are greater than 12000. In some cases, the SSANOS values can be more than the ICANOS. For instance, the SSANOS values are 28609.16 for the CUSUM-$p\rho$ chart in column [4]. When $p_1 = 0.01$ and $\rho_1 = 0.25$, there is 25% increase in correlation and the SSANSO values for all the charts are greater than 9520.65.

Table 4.5 SSANOS values some CUSUM control charts when $p_0 = 0.01, \rho_0 = 0.05$ and $s = \pm\infty$ and 0

			Shewhart	MBCUSUM		CUSUM-$p\rho$				CUSUM-$p\rho$ Combination		Three-CUSUM Combination	
						$p_t = 0.02$ & $\rho_t = 0.1$	$p_t = 0.02$ & $\rho_t = 0.03$	$p_t = 0.05$ & $\rho_t = 0.1$	$p_t = 0.05$ & $\rho_t = 0.03$	$p_t = 0.02$ & $\rho_t = 0.03$	$p_t = 0.05$ & $\rho_t = 0.03$	$p_t = 0.02$ & $\rho_t^1 = 0.1$ & $\rho_t^2 = 0.03$	$p_t = 0.05$ & $\rho_t^1 = 0.1$ & $\rho_t^2 = 0.3$
			$n = 100$	$p_t = 0.02$ & $\rho_t = 0.1$	$p_t = 0.05$ & $\rho_t = 0.1$								
s	p_1	ρ_1	[1]	[2]	[3]	[4]	[5]	[6]	[7]	[8]	[9]	[10]	[11]
0	0.01	0.05	16956.80	16931.60	16912.25	16953.89	16993.17	16962.51	17049.21	17100.65	16739.36	16932.92	16690.86
	0.02	0.05	1672.23	778.23	1132.31	824.66	782.98	1145.03	1145.52	816.29	1127.53	930.25	1449.47
	0.03	0.05	525.95	325.45	353.57	345.36	326.42	356.03	353.47	342.96	348.52	386.94	411.67
	0.04	0.05	268.57	206.17	188.27	215.36	208.97	189.58	188.09	215.59	188.55	242.00	213.37
	0.05	0.05	179.76	151.09	126.25	156.45	154.23	127.72	126.66	157.10	125.44	176.37	142.00
	0.06	0.05	140.85	119.40	94.52	122.26	121.32	95.52	94.99	123.76	96.02	139.25	106.09
	0.08	0.05	111.34	85.16	63.14	85.84	87.35	64.15	63.65	87.30	63.14	99.08	70.97
	0.1	0.05	102.96	66.20	47.84	66.41	68.73	48.12	48.06	68.05	47.68	77.42	53.46
	0.2	0.05	100.00	32.95	22.27	30.69	35.95	22.07	22.92	32.46	21.89	37.44	24.85
	0.3	0.05	100.00	23.25	15.24	19.79	27.46	14.66	16.02	21.04	14.68	25.19	16.76
	0.4	0.05	100.00	18.86	11.92	14.53	**24.75**	**11.16**	**12.91**	15.71	**11.29**	18.76	**12.86**
	0.5	0.05	100.00	16.62	10.10	11.40	25.43	9.10	11.23	12.26	9.16	14.50	10.52
$\pm\infty$	0.01	0.01	25811.76	14355.28	16315.59	25663.18	12209.17	20329.01	15446.39	16003.30	17378.88	26052.11	30445.35
	0.01	0.02	22955.49	14939.41	16548.43	22901.65	13215.29	19515.09	15817.72	16696.21	17435.56	26055.59	28837.35
	0.01	0.03	20682.16	15555.21	16688.69	20555.60	14319.31	18591.23	16132.69	17228.42	17286.28	24185.02	25692.80
	0.01	0.04	18602.87	16291.82	16811.33	18690.75	15594.39	17748.58	16749.11	17217.24	17029.00	20835.17	21141.73
	0.01	0.05	**16956.80**	**16931.60**	**16912.25**	**16953.89**	**16993.17**	**16962.51**	**17049.2**	**17100.65**	**16739.36**	**16932.92**	**16690.86**
	0.01	0.07	13600.36	18886.94	17173.97	13801.91	21370.11	15223.35	18296.13	17226.51	16041.93	9554.74	9239.53
	0.01	0.1	11191.04	21059.08	17452.87	11407.57	26726.34	13579.75	19392.54	14876.06	14837.71	6023.14	5762.77
	0.01	0.15	7983.19	25865.57	17535.45	8057.23	44941.73	10933.93	22040.10	11113.59	12396.19	3241.98	3172.58
	0.01	0.2	5994.42	32089.89	17380.85	6133.06	80183.19	8731.05	24983.03	8348.48	10248.66	2220.51	2170.11
	0.01	0.35	3102.85	56819.19	14331.90	3269.19	705751.23	4757.16	32552.92	4247.41	5397.37	1192.82	1197.47
		h	4.0000	3.0932	3.8792	3.0480	3.1293	3.8701	3.8714	3.3604	4.0678	3.6965	4.4943
										3.4534	4.0579	1.8816	1.8687
												1.2132	1.1421

Comparing the 11 control charts, when $s = \pm\infty$ and there is a decrease in correlation, the CUSUM-$p\rho$ chart in column [5] with $p_t = 0.02$ and $\rho_t = 0.1$ is designed to detect a decrease in ρ, and has the best performance and is uniformly better than the other charts. However, the SSANOS value is still very large for the smallest value of ρ_1. When $s = \infty$ and there is an

increase in correlation, the three-CUSUM chart combination in columns [10] and [11] have better performance than the other types of charts. The three-CUSUM chart combination has a CUSUM-ρ chart to monitor shifts only occur in the correlation and it is reasonable that this type of chart has better performance. The SSANOS values of the three-CUSUM chart combination in columns [10] and [11] show that even though these two charts are better than the other charts, detecting the shift in ρ with p remaining at p_0 still takes very long time.

From the discussion above in Table 4.4, it is difficult to detect a shift in correlation for all the charts we consider here, especially for small shifts in correlation. In practice, the major concern in a manufacturing process is the proportion of defectives and a shift in the correlation is not as important as a shift in the proportion. Therefore, it might not be necessary to detect a small shift in correlation. Table 4.5 provides similar conclusions as Table 4.4 and we will not discuss this table here.

4.4.2.2 Conclusions When Shift Only Occurs in the Proportion or Correlation

In this subsection, we discuss the performance of the charts when the shift actually only occurs in one parameter assuming that both p and ρ could shift. The CUSUM-$p\rho$ chart combination has been shown to be effective when the two parameters shift simultaneously in Section 4.4.1. In this section, we found that the CUSUM-$p\rho$ chart combination is also effective when shifts only occur in the proportion. The performance of the CUSUM-$p\rho$ chart is better than the other charts except for the MBCUSUM chart, which is designed to detect shift only occurs in the proportion and does not works well when the two parameters shift simultaneously. When the shift only occurs in the correlation, it is very difficult to detect it for all the charts. In practice, the actual shifts in the two parameters are usually unknown and it is desirable to use a control chart that is effective in detecting the shifts in both of the two parameters. In this case, we suggest using the CUSUM-$p\rho$ chart combination chart to monitor the two parameters. The MBCUSUM chart only works better than the CUSUM-$p\rho$ chart combination when the proportion shift but the correlation remains at the target value. However, practitioners usually do not know the actual shift and therefore, using the CUSUM-$p\rho$ chart combination is safer for detecting the unknown shifts in the two parameters.

4.4.3 Comparisons of Charts Performance for High Quality Process

The discussion in Section 4.4.2 is for a process with $p = 0.01$. In this section we will look at the performance of the CUSUM-type charts when $p = 0.001$. As the previous discussion has shown that the Shewhart chart is not effective for the shifts in both proportion and correlation and the three-CUSUM chart combinations can be beaten by the CUSUM-$p\rho$ chart combination when looking at overall performance, we will not discuss these two charts for the case of $p_0 = 0.001$. We will include the MBCUSUM chart and the CUSUM-$p\rho$ chart, which could be used when we actually know the direction of the shift. Table 4.6 shows the SSANOS values for 8 control charts with $p_0 = 0.001$ and $\rho = 0.2$ when shifts occur in both proportion and correlation. The ICANOS values for the charts in Table 4.6 all set to equal 16890.0. The ranges of the shifts in proportion vary for different directions and are relatively large, as the in-control proportion is 0.001.

In Table 4.6, columns [1], [3], [5], and [7] list the SSANOS values for the MBCUSUM, two CUSUM-$p\rho$ charts, and the CUSUM-$p\rho$ chart combination with $p_t = 0.002$. Columns [2], [4], [6] and [8] list the SSANOS values for the MBCUSUM, two CUSUM-$p\rho$ charts, and the CUSUM-$p\rho$ chart combination with $p_t = 0.005$. Comparing the charts in columns [1], [3], [4] and [7] with those in columns [2], [5], [6] and [8], respectively, it is noticed that with $p_t = 0.005$, the performance of the charts is better for most of the shifts than with $p_t = 0.002$. With $p_t = 0.002$, the charts only work well at very small shifts in proportion, for instance, when $p_1 = 0.002$.

In column [6], the CUSUM-$p\rho$ chart has $\rho_t = 0.15$ which is mis-specified for the positive direction shifts. However, when $s = 2.5, 5, 10$ and 15, we found that the performance of the chart in column [6] is better than that of column [3] with $\rho_t = 0.3$, which is correctly specified in direction. This comparison shows that when specifying the two pre-determined shifts, it is more important to appropriately specify p_t. When the actual shifts in proportion are close to p_t, even if ρ_t is mis-specified, the chart still works better than those charts with ρ_t appropriately specified but p_t is far away from the actual p_1. Similar conclusions can be reached when comparing the charts in column [4] and [5] when $s = -2.5$ and -5. When $p_0 = 0.001$, most of the shifts in proportion we consider here are close to $p_t = 0.005$. In general, the CUSUM-$p\rho$

chart combination in column [8] has better overall performance than the other charts when the two parameters shift simultaneously.

Table 4.6 SSANOS values of some CUSUM control charts when $p_0 = 0.001, \rho_0 = 0.2$ and $s = 2.5, 5, 10, 15, -2.5$ and -5

			MBCUSUM		CUSUM-$p\rho$				CUSUM-$p\rho$ Combination	
			$p_t = 0.002$	$p_t = 0.005$	$p_t = 0.002$ $\rho_t = 0.3$	$p_t = 0.002$ $\rho_t = 0.15$	$p_t = 0.005$ $\rho_t = 0.3$	$p_t = 0.005$ $\rho_t = 0.15$	$p_t = 0.002\&\rho_t = 0.3$ $p_t = 0.002\&\rho_t = 0.15$	$p_t = 0.005\&\rho_t = 0.3$ $p_t = 0.005\&\rho_t = 0.15$
s	p_1	ρ_1	[1]	[2]	[3]	[4]	[5]	[6]	[7]	[8]
	0.001	0.2	16799.46	16938.71	16576.85	17166.34	16728.72	16707.27	16960.63	16957.24
	0.002	0.2025	3177.20	3555.01	3775.14	3245.71	3632.39	3593.12	3406.97	3550.64
	0.005	0.21	709.64	676.34	873.09	720.86	707.37	688.26	804.84	677.96
	0.01	0.2225	298.10	267.49	367.56	304.58	276.58	269.86	361.73	268.21
2.5	0.02	0.2475	134.80	129.96	168.07	147.33	128.41	129.97	179.06	127.72
	0.05	0.3225	58.21	58.61	67.98	66.73	55.13	58.19	72.61	55.38
	0.08	0.3975	41.61	41.87	44.58	69.30	37.79	38.25	47.67	37.79
	0.1	0.4475	36.79	36.84	37.21	61.90	32.37	41.40	39.91	32.27
	0.15	0.5725	32.79	32.67	28.41	63.73	25.86	33.19	31.20	25.77
	0.002	0.205	3198.37	3597.51	3742.53	3265.46	3664.50	3594.94	3408.01	3562.16
	0.005	0.22	723.39	688.83	873.87	735.12	716.50	700.39	810.58	689.76
	0.01	0.245	307.53	277.85	374.17	319.18	285.12	279.30	369.86	276.80
5	0.02	0.295	144.92	138.89	173.21	161.21	136.05	139.55	187.03	135.68
	0.04	0.395	81.65	81.53	89.46	98.00	74.81	81.75	99.88	75.87
	0.05	0.445	71.24	71.29	74.27	116.39	63.91	83.87	83.56	64.61
	0.08	0.595	62.01	62.16	54.57	111.87	50.11	76.65	62.20	50.87
	0.002	0.21	3237.62	3631.65	3760.94	3315.31	3642.12	3650.52	3441.75	3613.61
	0.005	0.24	749.28	716.42	885.58	770.15	737.89	733.53	830.51	714.98
10	0.01	0.29	334.54	299.20	384.42	348.77	302.50	303.64	386.86	296.01
	0.02	0.39	172.18	162.33	185.68	199.69	153.58	164.53	204.68	153.54
	0.04	0.59	123.26	120.34	110.45	173.99	100.50	124.51	127.04	103.11
	0.002	0.215	3266.17	3657.00	3753.33	3376.24	3676.10	3733.00	3450.66	3624.22
15	0.005	0.26	772.65	753.07	890.33	810.55	755.88	764.34	851.88	737.23
	0.01	0.335	362.10	325.46	395.65	388.31	323.22	332.75	406.65	317.58
	0.02	0.485	211.11	195.37	204.26	256.06	177.23	201.13	225.98	178.37
	0.002	0.1975	3116.31	3491.88	3756.26	3195.77	3631.35	3516.43	3374.47	3500.11
	0.005	0.19	691.23	648.17	864.69	686.52	685.03	652.33	781.11	657.22
	0.01	0.1775	276.65	250.71	359.24	279.98	263.25	252.31	345.98	252.01
-2.5	0.02	0.1525	118.11	115.08	158.33	125.21	115.40	115.00	163.13	114.37
	0.04	0.1025	54.75	54.92	75.95	57.22	54.75	54.72	72.93	54.58
	0.05	0.0775	42.72	42.89	60.05	70.27	43.08	53.57	54.65	42.81
	0.08	0.0025	25.24	25.16	36.43	34.34	25.27	26.23	28.93	25.12
	0.002	0.195	3100.43	3488.94	3749.29	3177.12	3598.14	3531.36	3348.02	3470.72
	0.005	0.18	675.97	639.91	858.56	674.77	682.91	641.61	772.49	646.67
-5	0.01	0.155	267.36	243.00	355.51	268.46	255.75	242.44	337.16	244.43
	0.02	0.105	111.25	109.02	155.57	115.94	109.19	108.94	155.91	109.21
	0.04	0.005	49.46	49.38	72.75	50.28	49.80	49.42	64.69	49.57
		h	1.0950	1.5147	1.0368	1.2183	1.5883	1.5850	1.2555 1.5051	1.7507 1.6965

Table 4.7 shows the SSANOS values when the shift occurs only in the proportion or in the correlation. In the high quality process, we found that the shift in correlation is still difficult to detect for all the charts we discussed here. When the shift occurs only in the proportion, the

MBCUSUM chart still provides the best performance when $p_1 = p_t$. The overall performance of the 8 charts is good and similar here except the CUSUM-$p\rho$ chart in column [3] and the CUSUM-$p\rho$ chart combination in column [7], which consists of the CUSUM-$p\rho$ charts in column [3] and [4]. The relatively bad performance of the CUSUM-$p\rho$ chart in column [3] is caused by the fact that the tuning parameters p_t and ρ_t are not close to most of the actual shift combinations. Therefore, to apply the CUSUM-$p\rho$ chart in practice where the actual shifts are unknown, we can set the two tuning parameters to be in the middle of the ranges of shifts that could reasonably occur.

Table 4.7 SSANOS values of some CUSUM control charts when $p_0 = 0.001, \rho_0 = 0.2$ and $s = \pm\infty$ and 0

			MBCUSUM		CUSUM-pρ			CUSUM-pρ Combination	
			$p_t = 0.005$	$p_t = 0.002$ $\rho_t = 0.3$	$p_t = 0.002$ $\rho_t = 0.15$	$p_t = 0.005$ $\rho_t = 0.3$	$p_t = 0.005$ $\rho_t = 0.15$	$p_t = 0.002\&\rho_t = 0.3$ $p_t = 0.002\&\rho_t = 0.15$	$p_t = 0.005\&\rho_t = 0.3$ $p_t = 0.005\&\rho_t = 0.15$
s	p_1	ρ_1	[2]	[3]	[4]	[5]	[6]	[7]	[8]
	0.001	0.2	16938.71	16576.85	17166.34	16728.72	16707.27	16960.63	16957.24
	0.002	0.2	3534.46	3758.56	3229.75	3625.15	3570.64	3385.32	3543.66
	0.005	0.2	664.08	867.34	705.05	698.86	667.95	793.30	667.44
	0.01	0.2	259.27	363.53	292.08	269.27	261.40	353.57	259.25
0	0.02	0.2	122.50	163.27	135.20	121.73	122.17	171.37	120.92
	0.04	0.2	61.59	79.14	66.67	60.19	61.51	81.08	60.07
	0.05	0.2	49.51	63.21	69.98	48.39	49.08	63.22	48.44
	0.1	0.2	25.37	31.54	35.76	24.57	28.07	29.19	24.43
	0.2	0.2	13.52	15.82	25.37	12.65	14.28	14.62	12.61
	0.001	0.03	7930.07	26534.66	8937.10	15550.46	10383.13	12363.88	12176.09
	0.001	0.05	8401.04	24936.92	9557.24	15664.02	10848.87	12949.81	12929.14
	0.001	0.1	9463.09	21355.30	11326.15	16187.11	12468.52	14377.60	14725.37
	0.001	0.15	11032.31	18720.60	13850.20	16482.53	14418.33	15736.09	16130.38
±∞	0.001	0.2	16938.71	16576.85	17166.34	16728.72	16707.27	16960.63	16957.24
	0.001	0.25	19615.88	14769.92	21447.97	16848.38	19787.51	16938.75	17880.84
	0.001	0.3	22897.17	13374.80	27920.57	16610.72	23399.57	16578.16	18601.68
	0.001	0.4	32672.84	11231.34	51358.10	15868.62	34860.89	14727.02	19228.50
	0.001	0.5	49046.82	9737.90	108779.37	14489.88	55269.53	12911.18	18294.14
	0.001	0.6	79487.72	8861.22	280154.11	12914.01	97112.75	11592.68	16630.34
		h	1.5147	1.0368	1.2183	1.5883	1.5850	1.2555 1.5051	1.7507 1.6965

4.4.4 Conclusions from the Performance Comparisons

In this section, we proposed a CUSUM$-p\rho$ chart for monitoring the correlated binary process proportion and correlation. This chart has two pre-determined shifts used as tuning parameters, with one for the proportion and the other one for the correlation. The performance of the CUSUM$-p\rho$ chart depends highly on these pre-determined shifts. When the actual shifts in the two parameters are both close to its pre-determined shifts, respectively, the chart has very

good performance. However, when the actual shift combination is far away from the pre-determined shifts, the CUSUM$-p\rho$ chart does not work well. We found that the chart still works well if the pre-determined shift in proportion is close to the actual shift in proportion and the correlation does not change very much. The simulation results show that the pre-determined shift in the proportion is more significant than that of the correlation.

Based on the CUSUM$-p\rho$ chart, we developed the CUSUM$-p\rho$ chart combination to detect an increase in the proportion and an increase or a decrease in the correlation. The performance of the charts shown in this section indicates that the CUSUM $-p\rho$ chart combination has better overall performance considering that the shifts could occur in multiple directions. It is noted that when the pre-determined shifts in correlation are set to be the same values for two CUSUM$-p\rho$ chart combinations, the performance of the combination depends primarily on the pre-determined shifts in the proportion. The combination works well when the shift in proportion is close to p_t. The CUSUM $-p\rho$ chart combination can beat the three-CUSUM chart combination when considering overall performance.

Overall, the performance of the CUSUM $-p\rho$ chart and the CUSUM $-p\rho$ chart combination depends on the pre-determined shifts. In practice, to use these charts, practitioners need to have some general information about the likely size of the shift in the process to use the CUSUM$-p\rho$ chart. The pre-determined shifts can be selected based on that information, i.e. choose the pre-determined shifts close to the middle of the ranges of the shifts that could reasonably occur. In practice, it would usually be more important to detect a shift in the proportion than in the correlation, therefore, it is more important to specify the pre-determined proportion shift correctly.

An advantage of the proposed CUSUM-$p\rho$ chart or the CUSUM-$p\rho$ combination chart is that with appropriately specified tuning parameters, they have good performance and are easier to design than using several traditional CUSUM charts as a combination. In the CUSUM-$p\rho$ chart, there is only one control limit that needs to be specified. But when using two traditional CUSUM charts, we would need to specify two limits, which must be adjusted together to achieve the desired in-control performance. In the CUSUM-$p\rho$ chart combination, two control limits are adjusted to achieve the desired in-control performance. However, to detect an increase in the

proportion and an increase or a decrease in the correlation, three traditional CUSUM charts are needed and therefore multiple control limits need to be specified. Generally, beside the good performance of the proposed CUSUM-$p\rho$ chart and CUSUM-$p\rho$ chart combination, they are also easier to design compared with the traditional CUSUM chart combinations.

4.5 GLR-$p\rho$ Chart for Monitoring Proportion and Correlation

In Chapter 3, we proposed the MBGLR chart with an upper bound to monitor p in a correlated process. The MBGLR chart has been shown to have good performance in detecting shifts in p close to or smaller than the upper bound. In the MBGLR chart, the control statistic requires estimation of the shift p_1 and the upper bound is used in this estimation to avoid too frequent false alarms when the process is in control. This proposed MBGLR chart has been shown to have better performance over a wider range of shifts than the MBCUSUM chart for monitoring p. Therefore, when the shift is unknown, the MBGLR chart is a better choice than the MBCUSUM chart. In this section, the idea of the MBGLR chart will be extended to a GLR$-p\rho$ chart for monitoring the p and ρ. The chart performance will be compared with the proposed CUSUM$-p\rho$ chart combination, which was shown in Section 4.4 to have a better overall performance than the MBCUSUM chart, the individual CUSUM$-p\rho$ chart and the three-CUSUM chart combination.

4.5.1 The GLR$-p\rho$ Chart for Monitoring Proportion and Correlation

Consider a correlated binary process that is modeled as a two-state Markov chain model. It is assumed that the process has the in-control proportion and correlation p_0 and ρ_0 for X_i, $i = 1,2 \ldots \tau$, and a shift to an unknown $p_1 > p_0$ and an unknown ρ_1 occurs between observations τ and $\tau + 1$, where $0 \leq \rho_1 < \rho_0$ or $\rho_0 < \rho_1 < 1$. In the Phase II monitoring process, after each observation, we want to do a sequence of tests to see if there is any shift that was occurred at a prior observation. At observation k, the hypothesis test is based on all the past observations $X_1, X_2, \ldots . X_k$. The hypothesis test is:

$$H_0: p = p_0, \rho = \rho_0 \text{ for } X_i,\ i = 1,2, \ldots k$$

$$H_1: p = p_0, \rho = \rho_0 \text{ for } X_i,\ i = 1,2, \ldots \tau$$

$$p = p_1, \rho = \rho_1 \text{ for } X_i,\ i = \tau + 1, \tau + 2, \dots k$$

for some $p_1 > p_0$, $0 \le \rho_1 < \rho_0$ or $\rho_0 < \rho_1 < 1$, and some $\tau = 0,1, \dots k-1$. Under the alternative hypothesis, the likelihood function after the k^{th} binary observation is

$$L_k(\tau, p_0, \rho_0, p_1, \rho_1 | X_1, X_2, \dots X_k) = f(x_1, x_2, .., x_k | \tau, p_0, \rho_0, p_1, \rho_1)$$

$$= \begin{cases} \prod_{i=1}^{k} f(x_i | x_{i-1}, p_1, \rho_1), & \tau = 0 \\ \prod_{i=1}^{\tau} f(x_i | x_{i-1}, p_0, \rho_0) \prod_{i=\tau+1}^{k} f(x_i | x_{i-1}, p_1, \rho_1), & \tau \ge 1 \end{cases}$$

where $f(x_i | x_{i-1}, p, \rho)$ is the conditional probability mass function of X_i given X_{i-1} and $f(x_i | x_{i-1}, p, \rho) = f(x_1 | p, \rho)$ when $i = 1$. Then the likelihood function under the null hypothesis is

$$L_k(\infty, p_0, p_0, \rho_0, \rho_0 | X_1, X_2, \dots X_k) = f(x_1, x_2, .., x_k | \infty, p_0, p_0, \rho_0, \rho_0)$$

$$= \prod_{i=1}^{k} f(x_i | x_{i-1}, p_0, \rho)$$

The GLR$-p\rho$ statistic at the k^{th} binary observation is defined as the maximized log-likelihood ratio of the alternative hypothesis over the null hypothesis maximized over τ and p_1, i.e.

$$R_{p\rho,k} = \max_{\tau, p_1} ln \frac{L_k(\tau, p_0, \rho_0, p_1, \rho_1 | X_1, X_2, \dots X_k)}{L_k(\infty, p_0, p_0, \rho_0, \rho_0 | X_1, X_2, \dots X_k)}$$

$$= \max_{\tau} ln \frac{L_k(\tau, p_0, \rho_0, \hat{p}_1, \hat{\rho}_1 | X_1, X_2, \dots X_k)}{L_k(\infty, p_0, \rho_0, p_0, \rho_0 | X_1, X_2, \dots X_k)}$$

$$= \max_{0 \le \tau < k} \sum_{i=\tau+1}^{k} ln \frac{f(x_i | x_{i-1}, \hat{p}_1, \hat{\rho}_1)}{f(x_i | x_{i-1}, p_0, \rho_0)}$$

where $\hat{p}_1 = \max(p_0, p_{MLE})$, $\hat{\rho}_1 = \rho_{MLE}$, and p_{MLE} and ρ_{MLE} are defined as the maximum likelihood estimators of p_1 and ρ_1, respectively. The GLR-$p\rho$ statistic requires the calculation of

$\hat{p}_{MLE}$ and $\hat{\rho}_{MLE}$, and then maximizes $R_{p\rho,\mathrm{k}}$ over the possible change points τ. For the correlated binary case, similar to the case of the MBGLR statistic, it is difficult to obtain closed form expressions for $\hat{\tau}$, $\hat{p}_1$, and $\hat{\rho}_1$, and thus a grid search method was applied here. The chart signals when $R_{p\rho,\mathrm{k}} > h_{p\rho,G}$, where $h_{p\rho,G}$ is the control limit.

In the MBGLR chart, we found that an upper bound is needed due to the discreteness problem of the correlated binary process. In the GLR-$p\rho$, we found the same problem without upper bounds for the estimates of the proportion and correlation. Therefore, we will still use upper bounds for the estimates of the parameters as in the MBGLR chart. In the GLR-$p\rho$statistic, $\hat{p}_1 = \min(\max(p_0, \hat{p}_{MLE}), p_{ub})$ and $\hat{\rho}_1 = \min(\hat{\rho}_{MLE}, \rho_{ub})$, where ρ_{ub} is the upper bound for the estimate for ρ_1. In the monitoring process, we will only consider positive values for the correlation, i.e. $\hat{\rho}_1 = \max(0, \min(\hat{\rho}_{MLE}, \rho_{ub}))$.

4.5.2 The Performance of the GRL-$p\rho$ Chart

In this section, we will compare the performance of the GRL-$p\rho$ chart with the CUSUM-$p\rho$ chart combination. The CUSUM-$p\rho$ chart combination has been shown in Section 4.4 to have good overall performance for monitoring shifts in proportion and correlation. When specifying the pre-determined shifts in proportion and correlation in the chart combination, it is more important to correctly specify the pre-determined shift for the proportion than that for the correlation. It was noted in Chapter 3 that the upper bound of the MBGLR chart can be used as tuning parameter, where the chart is tuned to detect shifts close to or smaller than the upper bound p_{ub}. Therefore in the GRL-$p\rho$ chart, we will look at the performance of the chart with different values for the upper bounds for the shift in proportion and correlation, i.e. p_{ub} and ρ_{ub}. We will focus more on the comparisons of different p_{ub} values for GRL-$p\rho$ chart, as it is more important to detect a shift in proportion than that in correlation in practice.

It is noted that the estimate of shift in correlation is $\hat{\rho}_1 = \max(0, \min(\hat{\rho}_{MLE}, \rho_{ub}))$ and the lower bound of the estimate is 0. In the simulations, we found that using a positive lower bound for $\hat{\rho}_1$ gives better performance than using 0 as the lower bound for some of the shifts directions. Therefore, when comparing the chart performance, we use a lower bound $p_{lb} \geq 0$ for $\hat{\rho}_1$. In this subsection, we will compare the performance of the GRL-$p\rho$ charts with the CUSUM-$p\rho$ chart combination and the MBGLR chart with $p_0 = 0.01$ and $\rho_0 = 0.2$ and 0.05 as well as

the chart performance in a high quality process with $p_0 = 0.001$ and $\rho_0 = 0.2$. The performance will be studied by simulation and the geometric-type observation will be used as was used in previous simulation studies. We will use a window of 300 geometric-type observations for the GRL-$p\rho$ charts.

4.5.3 Comparisons of Chart Performance when the Proportion and Correlation Shift Simultaneously

We will first look at the chart performance with $p_0 = 0.01$ and $\rho_0 = 0.2$. The nine control charts compared here are one MBGLR chart, six GRL-$p\rho$ charts, and two CUSUM-$p\rho$ chart combinations. When comparing the charts, the control limits of each chart are selected at an appropriate value so that the ICANOS values of the charts are all close to 16890.0. The ICANOS values here match the ICANOS value of a Shewhart chart with $h = 5$ when $p_0 = 0.01$ and $\rho_0 = 0.2$. Besides this settings on the ICANOS values, we will look at the cases when the p_{ub} values of the MBGLR and the GRL-$p\rho$ charts are selected to be the same as the p_t values of the CUSUM-$p\rho$ chart combination. The ρ_{ub} and ρ_{lb} values for the GRL-$p\rho$ chart are selected to be the same as the $\rho_t's$ in the CUSUM-$p\rho$ chart combination. These cases are for fair comparisons among different types of charts.

Table 4.8 shows the SSANOS of the nine charts when $s = 2.5, 5, 10, 15, -2.5,$ and -5. Column [1] shows the SSANOS values of the MBGLR chart with $p_{ub} = 0.02$. This chart is designed to detect shifts that occur in the proportion but not in the correlation. Therefore, we would not expect to see good performance for this chart when the proportion and correlation shift simultaneously. Later, in a table with only proportion shifts, we will compare the GRL-$p\rho$ chart with the MBGLR chart to see how the chart designed for simultaneous shifts works when only one parameter changes. Columns [2]-[4] show the SSANOS values for three GRL-$p\rho$ charts, which have the same $p_{ub} = 0.02$ and $\rho_{ub} = 0.4$, but the ρ_{lb} are 0, 0.2 and 0.1, respectively. The GRL-$p\rho$ chart in column [2] with $\rho_{lb} = 0$ allows the estimates $\hat{\rho}_1$ to be any value between 0 and ρ_{ub}. The second case in column [3] with with $\rho_{lb} = p_0 = 0.2$ restrict the estimate to be greater than ρ_0. The reason we look at this case is to investigate the performance of the GRL-$p\rho$ chart with the lower bound on the estimate of $\hat{\rho}_1$ equal to ρ_0 and therefore there is no need to specify ρ_{lb} in practice. The third GRL-$p\rho$ chart in column [4] with $\rho_{lb} = 0.1$ impose the restriction

$0.1 \leq \hat{\rho}_1 \leq 0.4$, which provides a lower bound less than ρ_0. The GRL-$p\rho$ charts in columns [5]-[7] have the same lower and upper bound for $\hat{\rho}_1$, and the upper bounds for $\hat{p}_1$ are 0.05, 0.1, and 0.15, respectively. The last two columns [8] and [9] are the SSANOS values for the CUSUM-$p\rho$ chart combinations. In column [8], the chart combination consists of one CUSUM-pρ chart with $p_t = 0.02$ and $\rho_t = 0.4$, and one CUSUM-$p\rho$ chart with $p_t = 0.02$ and $\rho_t = 0.1$, where the value of p_t equals to the value of p_{ub} of the GRL-$p\rho$ chart in column [4] and $\rho_t = 0.4$ and $\rho_t = 0.1$ for the two the CUSUM-$p\rho$ charts equal to ρ_{ub} and ρ_{lb}, respectively, in the GRL-$p\rho$ chart in column [4]. The CUSUM-$p\rho$ chart combination in column [9] has a larger $p_t = 0.05$, and the pre-determined shifts of this chart are set to be equal to the values of the bounds for the GRL-$p\rho$ chart in column [5].

In Table 4.8, we found that the ICANOS values of the nine charts are close to 16890.0, but not close enough to make fair comparisons of the out-of-control SSANOS values and draw conclusions. Here we consider the ratio of $\frac{\text{SSANOS}_{p,\rho}}{\text{ICANOS}}$, where $\text{SSANOS}_{p,\rho}$ is the out-of-control SSANOS of a control chart when the shift in p is to p_1 and shift in ρ is to ρ_1. This ratio $\frac{\text{SSANOS}_{p,\rho}}{\text{ICANOS}}$ represents the number of observations needed to detect the shifts to p_1 and ρ_1 taking into account the differences between the ICANOS values of the charts. For a shift to p_1 and ρ_1, the $\min\left(\frac{\text{SSANOS}_{p,\rho}}{\text{ICANOS}}\right)$ of the all charts are calculated, and we define

$$v = \frac{\text{SSANOS}_{p_1,\rho_1}}{\text{ICANOS}} \Big/ \min\left(\frac{\text{SSANOS}_{p_1,\rho_1}}{\text{ICANOS}}\right)$$

The ratio v represent the comparison of the control chart to the best one to detect the shift to p_1 and ρ_1 among all the charts. The comparisons of the charts are presented with color shading based on v. The larger v is, the darker the shading is and the worse the chart performance is. The comparison in terms of v would be reasonable as long as there are only small differences in ICANOS values, but when the difference is large, comparisons based on v would not be reasonable. In the comparisons tables in this section for $p = 0.01$, the lightest color represent $v \in [1.00, 1.05]$ and the darkest color represent $v > 1.41$. When $p = 0.01$, the ranges of the SSANOS values for different chart are relatively large and we will use the lightest color represent $v \in [1.00, 1.30]$ and the darkest color represent $v > 3$.

Table 4.8 SSANOS values of the MBGLR, GLR-$p\rho$ and CUSUM-$p\rho$ chart combinations with $p_0 = 0.01$, $\rho_0 = 0.2$ and $s = 2.5, 5, 10, 15, -2.5$ and -5

			MBGLR	GLR-$p\rho$						CUSUM-$p\rho$ Combination	
			$p_{ub} = 0.02$	$p_{ub} = 0.02$ $\rho_{lb} = 0$ $\rho_{ub} = 0.4$	$p_{ub} = 0.02$ $\rho_{lb} = 0.2$ $\rho_{ub} = 0.4$	$p_{ub} = 0.02$ $\rho_{lb} = 0.1$ $\rho_{ub} = 0.4$	$p_{ub} = 0.05$ $\rho_{lb} = 0.1$ $\rho_{ub} = 0.4$	$p_{ub} = 0.1$ $\rho_{lb} = 0.1$ $\rho_{ub} = 0.4$	$p_{ub} = 0.15$ $\rho_{lb} = 0.1$ $\rho_{ub} = 0.4$	$p_t = 0.02$&$\rho_t = 0.4$ $p_t = 0.02$&$\rho_t = 0.1$	$p_t = 0.05$&$\rho_t = 0.4$ $p_t = 0.05$&$\rho_t = 0.1$
s	p_1	ρ_1	[1]	[2]	[3]	[4]	[5]	[6]	[7]	[8]	[9]
	0.01	**0.2**	**17175.42**	**16438.1**	**16152.3**	**16868.3**	**16873.9**	**16965.6**	**16725.0**	**16692.42**	**16931.82**
	0.015	**0.2125**	2284.49	2794.89	2642.10	2674.25	2773.36	2853.94	2915.91	2771.55	3544.66
	0.02	**0.225**	957.43	1191.51	1086.13	1120.47	1111.29	1139.38	1161.97	1118.46	1337.17
	0.025	**0.2375**	586.22	725.80	667.60	682.97	641.06	654.86	665.48	664.80	704.58
	0.03	**0.25**	421.05	521.45	474.05	491.73	439.31	444.75	453.47	472.71	452.94
2.5	**0.04**	**0.275**	274.86	336.34	303.53	317.01	262.58	264.27	266.85	302.38	252.55
	0.05	**0.3**	208.85	253.46	230.05	237.37	186.50	185.75	187.36	224.62	175.19
	0.06	**0.325**	170.68	204.84	183.71	192.86	146.21	143.11	143.43	179.54	134.99
	0.08	**0.375**	131.00	151.73	133.87	140.30	103.08	99.92	99.74	128.89	95.05
	0.1	**0.425**	110.44	120.92	105.03	110.82	82.07	78.09	77.44	100.84	74.93
	0.2	**0.675**	95.55	59.56	53.08	54.67	48.35	46.33	45.29	47.56	44.29
	0.015	**0.225**	2426.45	2941.76	2675.48	2769.59	2853.18	2943.81	2987.52	2836.37	3590.97
	0.02	**0.25**	1039.60	1266.36	1125.76	1187.85	1168.70	1201.62	1220.40	1167.00	1385.08
	0.025	**0.275**	649.91	787.63	692.62	732.04	682.61	697.68	709.20	704.29	740.79
	0.03	**0.3**	475.65	571.35	499.12	531.17	475.02	479.83	487.37	504.73	483.34
5	**0.04**	**0.35**	323.03	375.49	325.03	347.09	290.71	293.05	295.74	324.21	276.67
	0.05	**0.4**	256.30	283.16	242.74	260.38	211.94	209.72	211.94	238.62	197.61
	0.06	**0.45**	221.83	228.28	195.07	209.63	168.86	167.69	167.59	188.80	155.71
	0.08	**0.55**	193.44	163.46	140.16	149.02	124.94	122.15	122.00	131.34	115.00
	0.1	**0.65**	194.64	126.18	110.33	116.56	104.39	102.60	101.18	101.31	96.27
	0.015	**0.25**	2729.15	3158.73	2692.91	2892.84	2988.75	3065.89	3132.20	2832.15	3617.50
	0.02	**0.3**	1247.05	1372.90	1163.02	1262.83	1237.07	1272.33	1290.05	1191.76	1423.41
	0.025	**0.35**	820.94	858.73	724.76	783.13	742.17	753.39	761.52	719.94	783.50
10	**0.03**	**0.4**	636.84	615.52	515.04	565.58	517.99	527.86	530.83	509.32	521.21
	0.04	**0.5**	496.09	394.37	328.44	359.95	327.39	328.35	329.02	314.51	316.08
	0.05	**0.6**	471.35	281.03	242.47	261.40	245.80	245.19	245.02	226.03	235.64
	0.06	**0.7**	540.44	222.41	191.67	207.67	205.18	206.35	203.33	180.71	196.74
	0.015	**0.275**	3105.68	3194.14	2572.93	2908.73	2973.76	3062.32	3093.26	2751.93	3603.29
	0.02	**0.35**	1545.19	1400.26	1138.27	1249.47	1243.39	1274.08	1285.33	1128.23	1413.40
15	**0.025**	**0.425**	1098.65	851.23	685.36	765.63	739.42	756.05	760.54	674.23	789.80
	0.03	**0.5**	946.77	591.85	485.97	536.44	521.84	527.36	528.28	465.55	538.19
	0.04	**0.65**	1004.45	353.18	308.18	331.76	334.39	338.43	332.99	287.58	334.73
	0.015	**0.1875**	2050.60	2487.92	2518.33	2434.37	2530.24	2621.60	2666.44	2567.60	3429.66
	0.02	**0.175**	826.59	1001.55	996.00	972.74	968.87	1004.23	1013.65	964.48	1236.62
	0.025	**0.1625**	489.74	584.46	591.45	570.26	541.58	554.08	563.10	552.14	613.90
-	**0.03**	**0.15**	342.19	401.01	409.53	395.83	359.52	365.73	371.89	382.03	375.72
	0.05	**0.1**	151.27	168.45	182.77	170.83	136.57	137.13	137.64	162.87	128.19
	0.07	**0.05**	94.71	101.89	114.94	105.17	80.23	77.90	78.22	100.33	73.51
	0.08	**0.025**	79.50	84.35	96.72	87.46	65.42	63.15	62.97	83.41	60.13
	0.015	**0.175**	1953.83	2301.85	2394.60	2305.77	2396.57	2478.55	2537.74	2424.18	3360.05
	0.02	**0.15**	772.40	913.20	947.18	892.88	893.18	924.79	945.23	880.04	1158.37
-5	**0.025**	**0.125**	451.09	510.32	546.96	512.21	494.00	504.43	512.27	493.97	563.11
	0.03	**0.1**	312.73	345.22	378.96	350.01	320.19	326.84	331.41	334.74	335.33
	0.05	**0**	132.97	132.06	160.75	141.45	116.34	116.31	117.40	134.04	108.67
		h	2.987137	**4.5507**	**3.6958**	**4.1109**	**4.7782**	**5.0023**	**5.1242**	**3.4154** **3.8856**	**4.2441** **4.2556**

In Table 4.8, the MBGLR chart in column [1] has very bad performance when the shift in correlation is large, for instance, when $\rho_1 = 0.375, 0.425,$ and 0.675 for $s = 2.5$ and $\rho_1 = 0.45, 0.55,$ and 0.65 for $s = 5$. When the shifts in correlation are small and a relatively large shift

occurs in the proportion, the MBGLR chart designed to detect the shift in proportion works better than the GRL-$p\rho$ chart designed to detect simultaneous shifts in both parameters.

Comparing the GRL-$p\rho$ charts in columns [2]-[4] with same $p_{ub} = 0.02$ and $\rho_{ub} = 0.4$, it is noted that the GRL-$p\rho$ chart in column [2] with $\rho_{lb} = 0$ has the worst performance in all the positive directions. The GRL-$p\rho$ charts in columns [3] and [4] have similar performance. The GRL-$p\rho$ chart in column [3] with $\rho_{lb} = \rho_0 = 0.2$ works slightly better than GRL-$p\rho$ chart in column [4] with $\rho_{lb} = 0.1$ when the shift occurs in the positive direction and the later one works a bit letter when the shift direction is negative. This is because the GRL-$p\rho$ chart in column [3] has the restriction $\rho_{lb} = \rho_0 = 0.2$ and the estimated shifts cannot be smaller than p_0, which cannot provide an accurate estimate when the shifts are in the negative direction with $\rho_1 < 0.2$.

Comparing the GRL-$p\rho$ charts in column [4]-[7] with the same $\rho_{ub} = 0.4$ and $\rho_{lb} = 0.1$, we find that as p_{ub} increases, the overall performance of the chart gets better., but helps only to some point. Using a smaller upper bound on the estimate of the proportion gives a chart that works better at relative small shifts, and when p_{ub} gets larger, the performance of the GRL-$p\rho$ chart works relatively better at large shifts. For instance, the GRL-$p\rho$ chart in column [6] works better than the chart in column [7] at small shifts, but the chart in column [7] is better at relatively large shifts.

Comparing the CUSUM-$p\rho$ chart combinations in columns [8] and [9] with the GRL-$p\rho$ charts in columns [4] and [5] respectively, we found that the CUSUM-$p\rho$ chart combination works better than the GRL-$p\rho$ chart when the shifts combination in p and ρ are close to p_t and ρ_t of one of the CUSUM-$p\rho$ chart in the combination. While for shifts that are not close to p_t and ρ_t, the GRL-$p\rho$ chart works better. For instance, when $s = 10$ and 15, the shift combinations are very close to $p_t = 0.02$ and $\rho_t = 0.4$, and we found that the CUSUM-$p\rho$ chart combination in column [8] works quite well, but the CUSUM-$p\rho$ chart combination in column [9] with the pre-determined shifts far away from the shift combination does not work well.

In Table 4.9, we look at the chart comparisons when $p_0 = 0.01$ and $\rho_0 = 0.05$. The control limits of the 9 charts are selected so that the ICANOS values are close to 16956.6 which is the value for a Shewhart chart with $h = 4$. The p_{ub} of the MBGLR chart, the pre-determined shifts p_t and $\rho_t's$ in the CUSUM-$p\rho$ chart combinations, the p_{ub}, ρ_{ub} and p_{lb} of the GLR-$p\rho$

Table 4.9 SSANOS values of the MBGLR, GLR-$p\rho$ and CUSUM- $p\rho$ chart combinations with $p_0 = 0.01, \rho_0 = 0.05$ and $s = 2.5, 5, 10, 15, -2.5$ and 5

			MBGLR	GLR-$p\rho$						CUSUM-$p\rho$ Combination	
			$p_{ub} = 0.02$	$p_{ub} = 0.02$ $\rho_{lb} = 0$ $\rho_{ub} = 0.1$	$p_{ub} = 0.02$ $\rho_{lb} = 0.05$ $\rho_{ub} = 0.1$	$p_{ub} = 0.02$ $\rho_{lb} = 0.03$ $\rho_{ub} = 0.1$	$p_{ub} = 0.05$ $\rho_{lb} = 0.03$ $\rho_{ub} = 0.1$	$p_{ub} = 0.1$ $\rho_{lb} = 0.03$ $\rho_{ub} = 0.1$	$p_{ub} = 0.15$ $\rho_{lb} = 0.03$ $\rho_{ub} = 0.1$	$p_t = 0.02$&$\rho_t = 0.1$ $p_t = 0.02$&$\rho_t = 0.03$	$p_t = 0.05$&$\rho_t = 0.1$ $p_t = 0.05$&$\rho_t = 0.03$
s	p_1	ρ_1	[1]	[2]	[3]	[4]	[5]	[6]	[7]	[8]	[9]
	0.01	0.05	17220.22	15278.0	15990.43	16904.32	16686.38	16903.36	16976.53	17100.65	16739.36
	0.015	0.06	2004.39	2061.5	1763.82	2043.57	2259.86	2389.99	2444.35	2140.93	3195.63
	0.02	0.07	833.20	854.22	755.39	837.36	883.73	928.94	949.44	836.05	1153.08
	0.025	0.08	505.52	514.35	461.46	506.94	506.72	528.08	539.59	493.21	590.18
	0.03	0.1	357.61	364.93	333.35	361.65	343.65	355.84	363.50	351.62	370.70
2.5	0.04	0.12	229.39	235.91	212.14	230.24	203.78	207.96	210.40	226.00	203.01
	0.05	0.15	170.68	174.54	157.54	169.66	144.16	144.62	146.05	165.59	138.66
	0.06	0.17	139.75	138.93	125.27	134.74	110.95	110.54	110.71	131.70	105.80
	0.08	0.22	104.90	100.21	90.19	96.60	77.23	75.41	75.25	93.97	73.36
	0.1	0.27	84.89	78.66	70.59	75.43	60.41	57.95	57.52	73.81	57.05
	0.2	0.52	56.45	39.80	36.57	38.59	33.32	31.56	30.32	37.48	31.91
	0.015	0.07	59.44	34.22	31.91	32.71	30.93	30.16	28.50	32.15	30.26
	0.02	0.1	2104.15	2046.8	1987.79	2056.81	2273.06	2390.42	2454.72	2089.22	3192.12
	0.025	0.12	875.04	871.82	825.50	854.46	903.05	945.01	965.85	830.06	1166.10
	0.03	0.15	535.66	533.32	499.79	519.48	522.87	540.20	553.47	501.38	604.67
5.0	0.04	0.2	387.65	385.78	356.35	370.62	357.83	367.51	374.62	358.53	388.58
	0.05	0.25	256.87	243.33	228.41	237.90	217.49	220.14	221.97	228.41	217.25
	0.06	0.3	197.38	181.68	168.82	176.61	155.15	156.06	156.70	168.96	151.58
	0.08	0.4	164.42	144.94	135.11	140.86	122.83	122.13	122.19	135.21	117.49
	0.1	0.5	131.36	105.42	97.54	101.92	89.16	87.27	86.23	97.75	85.04
	0.015	0.1	117.00	84.35	78.57	81.67	72.90	71.01	69.58	78.55	69.81
	0.02	0.15	120.49	67.13	62.66	65.07	62.50	61.35	58.31	49.35	48.60
	0.025	0.2	2307.22	2135.1	1785.39	2046.03	2259.44	2364.91	2419.27	2073.19	3159.15
10	0.03	0.25	994.06	885.65	788.20	860.62	916.73	952.09	963.87	839.14	1180.39
	0.04	0.35	615.16	547.71	494.76	528.63	542.86	558.41	562.85	514.93	634.28
	0.05	0.45	465.67	395.83	359.31	379.68	379.23	387.32	391.71	367.63	413.46
	0.06	0.55	330.55	255.09	233.38	245.92	240.32	241.70	239.12	237.47	243.53
	0.015	0.12	277.37	191.03	176.13	185.05	179.12	179.23	176.44	175.94	178.59
	0.02	0.2	259.85	158.72	144.04	152.45	148.61	148.13	143.52	147.47	146.96
	0.025	0.27	274.73	132.95	123.73	129.19	128.33	127.21	119.08	95.44	95.88
15.	0.03	0.35	2494.10	2063.4	1764.86	1975.88	2192.36	2289.22	2323.48	1993.07	3095.76
	0.04	0.5	1119.00	878.18	798.90	845.01	910.24	938.62	945.40	818.70	1172.99
	0.045	0.57	735.51	547.28	494.63	524.00	549.08	561.64	561.62	502.79	641.81
	0.05	0.65	581.26	402.20	358.08	380.92	390.15	395.76	393.53	367.97	430.44
	0.013	0.04	453.79	262.75	238.66	252.09	257.73	256.67	249.50	241.02	266.32
	0.015	0.03	441.08	228.98	209.61	220.32	224.12	224.25	215.15	212.80	231.48
-	0.017	0.03	446.93	207.07	192.61	200.09	203.44	202.92	191.31	191.20	207.88
	0.02	0.02	516.64	198.04	184.55	192.02	192.97	193.10	178.04	142.34	145.94
	0.025	0.01	3533.49	3466.6	3599.93	3642.01	4057.33	4299.26	4449.38	3987.46	5639.61
	0.013	0.03	1914.58	1871.0	1977.22	1956.37	2180.22	2295.47	2369.90	2071.56	3223.26
-5	0.015	0.02	1218.55	1232.4	1261.18	1254.25	1367.90	1450.09	1494.66	1303.08	1979.28
	0.017	0.01	755.60	766.01	784.21	784.25	829.23	868.92	893.55	799.92	1103.17
	0.02	0	438.41	455.34	461.59	464.19	463.68	483.77	495.25	467.99	545.82
		h	3.1541	3.7242	3.3547	3.5376	4.3955	4.7089	4.8460	3.3604 3.4534	4.0678 4.0579

charts in Table 4.8 have similar settings in each column in Table 4.9 as in Table 4.8. As the in-control correlation $\rho_0 = 0.05$ is relatively small, we use $\rho_t = 0.03$ and 0.1 in the CUSUM-$p\rho$ chart combinations and $\rho_{ub} = 0.1$, and $p_{lb} = 0.03$ in the GLR-$p\rho$ charts. In Table 4.9, we found similar conclusions to those from Table 4.8 for the MBGLR chart, the GLR-$p\rho$ chart, and the CUSUM-$p\rho$ chart combinations.

Comparing the overall performance of the MBGLR chart, the GRL-$p\rho$ chart, and the CUSUM-$p\rho$ chart combination, we found that when there is small increase in correlation, the MBGLR chart works better than the GLR-$p\rho$ chart and the CUSUM-$p\rho$ chart combination with the same value of p_{ub}. When the shifts combinations are close the pre-determined shifts p_t and ρ_t in the CUSUM-$p\rho$ chart combination, the combination has the best performance, but the combination works very poorly when the shifts are quite different from the pre-determined shifts.

The GRL-$p\rho$ chart with a relatively large upper bound for the proportion works well over a wider range of shifts than the CUSUM-$p\rho$ chart combination. In practice, the shift combination is usually unknown, so using a GRL-$p\rho$ chart would be safer than using the CUSUM-$p\rho$ chart combination. From the aspect of designing a control chart, when using the CUSUM-$p\rho$ chart combination, we need to specify the control limits for the two CUSUM-$p\rho$ charts in the combination and adjust the two control limits to obtain the required ICANOS. The GLR-$p\rho$ chart is easier to design, as there is only one control limit that needs to be specified. It is found that when using a lower bound on the correlation p_{lb}, the GLR-$p\rho$ chart has much better performance when there are increases in both correlation and proportion, and the performance is slightly worse when there is large decreases in correlation compared to the GLR-$p\rho$ chart without a positive lower bound on the correlation.

4.5.3.1 Performance comparisons of the charts with shifts in either proportion or correlation

It was shown in Section 4.5.2.1 that the GLR-$p\rho$ charts with a relatively large upper bound on the proportion has good overall performance when there are simultaneous shifts in proportion and correlation. Now we will look at the performance of the GLR-$p\rho$ chart when the shift only occurs to either the proportion or the correlation. We are especially interested in looking at how the chart performs when there is only a shift in the proportion as this will be the major concern in most processes. In Section 4.4, we showed that a shift in only the correlation is very difficult to detect for the CUSUM-$p\rho$ chart, especially when the shift size is small. In this subsection, we will discuss the performance of the GLR-$p\rho$ chart in two directions with $s = \pm\infty$ and 0.

Table 4.10 SSANOS values of the MBGLR, GLR-$p\rho$ and CUSUM- $p\rho$ chart combinations with $p_0 = 0.01, \rho_0 = 0.2$ and $s = \pm\infty$ and 0

			MBGLR	GLR-$p\rho$						CUSUM-$p\rho$ Combination	
			$p_{ub} = 0.02$	$p_{ub} = 0.02$ $\rho_{lb} = 0$ $\rho_{ub} = 0.4$	$p_{ub} = 0.02$ $\rho_{lb} = 0.2$ $\rho_{ub} = 0.4$	$p_{ub} = 0.02$ $\rho_{lb} = 0.1$ $\rho_{ub} = 0.4$	$p_{ub} = 0.05$ $\rho_{lb} = 0.1$ $\rho_{ub} = 0.4$	$p_{ub} = 0.1$ $\rho_{lb} = 0.1$ $\rho_{ub} = 0.4$	$p_{ub} = 0.15$ $\rho_{lb} = 0.1$ $\rho_{ub} = 0.4$	$p_t = 0.02$&$\rho_t = 0.4$ $p_t = 0.02$&$\rho_t = 0.1$	$p_t = 0.05$&$\rho_t = 0.4$ $p_t = 0.05$&$\rho_t = 0.1$
s	p_1	ρ_1	[1]	[2]	[3]	[4]	[5]	[6]	[7]	[8]	[9]
	0.01	**0.2**	**17175.42**	**16438.1**	**16152.3**	**16868.3**	**16873.9**	**16965.6**	**16725.0**	**16692.42**	**16931.82**
	0.02	0.2	889.99	1045.45	1090.17	1050.42	1039.85	1071.50	1089.84	1050.22	1294.25
	0.03	0.2	376.71	446.17	462.28	445.17	398.70	405.94	412.66	429.90	415.73
	0.04	0.2	238.26	282.14	291.14	280.06	232.75	233.51	235.59	269.32	224.52
	0.05	0.2	175.46	206.53	211.02	205.25	161.04	160.00	162.01	195.83	151.03
	0.08	0.2	98.67	115.75	120.06	115.88	82.89	79.31	79.57	110.49	76.46
0	0.1	0.2	77.05	90.11	94.81	90.83	63.07	59.22	58.72	86.70	57.63
	0.2	0.2	39.40	43.29	48.54	45.71	29.65	26.77	25.44	43.46	26.96
	0.3	0.2	29.07	29.48	33.96	31.27	19.83	18.15	16.59	29.31	18.55
	0.4	0.2	24.57	22.19	26.42	23.74	15.40	14.13	12.58	21.75	14.50
	0.5	0.2	22.35	17.36	21.04	18.81	12.84	11.75	10.48	16.83	12.08
	0.6	0.2	21.63	14.06	17.01	15.22	11.17	10.26	9.13	13.29	10.38
	0.01	0.03	5988.07	2408.31	9429.32	3178.00	3581.76	3767.53	3862.44	5177.94	9821.88
	0.01	0.05	6647.45	2874.36	10610.2	3713.43	4199.17	4400.21	4504.83	6134.00	10887.61
	0.01	0.1	8853.72	4955.52	14802.7	6105.15	6782.88	7100.05	7235.83	9733.22	13684.10
	0.01	0.15	12174.88	9734.77	19034.0	11641.7	12360.5	12771.8	12841.1	14871.59	16037.43
	0.01	0.17	13908.51	12649.7	18974.9	14705.2	15037.1	15300.0	15338.4	16408.90	16700.82
$\pm\infty$	**0.01**	**0.2**	**17175.42**	**16438.1**	**16152.3**	**16868.3**	**16873.9**	**16965.6**	**16725.0**	**16692.42**	**16931.82**
	0.01	0.25	24923.69	9085.43	9222.30	11170.5	12091.8	12229.5	12262.5	12593.36	15599.48
	0.01	0.3	37086.68	5166.56	5238.70	6144.80	6924.15	7123.14	7206.02	8291.41	13035.62
	0.01	0.35	57212.29	3374.88	3321.74	3836.96	4362.85	4515.78	4560.58	5676.71	10339.57
	0.01	0.4	90118.62	2397.92	2400.95	2713.73	3076.50	3180.07	3223.20	4140.90	8029.92
	0.01	0.45	147239.97	1873.58	1869.38	2097.49	2361.87	2457.58	2481.21	3207.37	6200.12
	0.01	0.5	244108.70	1552.65	1556.02	1711.73	1934.09	1998.32	2011.48	2575.89	4887.97
		h	**2.9871**	**4.5507**	**3.6958**	**4.1109**	**4.7782**	**5.0023**	**5.1242**	**3.4154**	**4.2441**
										3.8856	**4.2556**

Table 4.10 shows the SSANOS values of the nine control charts considered in Table 4.8 with $p_0 = 0.01, \rho_0 = 0.2$ when $s = \pm\infty$ and 0. When $s = 0$, there is only a shift in the proportion and the correlation ρ_0 remains at the target value 0.2. Previous results for the MBGLR chart show that is chart works well for shifts close to or smaller than p_{ub}. Here, in Table 4.10 with $p_{ub} = 0.02$, the MBGLR chart in column [2] works well when $p_1 \leq 0.04$. The performance of the GLR-$p\rho$ chart varies depending on the values of p_{ub} and ρ_{lb}. It is noted that a larger p_{ub} results in better performance in detecting shifts in the proportion. In the CUSUM-$p\rho$ chart combinations in columns [8] and [9], as p_t increase, the chart has good performance for relatively large shifts in proportion but worse performance for small shifts. For instance, the CUSUM- $p\rho$ chart combination in column [8] works well when $p_1 \leq 0.03$ but the chart in

column [9] with a large p_t works well on the moderate and large shifts, but not for the small shifts. Comparing the GLR-$p\rho$ chart with the CUSUM- $p\rho$ chart combination, it is found that the overall performance of the GLR-$p\rho$ chart with a relatively large p_{ub} is better for detecting shifts in proportion than that of the CUSUM- $p\rho$ chart combination.

When $s = \pm\infty$, there is no shift in the proportion and $p_1 = p_0 = 0.01$. The performance of the MBGLR chart to detect the shift in correlation is the worst one compared with the other charts. The results make sense as the MBGLR chart applies to the shift only occurs in the proportion but not in the correlation.

The SSANOS values in columns [2[-[4] indicate that to detect the shifts in correlation, the GLR-$p\rho$ chart with no lower bound to the estimate of correlation in column [2] works better than the charts with $\rho_{lb} = \rho_0$ and 0.1 in columns [3] and [4]. The GLR-$p\rho$ chart in column [2] is almost uniformly better than the other charts when $s = \pm\infty$. Comparing the performance of the charts in columns [4]-[7], it is concluded that as p_{ub} increases, the performance in detecting shifts in correlation gets worse. This is as expected because there is no shift in proportion and a larger upper bound p_{ub}will hurt the performance. With a small $p_{ub} = 0.02$ and a lower bound $\rho_{lb} = 0.1$, the performance of the GLR-$p\rho$ chart is not as good as the chart with no lower bound, however, the performance is still better than the GLR-$p\rho$ chart with a relatively large upper bound.

The CUSUM- $p\rho$ chart combinations in columns [8] and [9] are designed to detect shifts simultaneously occurring to the proportion and correlation, especially for a known combination of shifts. We found the CUSUM- $p\rho$ chart combinations do not have good performance when $s = \infty$. Comparing the charts in column [8] and [9], as p_t increase, the performance gets worse, which is similar to the change pattern of p_{ub} in the GLR-$p\rho$ chart. Comparing the GLR-$p\rho$ chart with the CUSUM- $p\rho$ chart combination when $s = \infty$, we found that the GLR-$p\rho$ charts in columns [4]-[7] are uniformly better than the CUSUM- $p\rho$ chart combinations in columns [8] and [9]. This is true even when the GLR-$p\rho$ chart has a larger p_{ub} than that of the CUSUM- $p\rho$ chart combination.

In general, shifts in correlation are much more difficult to detect than simultaneous shifts in the two parameters and shifts occurring only in the proportion. To detect the shift in

correlation, a GLR-$p\rho$ chart with a small p_{ub} and no lower bound on ρ_1 works better than the other charts. When the shift occurs only in the proportion, we found that the GLR-$p\rho$ chart with a relatively large p_{ub} provides better overall performance than the CUSUM- $p\rho$ chart combination. Table 4.11 gives the SSANOS values of the charts for the case of $p_0 = 0.01$ and $\rho_0 = 0.05$. We found conclusions similar to the conclusions from Table 4.10 and thus will not discuss them here.

Table 4.11 SSANOS values of the MBGLR, GLR-$p\rho$ and CUSUM- $p\rho$ chart combinations with $p_0 = 0.01$, $\rho_0 = 0.05$ and $s = \pm\infty$ and 0

			MBGLR	GLR-$p\rho$						CUSUM-$p\rho$ Combination	
			$p_{ub} = 0.02$	$p_{ub} = 0.02$	$p_{ub} = 0.02$	$p_{ub} = 0.02$	$p_{ub} = 0.05$	$p_{ub} = 0.1$	$p_{ub} = 0.15$	$p_t = 0.02$&$\rho_t = 0.1$	$p_t = 0.05$&$\rho_t = 0.1$
				$\rho_{lb} = 0$	$\rho_{lb} = 0.05$	$\rho_{lb} = 0.03$	$\rho_{lb} = 0.03$	$\rho_{lb} = 0.03$	$\rho_{lb} = 0.03$	$p_t = 0.02$&$\rho_t = 0.03$	$p_t = 0.05$&$\rho_t = 0.03$
s	p_1	ρ_1	[1]	[2]	[3]	[4]	[5]	[6]	[7]	[8]	[9]
0	**0.01**	**0.05**	**17220.22**	**15278.0**	**15990.43**	**16904.32**	**16686.38**	**16903.36**	**16976.5**	**17100.65**	**16739.36**
	0.02	**0.05**	798.73	823.06	724.54	814.00	860.71	904.04	926.66	816.29	1127.53
	0.03	**0.05**	331.64	346.44	314.10	345.83	326.93	339.58	345.46	342.96	348.52
	0.04	**0.05**	209.31	217.74	196.71	218.75	190.19	194.88	197.60	215.59	188.55
	0.05	**0.05**	153.97	159.57	144.13	159.84	131.51	132.81	134.15	157.10	125.44
	0.06	**0.05**	121.54	126.90	114.66	126.36	100.08	99.10	100.25	123.76	96.02
	0.08	**0.05**	86.65	89.87	81.53	89.13	67.28	65.34	65.86	87.30	63.14
	0.1	**0.05**	67.31	70.17	63.10	69.24	50.81	48.34	48.40	68.05	47.68
	0.2	**0.05**	33.57	34.03	30.49	33.42	23.24	21.26	20.46	32.46	21.89
	0.3	**0.05**	23.67	22.60	19.99	21.94	15.44	14.00	13.11	21.04	14.68
	0.4	**0.05**	19.23	16.96	15.11	16.23	11.79	10.68	9.77	15.71	**11.29**
	0.5	**0.05**	16.80	13.43	12.12	12.79	9.78	8.78	7.90	12.26	9.16
$\pm\infty$	**0.01**	**0.01**	14262.62	8440.12	16932.96	12791.63	14165.64	15120.47	15702.9	16003.30	17378.88
	0.01	**0.02**	14882.40	10371.76	17263.50	14778.62	15707.13	16498.05	17086.1	16696.21	17435.56
	0.01	**0.03**	15601.81	12218.58	17340.08	16362.76	16605.47	17169.87	17529.2	17228.42	17286.28
	0.01	**0.04**	16402.86	14197.18	16971.21	17148.16	16916.55	17300.14	17564.2	17217.24	17029.00
	0.01	**0.05**	**17220.22**	**15278.0**	**15990.43**	**16904.32**	**16686.38**	**16903.36**	**16976.5**	**17100.65**	**16739.36**
	0.01	**0.075**	19653.37	13460.36	12068.92	13226.75	13985.94	14269.67	14193.1	17226.51	16041.93
	0.01	**0.1**	21701.27	9731.66	8296.72	9140.38	10289.28	10487.34	10464.6	14876.06	14837.71
	0.01	**0.15**	27088.45	5517.15	4835.73	5199.98	6047.77	6218.07	6220.12	11113.59	12396.19
	0.01	**0.2**	33927.04	3852.64	3361.93	3596.81	4220.81	4360.79	4329.67	8348.48	10248.66
	0.01	**0.35**	62352.31	2004.19	1813.15	1910.15	2225.64	2311.53	2250.88	4247.41	5397.37
	0.01	**0.4**	71275.41	1759.75	1591.98	1676.22	1951.04	2002.64	1946.43	1093.99	1482.19
	0.01	**0.5**	85141.29	1440.06	1306.82	1363.94	1566.97	1608.72	1528.47	902.83	1145.73
	0.01	**0.7**	49729.94	1171.21	1083.40	1132.39	1220.85	1252.41	1140.94	810.08	892.56
		h	**3.1541**	**3.7242**	**3.3547**	**3.5376**	**4.3955**	**4.7089**	**4.8460**	**3.3604**	**4.0678**
										3.4534	**4.0579**

The last case we look at here is a high quality process with $p_0 = 0.001$ and $\rho_0 = 0.2$. Table 4.12 shows the SSANOS values of four GLR-$p\rho$ charts with $\rho_{ub} = 0.3, \rho_{lb} = 0.15$, and $p_t = 0.002, 0.005, 0.01$ and 0.15 respectively. Columns [5]-[8] list the SSANOS values of four CUSUM- $p\rho$ chart combinations with $\rho_{t,1} = 0.3, \rho_{t,2} = 0.15$, and $p_t = 0.002$, 0.005, 0.01 and 0.015. The overall comparisons show that no matter which direction the shift

Table 4.12 SSANOS values of the GLR-$p\rho$ and CUSUM- $p\rho$ chart combinations with $p_0 = 0.001, \rho_0 = 0.2$ and $s = 2, 5, 10, 15, -2.5$ and 5

			GLR-$p\rho$				CUSUM-$p\rho$ Combination			
			$p_{ub} = 0.002$	$p_{ub} = 0.005$	$p_{ub} = 0.01$	$p_{ub} = 0.015$	$p_t = 0.002$ &$\rho_t = 0.3$	$p_t = 0.005$ &$\rho_t = 0.3$	$p_t = 0.01$	$p_t = 0.015$ &$\rho_t = 0.3$
			$\rho_{lb} = 0.15$	$\rho_{lb} = 0.15$	$\rho_{lb} = 0.15$		$p_t = 0.002$ &$\rho_t = 0.15$	$p_t = 0.005$ &$\rho_t = 0.15$	&$\rho_t = 0.3$ $p_t 0.01$	$p_t = 0.015$ &$\rho_t = 0.15$
s	p_1	ρ_1	$\rho_{lb} = 0.15$ [1]	$\rho_{ub} = 0.3$ [2]	$\rho_{ub} = 0.3$ [3]	$\rho_{ub} = 0.3$ [4]	[5]	[6]	$\rho_t = 0.15$ [5]	[6]
	0.001	**0.2**	**16836.97**	**16967.30**	**16721.87**	**17192.75**	**16960.63**	**16957.24**	**18523.27**	**18138.34**
	0.002	**0.2025**	3483.57	2914.70	2932.83	3066.71	3406.97	3550.64	4412.60	4705.89
	0.005	**0.21**	809.14	470.52	465.50	476.65	804.84	677.96	820.46	897.19
	0.01	**0.2225**	358.97	157.46	154.29	157.48	361.73	268.21	295.83	314.78
2.5	**0.02**	**0.2475**	170.52	67.82	67.99	68.06	179.06	127.72	131.01	135.45
	0.05	**0.3225**	66.98	29.38	29.66	29.63	72.61	55.38	55.56	55.96
	0.08	**0.3975**	44.34	20.84	20.76	20.75	47.67	37.79	38.04	38.11
	0.1	**0.4475**	37.67	18.07	18.12	18.06	39.91	32.27	32.44	32.58
	0.15	**0.5725**	30.12	15.56	15.52	15.64	31.20	25.77	25.95	26.08
	0.2	**0.6975**	28.70	16.50	16.49	16.58	29.03	24.78	24.92	25.18
	0.002	**0.205**	3479.99	2907.75	2936.62	3065.73	3408.01	3562.16	**4425.74**	4709.54
	0.005	**0.22**	819.12	481.08	475.60	491.37	810.58	689.76	**832.76**	914.97
	0.01	**0.245**	368.04	164.67	162.32	164.09	369.86	276.80	304.11	326.67
5	**0.02**	**0.295**	180.16	73.35	72.80	73.13	187.03	135.68	139.42	144.29
	0.04	**0.395**	94.06	41.43	41.44	41.42	99.88	75.87	76.41	76.99
	0.05	**0.445**	78.67	35.98	36.11	36.03	83.56	64.61	64.80	65.94
	0.08	**0.595**	59.68	30.98	30.77	30.89	62.20	50.87	51.17	51.74
	0.1	**0.695**	57.50	32.69	32.74	32.81	59.15	49.74	50.10	51.25
	0.002	**0.21**	3527.34	2929.18	2969.79	3107.81	3441.75	3613.61	4456.33	4723.23
	0.005	**0.24**	842.73	500.11	498.22	513.88	830.51	714.98	863.65	950.31
10	**0.01**	**0.29**	387.77	178.38	175.99	177.79	386.86	296.01	**327.34**	352.65
	0.02	**0.39**	201.87	86.52	85.98	85.90	204.68	153.54	**159.96**	167.04
	0.04	**0.59**	125.80	61.48	61.61	62.05	127.04	103.11	104.59	107.97
	0.05	**0.69**	118.26	65.21	65.23	65.45	118.88	100.55	103.65	106.31
	0.002	**0.215**	3576.96	2973.71	3025.43	3127.20	3450.66	3624.22	4548.16	4798.82
15	**0.005**	**0.26**	868.99	520.35	517.54	529.83	851.88	737.23	884.30	984.30
	0.01	**0.335**	411.45	195.45	191.95	195.77	406.65	317.58	350.34	379.70
	0.02	**0.485**	227.79	105.91	103.93	104.92	225.98	178.37	188.18	197.15
	0.04	**0.785**	192.06	124.95	124.85	126.35	187.98	171.77	179.80	187.85
	0.002	**0.1975**	3451.84	2830.92	2904.36	3022.39	3374.47	3500.11	**4371.89**	4658.65
	0.005	**0.19**	788.40	451.66	451.46	460.26	781.11	657.22	789.01	874.43
	0.01	**0.1775**	339.30	146.30	144.18	144.22	345.98	252.01	277.32	295.44
-2.5	**0.02**	**0.1525**	152.95	59.62	59.36	60.28	163.13	114.37	116.85	119.54
	0.04	**0.1025**	63.92	28.01	27.88	27.85	72.93	54.58	54.88	54.92
	0.05	**0.0775**	47.98	21.74	21.69	21.61	54.65	42.81	42.83	42.81
	0.08	**0.0025**	26.61	12.48	12.58	12.45	28.93	25.12	**25.23**	25.33
	0.002	**0.195**	3432.44	2839.31	2889.42	3002.31	3348.02	3470.72	**4373.64**	4641.03
-5	**0.005**	**0.18**	777.00	443.56	438.92	451.10	772.49	646.67	779.96	856.82
	0.01	**0.155**	331.29	139.92	139.30	139.82	337.16	244.43	268.55	284.70
	0.02	**0.105**	143.20	56.42	56.27	56.38	155.91	109.21	111.44	113.32
	0.04	**0.005**	55.57	25.09	25.09	25.00	64.69	49.57	50.06	49.85
		h	**1.4681**	**2.0852**	**2.2911**	**2.4693**	**1.2555**	**1.7507**	**1.9739**	**2.0098**
							1.5051	**1.6965**	**2.0253**	**1.9327**

occurs in, the overall performance of the GLR-$p\rho$ charts with $p_t = 0.005, 0.01,$ and 0.15 in columns [2]-[4] are much better than the other charts. There is no large difference in the SSANOS values for the three charts when the shifts are moderate and large. Table 4.12 shows that the advantage of the GLR-$p\rho$ chart compared to the CUSUM- $p\rho$ chart combination is clearer in a high quality process when two parameters shift simultaneously.

Table 4.13 SSANOS values of the GLR-$p\rho$ and CUSUM- $p\rho$ chart combinations with $p_0 = 0.001, \rho_0 = 0.2$ and $s = \pm\infty$ and 0

			GLR-$p\rho$				CUSUM-$p\rho$ Combination			
			$p_{ub} = 0.002$	$p_{ub} = 0.005$	$p_{ub} = 0.01$	$p_{ub} = 0.015$	$p_t = 0.002$ &$\rho_t = 0.3$	$p_t = 0.005$ &$\rho_t = 0.3$	$p_t = 0.01$	$p_t = 0.015$ &$\rho_t = 0.3$
				$\rho_{lb} = 0.15$	$\rho_{lb} = 0.15$	$\rho_{lb} = 0.15$	$p_t = 0.002$ &$\rho_t = 0.15$	$p_t = 0.005$ &$\rho_t = 0.15$	&$\rho_t = 0.3$ p_t0.01	$p_t = 0.015$ &$\rho_t = 0.15$
s	p_1	ρ_1	$\rho_{lb} = 0.15$ [1]	$\rho_{ub} = 0.3$ [2]	$\rho_{ub} = 0.3$ [3]	$\rho_{ub} = 0.3$ [4]	[5]	[6]	$\rho_t = 0.15$ s	p_1
	0.001	**0.2**	**16836.97**	**16967.30**	**16721.87**	**17192.75**	**16960.63**	**16957.24**	**18362.62**	**18101.51**
	0.002	**0.2**	3463.23	2880.53	2898.13	3023.24	3385.32	3543.66	4385.80	4649.29
	0.005	**0.2**	799.12	460.98	456.71	469.79	793.30	667.44	806.82	886.03
	0.01	**0.2**	348.99	151.03	148.98	152.20	353.57	259.25	285.57	305.46
0	**0.02**	**0.2**	160.75	63.54	63.20	63.69	171.37	120.92	124.35	126.92
	0.04	**0.2**	72.84	31.32	31.30	31.23	81.08	60.07	60.44	60.70
	0.05	**0.2**	56.26	24.94	25.00	25.03	63.22	48.44	48.59	48.40
	0.1	**0.2**	27.58	12.46	12.53	12.49	29.19	24.43	24.44	24.47
	0.2	**0.2**	14.33	6.20	6.27	6.26	14.62	12.61	12.65	12.61
	0.001	**0.03**	11335.93	11073.82	11306.58	11548.61	11166.00	12350.33	14475.11	13697.54
	0.001	**0.05**	12200.87	11815.26	12016.59	12215.12	11376.26	12938.55	14934.19	14301.04
	0.001	**0.1**	14437.10	13802.32	13816.60	14025.18	11890.96	14337.76	16137.97	15439.36
	0.001	**0.15**	16238.56	15643.70	15563.96	15751.84	12254.37	15728.32	17315.64	16732.13
	0.001	**0.2**	**16836.97**	**16967.30**	**16721.87**	**17192.75**	**16960.63**	**16957.24**	**18362.62**	**18101.51**
inf	**0.001**	**0.25**	16296.10	17089.32	17140.85	17813.14	16938.75	17880.84	19596.10	19522.93
	0.001	**0.3**	14814.98	16079.09	16344.18	17118.26	16578.16	18601.68	20616.21	20919.95
	0.001	**0.4**	11783.39	13172.01	13697.83	14439.41	14727.02	19228.50	21851.54	22924.48
	0.001	**0.5**	9653.92	11003.16	11512.41	12237.05	12911.18	18294.14	21232.25	22685.94
	0.001	**0.6**	8434.22	9799.77	10323.08	10925.32	11592.68	16630.34	18802.72	19854.10
	0.001	**0.8**	8690.15	10033.13	10399.72	10877.57	11091.16	13843.32	14308.22	14393.34
			11335.93	11073.82	11306.58	11548.61	11166.00	12350.33	14475.11	13697.54
		h	**1.4681**	**2.0852**	**2.2911**	**2.4693**	**1.2555**	**1.7507**	**1.9739**	**2.0098**
							1.5051	**1.6965**	**2.0253**	**1.9327**

In the end, we will look at Table 4.13, which provides the comparisons when the shift occurs only in the proportion or in the correlation. When $s = 0$ and the pre-determined shifts p_t and $\rho_t's$ of the CUSUM- $p\rho$ chart combination are equal to p_{ub}, ρ_{ub} and ρ_{lb}, respectively, the performance of the GLR-$p\rho$ chart is better than the CUSUM- $p\rho$ chart combination except for very small shifts in the proportion.

When $s = \infty$, we found that the performance of all the charts is bad, i.e. the shift in correlation is very difficult to detect in the high quality process. When $\rho_1 = 0.8$, which is a large shift and 4 times of the in-control correlation, for most of the charts, it takes more than 10,000 observations to detect the shift. Under this overall bad performance, we found that the GLR-$p\rho$ chart can still beat the CUSUM- $p\rho$ chart combination for both increases and decreases in correlation except at very small decreases.

4.5.3.2 Conclusions

In this section, we compared the performance of the GLR-$p\rho$ chart with the CUSUM- $p\rho$ chart combination. When there are simultaneous shifts in proportion and correlation, and as the upper bound for the proportion p_{ub} gets larger, the GLR-$p\rho$ chart has better overall performance than that with a smaller p_{ub} assuming the charts have the same ρ_{ub} and ρ_{lb} for correlation. We found $p_{ub} > 0.05$ can provide good performance over a wider ranges of the shifts when $p_0 = 0.01$. It is noted that the specification of the lower bound for correlation affects the performance of the chart. A lower bound on correlation p_{lb} is needed so that the GLR-$p\rho$ chart can have better performance when there are increases in both correlation and proportion. However, when the correlation decreases, the GLR-$p\rho$ chart without a positive lower bound on correlation is more effective.

When a shift occurs only in the proportion, the MBGLR chart performs well when the shift is smaller than or close to p_{ub}. With the same p_{ub}, the GLR-$p\rho$ chart has slightly worse performance than the MBGLR chart when the shift is smaller than or equal to p_{ub}, but when the shift gets larger, the GLR-$p\rho$ chart can detect the shift faster than the MBGLR chart. When a shift occurs only in the correlation, the GLR-$p\rho$ chart cannot detect small shifts in correlation as well as the CUSUM-$p\rho$ chart, but neither chart is effective in this case.

In general, the overall performance of the GRL-$p\rho$ chart is better than that of the CUSUM-$p\rho$ chart combination when the shifts are unknown, especially in a high quality process. The GRL-$p\rho$ only works poorly when the shifts occur only in the correlation. However, in this case, the other control charts do not work very well either.

4.6 Simulated Data Example

In the previous subsections, we discussed the performance of the CUSUM-$p\rho$ chart, the CUSUM-$p\rho$ chart combination, and the GLR-$p\rho$ chart. In this section, we will use a simulated data example to illustrate the monitoring process.

First, we simulated 100,000 in-control binary observations from $p_0 = 0.01$ and $\rho = 0.05$ as Phase I. Then in Phase II, we first simulated 1,000 in-control observations to allow the

process to reach a steady state. Then 2,000 out-of-control observations are simulated from $p_1 = 0.02$ and $\rho_1 = 0.1$. In this case, both the proportion and the correlation increased.

Using Equation (3.1), the estimated proportion and correlation from the Phase I data are $\hat{p}_0 = 0.0101$ and $\hat{\rho}_0 = 0.0507$ from the Phase I data. The corresponding transition probabilities are $p_{01} = 0.0096$ and $p_{11} = 0.0603$. The control limits used for the charts are specified using the estimated parameters and desired ICANOS values. Here, we use ICANOS=16890.0 as in our simulation study. In Phase II, we use two CUSUM $-p\rho$ charts, one CUSUM $-p\rho$ chart combination, and one GLR$-p\rho$ chart to monitor the process.

Figure 4.2 shows the plot of the transitions between 0 and 1 for Phase II of the simulated data according to whether $(X_{k-1}, X_k) = (1,0), (0,0), (1,1)$, and $(0,1)$. The representation of (X_{k-1}, X_k) corresponds to the increasing order of the likelihood ratio. From Figure 4.2, with small p_1, most of the transitions are $(X_{k-1}, X_k) = (0,0)$ and the plot shows a horizontal solid line. It is also noted that after the change point, at observation 1000, there is increase in the number of $(1,0)$ transitions or corresponding $(0,1)$ transitions

Figure 4.2 Transitions of the Phase II data according to the value of (X_{k-1}, X_k)

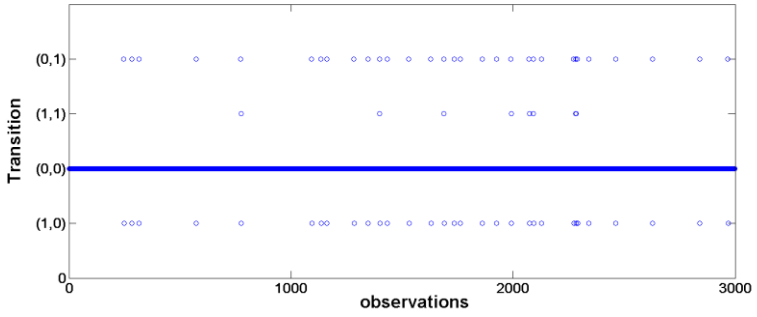

Figures 4.3 shows the monitoring process in Phase II using two individual CUSUM$-p\rho$ charts. The first 1,000 observations are in-control and the remaining 2,000 observations are out-of-control. The upper chart in Figure 4.3 is the CUSUM $-p\rho$ chart with $p_t = 0.02, \rho_t = 0.1$, where the actual shifts are equal to the pre-determined shifts. With $\hat{p}_0 = 0.0101$, $\hat{\rho}_0 = 0.0507$ and ICANOS $= 16890.00$, the control limit is $h = 3.0509$. This chart detects the shift in 691 observations. The lower chart in Figure 4.3 is the CUSUM$-p\rho$ chart with $p_t = 0.02$ and $\rho_t = 0.03$. The control limit is 3.1342 and the shift is detected at the 1075th observation after the change point. In this case, it is not surprising that the upper CUSUM $-p\rho$ chart signals

first, because the actual shifts are the same as the shifts that the CUSUM$-p\rho$ chart is designed to detect.

Figure 4.3 Monitoring Phase II using the CUSUM$-p\rho$ charts

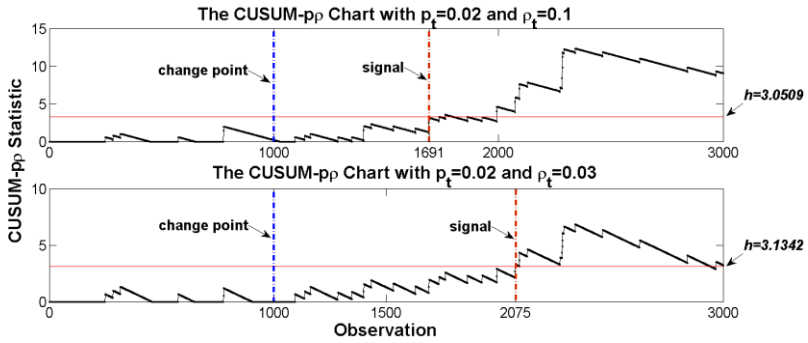

Figure 4.4 shows the monitoring process using the CUSUM-$p\rho$ chart combination. In Figure 4.4, the upper chart is the CUSUM$-p\rho$ chart with $p_t = 0.05, \rho_t = 0.15,$ and the lower one is the CUSUM$-p\rho$ chart with $p_t = 0.05, \rho_t = 0.03$. The control limits for the two charts are 4.6078 and 4.4330, respectively. The CUSUM$-p\rho$ chart with $p_t = 0.05, \rho_t = 0.15$ in the chart combination signals at observation 2093 and the number of observations to signal is 1093. This signals faster than the CUSUM$-p\rho$ chart with $p_t = 0.05, \rho_t = 0.03$ and therefore the chart combination signals at the 1093th observation after the change point. The actual shift in the proportion is not close to $p_t = 0.05$ in the CUSUM-$p\rho$ chart combination and the chart combination signals slower than both of the two individual CUSUM-$p\rho$ charts with $p_1 = p_t$ in Figure 4.3. This result is consistent with the simulation results discussed in Section 4.4, from which we conclude the CUSUM-$p\rho$ chart works well when the tuning parameters are correctly specified.

Figure 4.4 Monitoring using the CUSUM$-p\rho$ chart combination

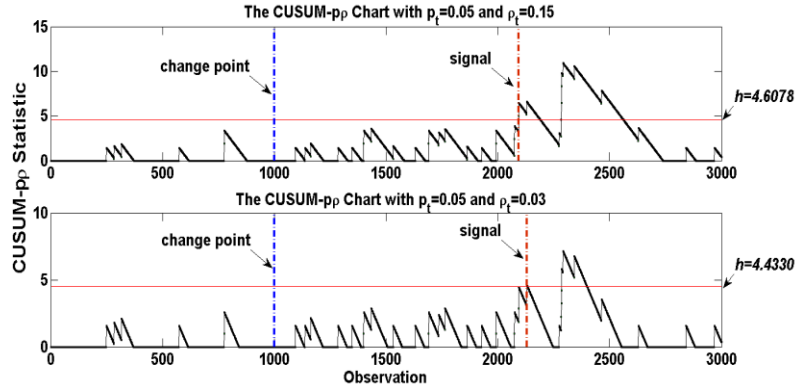

In the end, we use the GLR-$p\rho$ chart with $p_{ub} = 0.05, \rho_{ub} = 0.15$, and $\rho_{lb} = 0.03$ to monitor the Phase II data. The bounds of the GLR-$p\rho$ chart are set to be the same as the tuning parameters values in the CUSUM-$p\rho$ chart combination, which are not very close to the actual shifts. With the estimated in-control parameters and desired ICANOS, $h = 4.4297$. In Figure 4.5, the number of observations to signal for the GLR-$p\rho$ chart is 993. It is noted that the GLR-$p\rho$ chart does not signal as fast as the CUSUM-$p\rho$ chart with p_t and ρ_t both correctly specified in Figure 4.3, but the detection of the GLR-$p\rho$ chart is faster than the CUSUM-$p\rho$ chart combination in Figure 4.4. This result confirms the comparisons between the GLR-$p\rho$ chart and the CUSUM-$p\rho$ chart combination in Section 4.5: the CUSUM-$p\rho$ chart combination does not work very well when the tuning parameters are not close to the actual shifts, but the GLR-$p\rho$ chart works well on a wide range of shifts.

Figure 4.5 Monitoring using the GLR$-p\rho$ chart

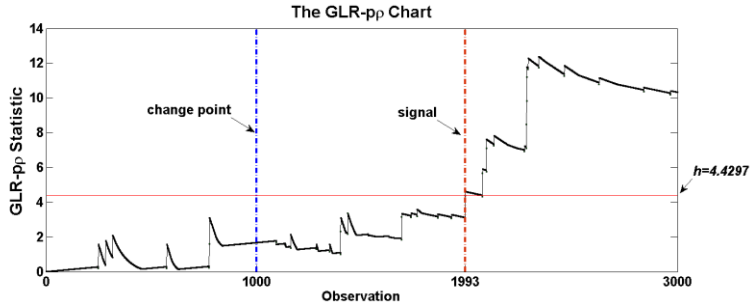

Figure 4.6 The estimated $\hat{p}_1, \hat{\rho}_1$, and $\hat{\tau}$ of the GLR-$p\rho$ chart

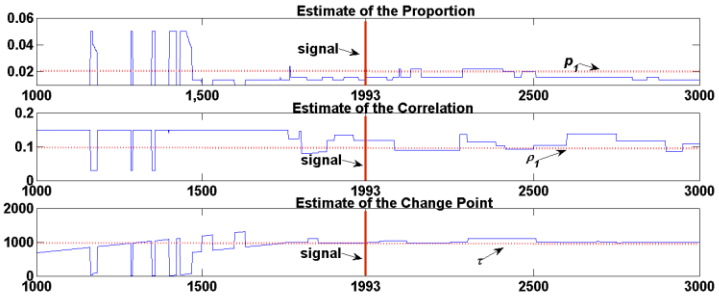

Figure 4.6 shows the value of $\hat{p}_1$, $\hat{\rho}_1$, and $\hat{\tau}$ estimated when the GLR-$p\rho$ chart is applied to monitor the process. Figure 4.6 shows that the estimation of shifts and change point are stable when the GLR-$p\rho$ chart signals at observation 1993 with $\hat{p}_1 = 0.011$, $\hat{\rho}_1 = 0.130$, and $\hat{\tau} = 1010$. The estimate of the proportion is not very close to the actual shift, because there were

relatively few defectives observed between the estimated change point and the signal point at observation 1993.

4.7 Conclusions

In Chapter 4, we discussed the monitoring process when there are shifts in the proportion and correlation of the correlated binary process. The work in this chapter is an extension from the MBCUSUM chart and the MBGLR chart. In this chapter, we proposed the CUSUM-$p\rho$ chart, the CUSUM-$p\rho$ chart combination, the three-CUSUM combination, and the GLR-$p\rho$ chart to monitor the two parameters. The performance of the charts was compared by simulation and it was concluded that the overall performance of the CUSUM-$p\rho$ chart combination is better than using an individual CUSUM-$p\rho$ chart, while a GLR-$p\rho$ chart has better performance than the CUSUM-$p\rho$ chart combination when the shifts are unknown. The GLR-$p\rho$ chart with a relatively large upper bound for p can detect a very wide range of shifts. When monitoring a high quality process, the advantage of the GLR-$p\rho$ chart is more obvious.

In general, it is suggested that in the unlikely case in which the shifts in proportion and correlation are both known, a CUSUM-$p\rho$ chart can be used to achieve good performance. When the shifts values are unknown, but there is information about the possible shift ranges, we could use a CUSUM-$p\rho$ chart combination and set the pre-determined shifts close to the middle of ranges where the shifts could reasonably occur. With no information about the shifts, a GLR-$p\rho$ chart with a relatively large upper bound on the proportion is suggested. A lower bound on the correlation will help improve the performance of the chart when there are increases in both correlation and proportion. We found that with a relatively large upper bound on the proportion and with bounds for the correlation that are not very far away from the in-control proportion, the GLR-$p\rho$ chart has good overall performance.

To use the GLR-$p\rho$ chart in practice, we would need to specify the control limit for the chart. The control limits of the GLR-$p\rho$ charts discussed in this chapter were obtained from a linear equation of the control limit and $log(\text{ICANOS})$ using the simulated data for each specific parameter settings (similar to Equation (3.5) in Chapter 3). In Chapter 3, we found that the intercept and the slope of the equation have a linear relationship with p_0, ρ_0 and p_{ub} for the

MBGLR chart (see Equations (3.3) and (3.4) in Chapter 3). The GLR-$p\rho$ chart has two more parameters ρ_{ub} and ρ_{lb} compared to the MBGLR chart and therefore the equations for the intercept and the slope with in-control parameters and the bounds can be more complicated than Equations (3.3) and (3.4) in Chapter 3 for the MBGLR chart. However, the design of the GLR-$p\rho$ chart is still easier than the design of the CUSUM-$p\rho$ chart combination, as there is only one control limit that needs to be specified for the GLR-$p\rho$ chart but there are two control limits that need to be specified and adjusted with each other for the CUSUM-$p\rho$ chart combination.

Chapter 5. The GLR Chart for Monitoring Correlated Binary Data when $n > 1$

5.1 Process Description and Sampling Plan

In Chapters 3 and 4, the correlated binary observations were inspected from a continuous stream and the sample size was $n = 1$. It sometimes happens in practice that the binary observations are aggregated into samples of size $n > 1$. In this chapter, we assume that samples of size n are taken at each sampling point and these samples are far enough apart in time to assume independence between samples, but there is still correlation between the observations in a sample. In this case, we will assume that a shift in the proportion can only occur in the time interval between samples and thus that the binary observations within one sample will have the same proportion of defectives. In this chapter, we assume the correlation remains at the target value as in Chapter 3 as the shift in proportion in the primary concern in a process. This chapter includes the derivation of the proposed GLR chart for the case when $n > 1$, and the chart comparisons when the in-control proportion is $p_0 = 0.01$ and sample size $n = 100$ and 10.

The number of defectives in a sample T is assumed to follow the Markov Binomial distribution $MB\ (n, p, \rho)$ suggested by Weiss (2009). The distribution of T is given by:

$$f(t|p,\rho) = \begin{cases} (1-p)p_{00}^{n-1}, & t = 0 \\ pp_{11}^{t-1}p_{10}^{2}p_{00}^{n-t-2}\sum_{a=0}^{2}\binom{2}{a}\left(\frac{p_{00}}{p_{10}}\right)^{a} \\ \times \sum_{r=0}^{t-1}\binom{n-t-1}{r+1-a}\binom{t-1}{r}\left(\frac{p_{01}p_{10}}{p_{00}p_{11}}\right)^{r}, & 0 < t < n \\ pp_{11}^{n-1}, & t = n \end{cases} \tag{5.1}$$

where $E(T) = np,\ V(T) = np(1-p)\frac{1+\rho}{1-\rho}\left(1 - \frac{2\rho(1-\rho^n)}{n(1-\rho^2)}\right) \approx np(1-p)\frac{1+\rho}{1-\rho}$ for larg n. It is noted that the binomial distribution is a special case of the Markov binomial distribution when $\rho = 0$.

5.2 Derivation and Design of the GLR Chart

Consider the sequence T_1, T_2 ... representing the number of defectives from a sequence of samples of size n, where these samples are assumed to be independent. The hypothesis about the process proportion change assumes that there is an increase in p to p_1 that occurs between samples τ and $\tau + 1$. Therefore the likelihood at the s^{th} sample under the null hypothesis is

$$L_k(\infty, p_0, p_0, \rho | t_1, \dots, t_s) = \prod_{i=1}^{s} f(t_i | \infty, p_0, \rho)$$

And under the alternative hypothesis, the likelihood is

$$L_k(\tau, p_0, p_1, \rho | t_1, \dots, t_s) = \prod_{i=1}^{\tau} f(t_i |\, p_0, \rho) \prod_{i=\tau+1}^{s} f(t_i | p_1, \rho)$$

Then the GLR statistic at sample s is

$$R_s = ln \frac{\max\limits_{0 \le \tau < s, p_0 < p_1 \le 1} L_k(\tau, p_0, p_1, \rho | t_1, \dots, t_s)}{L_k(\infty, p_0, p_0, \rho | t_1, \dots, t_s)} = \max_{0 \le \tau < s, p_0 < p_1 \le 1} \sum_{i=\tau+1}^{s} ln \frac{f(t_i | p_1, \rho)}{f(t_i | p_0, \rho)}$$

If a window of size m is applied to the GLR statistic, then the control statistic can be written as

$$R_s = \max_{\max(0, k-m-1) \le \tau < s} \sum_{i=\tau+1}^{s} \ln\left(\frac{f(t_i |\, \hat{p}_1, \rho)}{f(t_i | p_0, \rho)}\right)$$

where $\hat{p}_1 = \max(p_0, \hat{p}_{MLE})$. Here $\hat{p}_{MLE}$ is the MLE of p_1 and is obtained by the grid search method as was done for the case with $n = 1$ in Chapters 3 and 4. In Chapters 3 and 4, an upper bound is needed for $\hat{p}_1$ in the MBGLR chart and the GLR-$p\rho$ chart. We found the upper bound is not necessary in the case with $n > 1$, as the discreteness problem is not severe as the case with $n = 1$. The Markov binomial GRL statistic will signal if $R_s \ge h_T$, where h_T is a pre-determined control limit chosen to achieve the desired in-control performance. We call this chart the Markov binomial GLR chart and it will be referred as the MBNGLR chart in later sections.

To apply this MBNGLR chart, the window size and the control limit need to be specified. The observations stored in the window are the values of T_s. Simulation results (not shown here) confirmed that the window size m in the MBNGLR chart can be determined in the same way as

m for a MBGLR chart, i.e. m can be chosen to satisfy $n * m = \text{ICANOS}$, which is sufficiently large to obtain almost the same performance as the MBNGLR chart with no window, in terms of detecting even a very small shift. We will follow this rule and choose m be a value rounded to the hundred as close as possible to $\frac{\text{ICANOS}}{n}$.

Preliminary results using particular values of p_0 and n show that the control limit has a linear relation with log-scale of ICANOS similar as in the correlated binary case. Based on the preliminary results, we expect to get a fitted linear regression line for obtaining the control limit as the case with $n = 1$. More work is needed on determining h, and this future work will be discussed more in the next chapter.

5.3 Chart Performance Comparisons

In this section, we will compare the performance of the MBNGLR chart with several traditional control charts and a modified GLR chart for detecting shifts in p when the number of defectives from each sample follows the Markov binomial distribution. The traditional control charts are modified from the original Shewhart and CUSUM charts with correlation accounted for in the distribution of the control statistics. We will first introduce the competing control charts for the MBNGLR chart and then discuss the numerical results of the comparisons.

5.3.1 Shewhart-Type Chart

Weiss (2009) suggested a Shewhart-type chart to monitor T_s. This Shewhart chart was designed to detect both increases and decreases in p. In the case in which only increases in p are being considered, a signal is given if $T_s > h_s$, where the control limit h_s is some positive integer. For a control limit h_s, the ICANOS satisfies

$$\text{ICANOS} = \frac{n}{P(T_s > h_s | p = p_0)}$$

Therefore, for this Shewhart-type chart, there will be only a few ICANOS values available corresponding to the integer values for h_s. When the chart performance is compared in a later section, h_s will be selected first and the corresponding ICANOS will be calculated from the above

equation. The other control charts will then be set to have in-control performance similar to this Shewhart-type chart.

5.3.2 CUSUM Chart

In Chapter 3, the MBCUSUM chart was considered for monitoring p when $n = 1$. When $n > 1$, we propose a Markov Binomial CUSUM (MBNCUSUM) chart with control statistic

$$C_s^n = \max\{0, C_{s-1}^n\} + L_s^n, \quad s = 1,2,3, \ldots \text{ and } C_{T_0} = 0$$

where

$$L_s^n = ln\frac{f(t_s|p_t, \rho)}{f(t_s|p_0, \rho)}$$

for some pre-determined shift p_t. Then the MBNCUSUM chart will signal if $C_s^n > h_c^n$, where h_c^n is the control limit for the MBNCUSUM chart. If the MLE of p_1 in the MBNGLR chart happens to always equal the pre-determined shift size p_t in the CUSUM chart, then the two charts will be equivalent if the control limits are the same.

5.3.3 Shewhart-CUSUM Chart Combination

It is known that the Shewhart-type chart is sensitive to large shifts and the MBNCUSUM chart is designed to detect a shift equal to p_t. Therefore one can combine the two types of charts with a small p_t used for the CUSUM chart to have better overall performance than using each chart individually. In the Shewhart-CUSUM combination, the pre-determind shift size p_t is selected to be relatively small and the CUSUM chart will then effectively detect a relatively small shifts. The Shewhart chart will easily detect the relatively large shifts. We use h_s and h_c^n to denote the control limits of the Shewhart and CUSUM charts, respectively, and they are selected so that the ICANOS of the combined chart achieves the same desired ICANOS as the Shewhart-type chart. However, unlike in the normal distribution case where we can easily find many combinations of h_s and h_c^n, it is not easy to find acceptable pairs of h_s and h_c^n in the correlated binomial case. The control limit h_s of the Shewhart chart in the combination can only take integer values, which provides us with very limited ICANOS values that are achievable. Therefore, we will first select an integer control limit for the Shewhart chart in the combination and then adjust the control limit of the CUSUM chart to obtain the desired ICANOS.

5.3.4 EWMA-GLR Chart

The original GLR algorithm maximize the likelihood ratio with $\hat{p}_1 = \hat{p}_{MLE}$. Another estimate for p_1 used in literature is an EWMA-type estimator which is a weighted sum of the cumulative information from the past sample and the current sample. The EWMA-type estimator was used by Lee, Wang, Peng and Sun (2012) in the GLR chart for monitoring shifts in proportions for multinomial observations and can avoid the case when $\hat{p}_{MLE}$ is estimated to be 0 or 1. For the GLR chart, consider the EWMA-type estimator of p_1 at the s^{th} sample:

$$\hat{p}_{1,s} = \lambda * \max(p_0, \hat{p}_{MLE}) + (1-\lambda)\hat{p}_{1,s-1}$$

where $s = 1, 2, \dots$, $\hat{p}_{1,0} = p_0$ and λ is a tuning parameter with $0 < \lambda \leq 1$. The parameter λ determines the rate at which new information enters into the calculation of the EWMA estimate. When $\lambda = 1$, the EWMA type estimates is equivalent to the estimate in the original GLR algorithm.

Based on the EWMA-type estimator, we propose an EGLR chart with statistic at sample s is

$$ER_s = \max_{0 \leq \tau < s} \sum_{i=\tau+1}^{s} ln \frac{f(t_i|\hat{p}_{1,s}, \rho)}{f(t_i|p_0, \rho)}$$

Applying a window size m to the EGLR statistic, the control statistic can be written as

$$ER_s = \begin{cases} \max\limits_{0 \leq \tau < s} \sum\limits_{i=\tau+1}^{s} \ln\left(\frac{f(t_i|\,\hat{p}_{1,s}, \rho)}{f(t_i|p_0, \rho)}\right), & if\ s < m \\ \max\limits_{s-m-1 \leq \tau < s} \sum\limits_{i=\tau+1}^{s} \ln\left(\frac{f(t_i|\hat{p}_{1,s}, \rho)}{f(t_i|p_0, \rho)}\right), & if\ s \geq m \end{cases}$$

A signal by the EGLR chart is given at sample s if $ER_s \geq h_{er}$, where the control limit h_{er} can be chosen to give specified in-control performance. The window size of the EGLR chart m can be chosen to satisfy $n * m = \text{ICANOS}$.

5.3.5 Chart Performance Comparisons

In this subsection, the MBNGLR chart is compared with the Shewhart chart, the MBNCUSUM chart, the Shewhart-CUSUM chart combination, and the EGLR chart when

$p_0 = 0.01$ and $\rho = 0.05$. We consider shifts smaller than 0.2, which is 20 times of the in-control proportion.

First we consider the case of $n = 100$. The Shewhart chart for this case has ICANOS $= 16956.24$ when $h_s = 4$. Then the other charts compared are set to have in-control performance close to 16956.24. The EGLR chart with $\lambda = 0.02$ and two CUSUM charts with $p_t = 0.015$ and 0.02 are shown in Table 4.2. The two Shewhart-CUSUM chart combinations are also shown in Table 4.2. The control limit of the Shewhart chart must increase when it is combined with the CUSUM chart so that the chart combination has the desired ICANOS. The MBNGLR chart and the EGLR charts have the window size equal to 200. From the discussion on window size, $n * m$ can be set at least equal to the number of $T_s's$, and m on average is about 169.5624. This storage volume is reasonable and does not cause a large calculation burden. Therefore we use a window size equal to 200 in all the simulation in this case.

In Table 5.1, even though it is desired that the ICANOS values of the eight charts to be close to 16956.24, for the CUSUM charts and Shewhart-CUSUM chart combinations it is difficult to get the ICANOS very close to 16956.24. When the SSANOS values are not close enough, it is unfair to compare the out-of-control SSANOS values and draw conclusions. Therefore we consider the ratio $v = \frac{\text{SSANOS}_{p_1}}{\text{ICANOS}} / \, min(\frac{\text{SSANOS}_{p_1}}{\text{ICANOS}})$ as a measure of the performance of the control chart as in Chapter 4.

The ratio v represent the comparison of the control chart to the best one to detect the shift to p_1 among the all charts. The larger v is, the worse the chart performance is. In Tables 5.1 and 5.2, the values of v are used to determine the color shading.

Table 5.1 shows that the performance of the Shewhart chart in column [1] at small shifts is bad compared with the other charts, but this chart can detect relatively large shifts such as those greater than 0.05 very fast. The MBNGLR chart in column [2] has overall better performance than most of the other charts. It can detect shifts from 0.02 to 0.2 relatively fast, but is worse only at very small shifts. The EGLR chart with $\lambda = 0.02$ can detect small shifts around 0.013 to 0.02 very fast, but cannot beat the other charts at moderate or large shifts. The CUSUM charts provide relatively good performance at shifts around p_t, but are worse at other shifts. For instance, when $p_t = 0.015$ in column [4], the CUSUM chart can detect shifts 0.013, 0.015, and

0.02 very fast, but does not work well for shifts greater than 0.025. We find that the Shewhart-CUSUM chart combination with $p_t = 0.015$ in column [6] provides overall performance that is as good as the MBNGLR chart. It is slightly better than the MBNGLR chart at very small shifts and slightly worse at large shifts. This is as expected as the Shewhart chart dominates the detection of large shifts and the MBNCUSUM chart with a small tuning parameter dominates the detection of small shifts. The other Shewhart-CUSUM chart combination in column [7] does not work as well as the one in column [6]. This indicates that that the selection of the tuning parameter and control limits significantly affects the performance of the chart combinations. Combined with a Shewhart chart, the CUSUM chart will have overall better performance than an individual CUSUM chart when using the same tuning parameter in the individual CUSUM chart as used in the chart combination.

Table 5.1 Comparisons of MBNGLR, EWMA-GLR, Shewhart, CUSUM, and Shewhart-CUSUM chart combinations with $p_0 = 0.01, \rho = 0.05, n = 100$

	Shewhart	MBNGLR	EGLR	MBNCUSUM		Shewhart-CUSUM	
			$\lambda = 0.02$	$p_t = 0.015$	$p_t = 0.02$	$p_t = 0.015$	$p_t = 0.02$
p	[1]	[2]	[3]	[4]	[5]	[6]	[7]
0.01	16929.65	16986.26	16690.46	16096.76	16154.84	16947.25	17702.05
0.013	6814.24	4030.48	3257.64	3296.75	3804.05	3358.94	3997.24
0.015	4233.35	2197.73	1840.04	1828.98	2047.78	1853.32	2109.46
0.02	1675.24	889.86	837.55	816.79	814.25	826.46	831.86
0.025	866.90	531.72	546.29	533.87	502.48	537.01	512.03
0.03	521.35	377.11	410.44	401.89	367.68	405.08	376.18
0.04	269.15	243.38	279.58	281.23	246.94	278.19	253.07
0.05	179.05	184.66	216.76	223.81	192.75	218.11	196.74
0.06	141.18	152.07	180.52	190.2	161.37	181.62	163.54
0.08	111.31	119.27	140.32	151.88	126.54	139.06	127.14
0.1	103.05	106.36	118.80	128.46	110.14	117.27	110.48
0.15	100.07	100.21	101.53	103.42	100.46	101.18	100.50
0.2	100.00	100.00	100.06	100.17	100.01	100.04	100.02
h	4.0000	3.6102	2.2441	2.5410	3.0900	$h_s = 7.0000$ $h_c = 2.4838$	$h_s = 7.0000$ $h_c = 3.1325$

In general, the MBNGLR chart can beat most of the control charts considered here with better overall performance over a wide range of shifts. The Shewhart- CUSUM chart combination is comparable with MBNGLR chart in terms of performance, but has the challenges of selection of appropriate tuning parameters and is more difficult to design due to combining of two types of charts with two control limits to specify. It is noted that usually the CUSUM chart designed to detect the shift equal to the tuning parameter has the best performance among all the charts at that shift, and the Shewhart chart is difficult to beat for large shift sizes.

The results of chart comparisons for a second case with $n = 10$ are presented in Table 5.2. With $h_s = 2$, the Shewhart chart has ICANOS $= 17256.5$, or equivalently ICANSS $= 1725.65$. The ICANOS values in the second case in Table 5.2 are set to be close to those in the first case in Table 5.1. This allows comparisons between the two sampling plans, one with a large sample size and one with a relatively small sample size. The window sizes used for the MBNGLR chart and the EGLR chart are set to be 2000. We will use the same tuning parameters λ and p_t respectively for EGLR charts and the MBNCUSUM charts as in Table 5.1.We reach similar conclusions as those from Table 5.1. The MBNGLR chart can beat most of the other types of charts with good overall performance as well as easy design.

Now we compare the two sampling plans. In Table 5.2, we see that using $n = 100$ gives a smaller SSANOS when detecting small shifts, while using $n = 10$ gives a smaller SSANOS when detecting large shifts. Therefore we conclude that taking small samples (which could presumably be taken frequently) would be better for detecting large shifts, while taking larger samples (which would presumably be taken less frequently) would be better for detecting small shifts.

Table 5.2 Comparisons of MBNGLR, EWMA-GLR, Shewhart, CUSUM, and Shewhart-CUSUM chart combinations with $p_0 = 0.01, \rho = 0.05, n = 10$

	Shewhart	MBNGLR	EGLR	MBNCUSUM		Shewhart-CUSUM	
			$\lambda = 0.02$	$p_t = 0.015$	$p_t = 0.02$	$p_t = 0.015$	$p_t = 0.02$
p	[1]	[2]	[3]	[4]	[5]	[6]	[7]
0.01	17250.06	17295.88	17198.34	17088.21	16803.13	16698.46	16505.43
0.013	10615.41	8153.81	7680.97	8419.95	8200.23	8227.38	7382.13
0.015	8045	4697.92	4140.04	4062.97	4459	4618.22	4320.49
0.02	4517.66	1890.74	1833.76	1753.11	1715.13	1832.74	1827.34
0.025	2823.78	1540.83	1546.85	1530.3	1425.59	1466.14	1538.12
0.03	1901.51	1177.11	1193.53	1181.04	1173.56	1157.95	1105.64
0.04	1003.88	950.61	990.01	978.43	946.94	933	958.19
0.05	604.4	672.75	716.76	713.81	795.86	785.56	720.09
0.06	398.47	429.46	427.53	430.98	454.75	443.58	420.28
0.08	207.21	227.43	230.23	245.55	231.46	220.48	227.49
0.1	125.76	135.21	139.72	139.75	137.23	138.69	139.18
0.15	53.2	56.89	59.53	59.33	60.24	62.33	58.74
0.2	30.75	32.78	34.39	35.95	38.01	37.14	38.06
h	2.0000	6.1753	4.8645	2.8160	3.7096	$h_s = 4.0000$ $h_c = 2.9816$	$h_s = 4.0000$ $h_c = 2.0966$

It is noted that when shift size is large, for instance $p = 0.15$, using $n = 100$, requires to at least one sample to detect a shift, and therefore the SSANOS is always at least 100. The comparisons between $n = 100$ and $n = 10$ based on the SSANOS can be a bit misleading when

shifts are large. We can consider using the steady state average time to signal (SSATS) instead of the SSANOS. The SSATS is related to the SSANOS by the equation: $\text{SSATS} = \frac{\text{SSANOS}}{n} * d - (\frac{d}{2})$, where d_t is the time difference between two consecutive samples. For example, assume in the first sampling plan that samples of $n = 100$ are taken every 10 hours, while in the second sample plan sample of $n = 10$ are taken every hour. We compare the SSATS value of the MBNGLR chart for large shifts. With $n = 100$, the SSANOS value is 100 for shift of size 0.2 and then this corresponds to an SSATS value of 5 hours. With $n = 10$, the SSANOS value is 32.78 for shift of size 0.2 and the corresponding SSATS values is 2.778 hours. We again obtain the conclusions that the sampling plan with $n = 10$ can detect shifts faster than the plan with $n = 100$, but the relative difference in performance has changed a bit.

5.4 Discussion

In section 5.3, the proposed MBNGLR chart was compared to the Shewhart, MBNCUSUM, Shewhart-CUSUM combination, and the EGLR charts. The performance of the charts was compared based on the ratio of $\frac{\text{SSANOS}}{\text{ICANOS}}$ and the MBNGLR chart was recommended based on its overall good performance and the ease with which it can be designed. Evaluation of different sampling plans indicated that taking samples frequently, i.e. with small sample size is suggested for detecting large shifts, while a large sample size is suggested for detecting small shifts. This conclusion is also confirmed by simulation results (not shown here) for Shewhart, MBNGLR and MBNCUSUM charts when $p_0 = 0.1$.

Chapter 6. Conclusion and Future Work

6.1 Conclusions

The first part of the dissertation focuses on monitoring the process proportion with binary data following the two-state Markov chain model. The binary observations are assumed to come from a continuous stream and will be available for inspection immediately. The sample size is considered to be $n = 1$. Binary processes can be well monitored by the traditional types of charts when the observations are independent. The Shewhart types chart can detect large shifts very well while the CUSUM-type charts can be designed to detect shifts according to the tuning parameter selected. However, when correlation, is present, these traditional charts do not have robust in-control performance. In this situation, the MBCUSUM chart proves to be a better choice because it takes the correlation into account as well as has overall good performance in detecting changes in proportion.

We proposed the Markov binary GLR chart with an upper bound as a tuning parameter. The MBGLR chart is shown to quickly detect shifts less than or equal to the upper bound. The design of the MBGLR chart requires the specification of the window size, control limit, and the upper bound. The calculation of MBGLR statistic requires maximization over all the past samples, and a moving window can be used to relieve part of the computational burden. The window size is required to include a sufficiently large number of observations to get robust in and out-of-control performance, as in the case of no window. It was found that the control limit of the MBGLR chart and the log scale of in-control ANOS have a linear relationship for many combinations of p_0, ρ and p_{ub}. Fitted linear regression equations are provided for practitioners to use in finding the control limit for given values of p_0, ρ, p_{ub}, and the desired ICANOS. The upper bound of the MBGLR chart is optimized using a loss function END, which counts the overall extra number of defectives produced when the process proportion shifts. It is shown that the upper bound selection depends on the possible maximum shift that can occur as well as the prior distribution of the possible shift. When all shifts have an equal chance to occur, it is suggested that the upper bound be selected to be equal to the maximum shift. The MBGLR chart and the MBCUSUM chart are optimized with respect to the upper bound and the pre-determined shift

size, respectively, using the END under different combinations of $p_0, \rho,$ maximum shift, and the prior distribution. It is concluded that the optimized MBGLR chart is better than the optimized MBCUSUM chart with less loss in terms of END. The optimized MBGLR chart can be much better than the optimized MBCUSUM chart when there is a wide range of possible shifts, and especially for the high quality processes with small values of p_0.

The second part of the proposal is an extension of the first part and investigated control charts for monitoring a process in which the proportion and correlation can shift simultaneously. We extended the idea of the MBCUSUM chart and the MBGLR chart and proposed the CUSUM-$p\rho$ and GLR-$p\rho$ charts. The CUSUM-$p\rho$ chart with two tuning parameters is a good choice when the shifts in proportion and correlation are known. This chart is better than using two traditional CUSUM charts in the sense that it only has one control limit that needs to be specified and therefore is easier to design. Based on the proposed CUSUM-$p\rho$ chart, we proposed the CUSUM-$p\rho$ chart combination to detect both increases and decreases in the correlation and increases in the proportion. The overall performance of this chart combination in most of the possible directions can beat the other CUSUM-type charts. When the actual shifts are unknown, using a GLR-$p\rho$ chart with a relatively large upper bound can provide better performance over a wider range of shifts than the CUSUM-type charts.

In monitoring a correlated binary process, we found that shifts in correlation are difficult to detect compared with shifts in proportion. The GLR-$p\rho$ chart, as well as the other charts, cannot detect small shifts in correlation very fast. However, when detecting shifts in proportion or simultaneous shifts in the two parameters, with a relatively larger upper bound on the proportion, the detection is very fast for most of the shifts in various directions.

The last part of the dissertation considers the situation in which samples are taken as a group with $n > 1$, when consecutive samples are taken with a long enough time difference between them that we can assume independence for the samples. Within one sample, the number of defectives follows a Markov binomial distribution which arises when the individual observations in a sample follow the two-state Markov chain model. There are several possible sampling plans and assumptions about shifts available for this case. We assume that the shift only occurs between samples and the Markov binomial GLR chart is proposed to detect an increase in the proportion while the correlation remains at the in-control value. The proposed

MBNGLR chart is compared with traditional types of charts and it is shown to beat those charts in terms of overall better performance and ease of design. Besides the comparisons of different charts, we found that the sample size selection affects the ability to detect shifts. For a given sampling rate per unit time, a large sample size with a long sampling interval provides better performance in detecting small shifts, while a small sample size with a short sampling interval detects large shifts faster.

6.2 Future Topics

So far, we have proposed several charts for monitoring the proportion and correlation in correlated binary process. The charts include CUSUM-type charts, chart combinations, and GLR charts. To monitor the proportion, we proposed a MBGLR chart and compared the chart performance with the MBCUSUM chart. The design methodology was investigated for the MBGLR chart in Chapter 3. The work in Chapter 3 assumes that the binary observations (case of $n = 1$) follow a two-state Markov chain model where the current observation only depends on the previous one. A more general model can be considered in the future, such as a higher order Markov chain model. Higher order models contain more parameters and the development of control charts for monitoring the proportion would probably need to assume that other parameters are unchanged.

In Chapter 4, the CUSUM-$p\rho$ chart, the CUSUM-$p\rho$ chart combination, and the GLR-$p\rho$ chart were proposed to monitor the shifts in both the proportion and the correlation. We did a complete performance comparison of these charts on wide shift ranges. However, the design methodology for the GLR-$p\rho$ chart needs to be investigated in the future, especially providing an equation to find the control limit as was done for the MBGLR chart in Chapter 3. It is also shown that the performance of the GLR-$p\rho$ works much better than the CUSUM-$p\rho$ chart in the high quality process. Another future work is to investigate the performance of GLR- $p\rho$ when the in-control parameters are at extreme cases, for instance, at very small values of proportion.

The last part in the dissertation investigates using a GLR chart for monitoring a proportion when observations are grouped into samples. The correlated binary observations are available with a long enough time period between samples to assume independence has been

completed. We proposed a MBNGLR chart for monitoring the process proportion in this case and the chart is compared with an EWMA-GLR chart and a Shewhart-CUSUM chart combination. In the future, more comparisons need to be done to obtain more general conclusions for this situation. Also, development of the design methodology for the MBNGLR chart is also in need.

When the MBGLR chart and the GLR- $p\rho$ are applied, it is necessary to obtain the maximum-likelihood estimates of the parameters and change point. We used the grid search method to find the global maximum point of the objective function for estimating the parameters and the change point. One future issue is to investigate the smoothness of the objective function, especially in the cases with extreme in-control parameters.

In the work of the dissertation, we assume that the parameters are known or well estimated from Phase I data. When the parameters are estimated from Phase I data, it is necessary to have large enough dataset. When the parameters are not accurately estimated, the performance of the chart will be affected. Therefore one future research topic is to evaluate the effect of estimating the in-control parameters from Phase I data.

Appendix

Appendix A

When the binary observations are independent, the sequence can be written as equivalent geometric observations. Applying this idea to the correlated binary sequences $X_1, X_2, \ldots$, the number of items observed until a defective is observed can be defined as a geometric-type random variable Y. The geometric-type random variables are used to speed up the simulation used to obtain the numerical results in this proposal. When p is small most of the observations from the correlated binary process will be 0 with an occasional 1. The GLR chart will only signal when a 1 is observed, so in simulating observations it is much faster to simulate the geometric-type variables Y instead of the individual correlated binary observations. The geometric-type sequence $Y_1, Y_2, \ldots Y_t$ corresponding to the binary sequence $X_1, X_2, \ldots X_k$ satisfies $\sum_{j=1}^{t} Y_j = k$ and $X_k = 1$.

Shepherd et al. (2007) showed that the geometric-type random variables $Y_1, Y_2, \ldots$ are independent and derived their distributions. The distribution of the first geometric- type observation Y_1 depends on the starter of the binary correlated sequence $X_i, i = 1, 2, 3 \ldots$. With probability p we have $X_1 = 1$, and this gives $Y_1 = 1$. If $X_1 = 0$, then the first defective item would be observed after a sequence of non-defective items and for $k = 2, 3, \ldots$

$$P(Y_1 = y_j) = P(X_k = 1 \text{ and } X_i = 0, i = 1,2,3 \ldots k-1)$$

where $y_t > 1$. Since the sequence $X_i, i = 1, 2, 3 \ldots$ is a two state Markov Chain and the current state only depends on the previous state, the above equation becomes:

$$\begin{aligned} f(Y_1 = y_t) &= f(X_k = 1 | X_{k-1} = 0) f(X_{k-1} = 0 | X_{k-2} = 0) \ldots f(X_2 = 0 | X_1 = 0) f(X_1 = 0) \\ &= p_{01}(p_{00})^{y_t - 2}(1-p) \end{aligned}$$

For the rest of the observations $Y_t, t = 2, 3 \ldots$, the outcome $Y_t = 1$ means that after the $(t-1)^{th}$ defective observation in the correlated binary sequence, we immediately observe the t^{th} defective. Thus

$$f(Y_t = 1) = f(X_{\sum_{j=1}^{t} Y_j} = 1 | X_{\sum_{j=1}^{t-1} Y_j} = 1) = p_{11}$$

If $Y_t = y_t$, where $y_t > 1$, then after the $(t-1)^{th}$ defective in the correlated binary sequence, $y - 1$ non-defective items would be observed before the t^{th} defective occur, i.e. the corresponding binary sequence will be 10, 00,00,00,…,01. Thus,

$$f(Y_t = y_t) = f\left(X_{\sum_{j=1}^{t} Y_t} = 1 \middle| X_{\sum_{j=1}^{t} Y_t - 1} = 0\right) f\left(X_{\sum_{j=1}^{t} Y_t - 1} = 0 \middle| X_{\sum_{j=1}^{t} Y_t - 2} = 0\right) \ldots.$$

$$\ldots f\left(X_{\sum_{j=1}^{t-1} Y_t + 2} = 0 \middle| X_{\sum_{j=1}^{t-1} Y_t + 1} = 0\right) f\left(X_{\sum_{j=1}^{t-1} Y_t + 1} = 0 \middle| X_{\sum_{j=1}^{t-1} Y_t} = 1\right)$$

$$= p_{01}(p_{00})^{y_t - 2} p_{10}$$

Then the distribution of Y_t is:

$$f(y_t | p, \rho) = \begin{cases} p, & if\ t = 1\ and\ y_1 = 1 \\ p_{01}(p_{00})^{y_t - 2}(1-p), & if\ t = 1\ and\ y_1 \geq 2 \\ p_{11}, & if\ t \geq 2\ and\ y_t = 1 \\ p_{01}(p_{00})^{y_t - 2} p_{10}, & if\ t \geq 2\ and\ y_t \geq 2 \end{cases}$$

Let Y_δ be the geometric-type observation such that δ is the smallest integer with $\sum_{j=1}^{\delta} Y_j$ satisfying $\sum_{j=1}^{\delta} Y_j \geq \tau$. In simulation, the geometric-type observations are simulated from $p = p_0$ until $\sum_{j=1}^{\delta} Y_j \geq \tau$. If $\sum_{j=1}^{\delta} Y_j = \tau$, then $X_\tau = 1$. We continue simulated sequence $Y_{\delta+1}, Y_{\delta+2}, \ldots$ from the distribution of Y using $p = p_1$. If $\sum_{j=1}^{\delta} Y_j > \tau$, then $X_\tau = 0$. Then $X_{\tau+1}, X_{\tau+2}, \ldots$ are simulated using $p = p_1$ until a defective is observed. After this defective, we continue simulating the geometric-type observations with $p = p_1$.

Before we discuss the equivalence of the likelihood functions in the GLR statistics using Y and using X, we first argue that a signal given at X_k satisfies $X_k = 1$. Suppose a signal is given at X_k with $X_k = 0$ and let $X_{k^*} = 1$ be the last defective observation. Then we will have a sequence $X_{k^*}, X_{k^*+1}, \ldots X_k$ with all observations being non-defective and the contribution of this sequence to the likelihood ratio will reduce the value of R_k compared to the value of R_{k^*}. Thus if a signal is not given at k^*, the chart would not signal at k. Therefore, if k is the first time that a

signal is given, then X_k must satisfy $X_k = 1$. We will show the equivalence of the equivalence of the likelihood function in the GLR statistic using Y and using X based on this argument.

Now we will show that the likelihood function in the GLR statistic using Y is equivalent to the one using the binary variable X. First, we consider the case with a signal given before the change point. Suppose the signal is given at X_k with $k \leq \tau$ and the binary sequence $X_1, X_2, \dots X_k$ corresponds to the geometric-type sequence $Y_1, Y_2, \dots, Y_t$ with $\sum_{j=1}^{t} Y_j = k$ and $\sum_{i=1}^{k} X_i = t$. Suppose $Y_t = y_t$ for $t = 1, 2, \dots$, then in the binary sequence, we observe defectives at $X_{y_1}, X_{y_1+y_2}, \dots X_k$. To show that the likelihood function based on $X_1, X_2, \dots X_k$ is equivalent to that based on $Y_1, Y_2, \dots, Y_t$, we only need to show:

$$f(X_1 | p_0, \rho) f(X_2 | X_1, p_0, \rho) \dots f\left(X_{y_1} | X_{y_1-1}, p_0, \rho\right) = f(Y_1 | p_0, \rho) \tag{A.1}$$

$$f\left(X_{y_1+1} | X_{y_1}, p_0, \rho\right) \dots f\left(X_{y_1+y_2} | X_{y_1+y_2-1}, p_0, \rho\right) = f(Y_2 | p_0, \rho) \tag{A.2}$$

…

$$f(X_{\sum_{j=1}^{t-2} y_j+1} | X_{\sum_{j=1}^{t-2} y_j}, p_0, \rho) \dots f(X_{\sum_{j=1}^{t-1} y_j} | X_{\sum_{j=1}^{t-1} y_j-1}, p_0, \rho) = f(Y_{t-1} | p_0, \rho)$$

$$f\left(X_{\sum_{j=1}^{t-1} y_j+1} \middle| X_{\sum_{j=1}^{t-1} y_j}, p_0, \rho\right) \dots f\left(X_k \middle| X_{\sum_{j=1}^{t} y_j-1}, p_0, \rho\right) = f(Y_t | p_0, \rho).$$

When $X_1 = 1$, we have $Y_1 = 1$, and the left side of Equation (A.1) becomes $f(X_1 | p_0, \rho)$ and equals to p_0. The right side of Equation (A.1) $f(Y_1 | p_0, \rho) = p_0$ when $Y_1 = 1$. When $X_1 = 0$, we have $Y_1 > 1$, and the left side of Equation (A.1) satisfies:

$$f(X_1 | p_0, \rho) f(X_2 | X_1, p_0, \rho) \dots f\left(X_{y_1} | X_{y_1-1}, p_0, \rho\right) = (1-p) p_{00}^{y_1-2} p_{01}$$

The right side of Equation (A.1) is $f(Y_1 | p_0, \rho) = (1-p) p_{00}^{y_1-2} p_{01}$. Thus the equivalence in Equation (A.1) is true.

The proofs of equality for the other equations are similar and we will only show that Equation (A.2) is true. When $Y_2 = 1$, we have $X_{y_1+y_2} = 1$. Then the left side of Equation (A.2) becomes $f\left(X_{y_1+y_2} | X_{y_1+y_2-1}, p_0, \rho\right) = p_{11}$ and the right side of Equation (A.2) is $f(Y_2 | p_0, \rho) = p_{11}$ when $Y_2 = 1$. When $Y_2 > 1$, the corresponding binary sequence starts with a non-defective

with the previous one being defective, and after another $y_2 - 2$ non-defective observations, the sequence reaches the last one being defective. Therefore the left side of Equation (A.2) satisfies:

$$f(X_{y_1+1}|X_{y_1}, p_0, \rho) \dots f(X_{y_1+y_2}|X_{y_1+y_2-1}, p_0, \rho) = p_{10}(p_{00})^{y_2-2}p_{01}$$

The right side of Equation (A.2) $f(Y_2|p_0, \rho)$ is $p_{10}(p_{00})^{y_2-2}p_{01}$ following the distribution of Y. The equivalence of Equation (A.2) is true.

So far, we have showed that the equivalence of the likelihood function using the correlated binary sequence is equivalent to that using the geometric-type sequence when there is a signal observed before the change point τ. Now we consider the case in which the signal is observed after the change point. Now we consider the sequence $X_1, X_2, \dots X_k$ corresponding to the geometric-type sequence $Y_1, Y_2, \dots, Y_t$ with $\sum_{j=1}^{t} Y_j = k$ and $0 \leq \tau < k$. In the GLR statistic the likelihood ratio only consists of density functions of $X's$ after the change point, so we will only need to show the equivalence of likelihood functions based on geometric-type random variables and that based on binary variables between the change point τ and the current sample.

As in the discussion of the simulation of Y, Y_δ is the geometric-type observation satisfying $\sum_{j=1}^{\delta} Y_j \geq \tau$. We first consider the case with $\sum_{j=1}^{\delta} Y_j = \tau$ and $X_\tau = 1$ and the correlated binary sequence $X_{\tau+1}, X_{\tau+2}, \dots X_k$ corresponds to the geometric-type sequence $Y_{\delta+1}, Y_{\delta+2}, \dots Y_t$. We observe defectives at $X_{\tau+y_{\delta+1}}, X_{\tau+y_{\delta+1}+y_{\delta+1}}, \dots, X_{\tau+\sum_{j=\delta+1}^{t} y_j}$. To prove the equivalence of the likelihood function based on $X_{\tau+1}, X_{\tau+2}, \dots X_k$ and that based on $Y_{\delta+1}, Y_{\delta+2}, \dots Y_t$, we only need to show:

$$f(X_{\tau+1}|\, p_1, \rho) f(X_{\tau+2}|X_1, p_1, \rho) \dots f(X_{\tau+y_1}|X_{y_1-1}, p_1, \rho) = f(Y_{\delta+1}|p_1, \rho),$$

$$f(X_{y_1+1}|X_{y_1}, p_1, \rho) \dots f(X_{y_1+y_2}|X_{y_1+y_2-1}, p_1, \rho) = f(Y_{\delta+2}|p_1, \rho),$$

…

$$f(X_{\tau+\sum_{j=\delta+1}^{t-2} y_j+1}|X_{\tau+\sum_{j=\delta+1}^{t-2} y_j}, p_1, \rho) \dots f(X_{\tau+\sum_{j=\delta+1}^{t-1} y_j}|X_{\tau+\sum_{j=\delta+1}^{t-1} y_j-1}, p_1, \rho) = f(Y_{t-1}|p_1, \rho)$$

$$f(X_{\tau+\sum_{j=\delta+1}^{t-1} y_j+1}|X_{\tau+\sum_{j=\delta+1}^{t-1} y_j}, p_1, \rho) \dots f(X_{\tau+\sum_{j=\delta+1}^{t} y_j}|X_{\tau+\sum_{j=\delta+1}^{t} y_j-1}, p_1, \rho) =$$
$$f(Y_t|p_1, \rho).$$

It is noticed that the proof of the above equations are similar to that of Equation (A.2). The difference is the equations above, the binary and the geometric-type variables have parameters p_1 and ρ while in Equation (A.2), the parameters are p_0 and ρ. However, the difference in the value of p does not affect the proof on the equivalence of these equations and therefore we will omit the proof of these equations here.

When a signal is observed after the change point, the second case we consider is $\sum_{j=1}^{\delta} Y_j > \tau$ and $X_\tau = 0$. In this case, the geometric-type sequence $Y_\delta, Y_{\delta+1}, \dots Y_t$ corresponds to $X_{a+1}, \dots X_\tau, \dots X_b, X_{b+1}, \dots X_k$, where X_a is the last defective observation before the change point and X_b is the first defective after the change point. Then $Y_{\delta+1}, \dots Y_t$ corresponds to $X_{b+1}, \dots X_k$ with p shift to p_1 and Y_δ corresponds to $X_{a+1}, \dots, X_\tau, \dots X_b$. The equivalence in the likelihood functions based on $Y_{\delta+1}, \dots Y_t$ and that based on $X_{b+1}, \dots X_k$ can be shown similarly as the proofs for Equation (A.2). Y_δ, which covers the change point in the binary sequence was simulated from the original binary sequence and therefore the likelihood functions are equivalent using the correlated binary sequence and the geometric-type sequence.

Appendix B

In Appendix A we showed that the equivalence of the likelihood functions in the GLR statistic using the binary variables and the geometric-type random variables. Now we discuss the relationship between the window size m for binary observations and the window size m' for the geometric-type observations.

In the simulation, a sequence of $Y_{t-m'}, Y_{t-m'-1}, \dots . Y_{t-1}$ will be stored in the window. In a window, storeing m' geometric-type observations is equivalent to storing a binary sequence of random length. Shepherd et. al (2007) proved that the geometric-type random variables Y_t satisfy:

$$E(Y_1) = \frac{p_{10}}{p_{01}(p_{01} + p_{10})} = \left(\frac{1}{p} - 1\right) * \frac{1}{1-\rho}$$

$$E(Y_t) = \frac{p_{10}}{p_{01}} = \frac{1}{p} - 1$$

In the correlated binary case, the window size of binary observations m and equivalent geometric observations m' satisfy:

$$E(m) = m' * E(Y_t) = \begin{cases} \frac{m'(1-p)}{p(1-\rho)} & if\ t = 1 \\ \frac{m'(1-p)}{p} & if\ t > 1 \end{cases}$$

when Y_1 is not in the window. When Y_1 is in the window and $m' > 1, E(m) = E(Y_1) + (m' - 1)E(Y_2)$.

It is noted that in the independent case, m' satisfies $E(m) = m' \times \frac{1}{p}$, where $\frac{1}{p}$ is the expectation of geometric random variable. It is noted that in the correlated binary case $E(m)$ depends on p when $t > 1$ and as the proportion shifts from p_0 to $p_1 > p_0$, $E(m)$ decreases. When $t = 1$, $E(m)$ is affected by both p and ρ. As ρ increases, $E(m)$ gets larger.

Since we consider relatively small correlations in this proposal and the distribution of Y_1 has little effect on the SSANOS because we assume that the shift occurs after the process reaches a steady state, we will only consider the case when $t > 1$. When the window size m of the correlated binary variable is required to be equal to a particular value w, then in the simulation, m' is set to be $\frac{wp_0}{1-p_0}$ where p_0 is the in-control value of p_0.

References

Altham, P. M. E. (1978). "Two Generalizations of the Binomial Distribution". *Applied Statistics,* 27(2), pp. 162–167.

Alwan, L.C. and Roberts, H.V. (1995). "The Problem of Misplaced Control Limits". *Applied Statistics-Journal of The Royal Statistical Society Series* C 44(3), pp. 269-278.

Apley, D. W. and Shi, J. (1999). "The GLRT for Statistical Process Control of Autocorrelated Processes". *IIE Transactions,* 31, pp. 1123-1134.

Basseville, M. and Nikiforov, I. V. (1993). Detection of Abrupt Changes: Theory and Applications. Eaglewood Cliffs, NJ: Prentice-Hall.

Bhat, N., and Lal, R. (1990). "Attribute Control Charts for Markov Dependent Production Processes". *IIE Transactions,* 22, pp. 181-188.

Blatterman, D. K. and Champ, C. W. (1992). "A Shewhart Control Chart Under 100% Inspection for Markov Dependent Attribute Data". *Proceedings of the 23 rd Annual Modeling and Simulation Conference, Pittsburg, PA*, pp. 1769-1774.

Blatterman, D. K. and Rigdon, S. E. (1994). "A CUSUM Quality Control Chart Under 100% Inspection for Markov Dependent Attribute Data". *Proceedings of the Third Industrial Engineering Research Conference, Atlanta, GA,* pp. 34-39.

Blostein, S. D. (1991). “Quickest Detection of a Time-Varying Change in Distribution”. *IEEE Transactions on Information Theory*, 37, pp. 1116-1122.

Bourke, P. D. (1991). “Detecting a Shift in Fraction Non-conforming Using Run-Length Control Charts with 100% Inspection”. *Journal of Quality Technology,* 23, pp. 225-238.

Broadbent, S. R. (1958). “The Inspection of a Markov Process”. *Journal of the Royal Statistical Society Series B-Statistical Methodology,* 20, pp. 111-119.

Capizzi, G. (2001). “Design of Change Detection Algorithms Based on the Generalized Likelihood Ratio Test”. *Environmetrics*, 12, pp. 749-756.

Champ, C. W. , Blatterman, D. K. and Rigdon, S. E. (1994). “A CUSUM Quality Control Chart Under 100% Inspection for Markov Dependent Attribute Data”. *Proceedings of the Third Industrial Engineering Research Conference, Atlanta, GA,* pp. 34-39.

Chen, R. (1978). “A surveillance system for congenital malformations”. Journal of American Statistical Association (73) 362, pp. 323-327.

Deligonul, Z.S. and Mergen, A.E.(1987). “Dependence Bias in Conventional p Charts and its Correction with an Approximate Lot Quality Distribution”. *Journal of Applied Statistics,* 14, pp. 75-81.

Gan, F. F. (1991). "An Optimal Design of Cusum Quality Control Charts". *Journal of Quality Technology*, 23, pp. 279-286.

Gan, F. F. (1993). "An Optimal Design of CUSUM Control Charts for Binomial Counts". *Journal of Applied Statistics*, 20, pp. 445-460.

Gupta, R. C. and Tao, H (2010). "A generalized correlated binomial distribution with application in multiple testing problems". *Metrika*, 71, pp. 59-77

Hisakado, M, Kitsukawa, K. and S. Mori (2006), "Correlated Binomial Models and Correlation Structures". *Journal of Physics*, A39 15365.

Huang, W. "GLR Control Charts for Monitoring a Proportion". Ph.D. Dissertation, Virginia Polytechnic Institute and State University, 2011.

Huang, W., Reynolds M. R. Jr. and Wang. S. (2012) "A binomial GLR control chart for monitoring a proportion". *Journal of Quality Technology* 44, pp. 192-208.

Huang, W., Wang, S. and Reynolds, M. R., Jr. (2013). "A Generalized Likelihood Ratio Chart for Monitoring Bernoulli Processes". *Quality and Reliability Engineering International*, 29(5), pp. 665-679.

Lou. J. and Reynolds, M. R., Jr. (2012). "Maximum-Likelihood-Based Diagnostics after a Signal from Control Charts". *Journal of Quality Technology* 44, pp. 321-347.

Kupper，L．L．and Hasman, J. K. (1978)．“The Use of a Correlated Binomial Model for the Analysis of Certain Toxicological Experiment”. *Biometrics*, 34, pp: 69-74.

Lai, T. L. (1995). “Sequential Changepoint Detection in Quality-Control and Dynamical-Systems”. *Journal of the Royal Statistical Society Series B-Methodological*, 57, pp. 613-658.

Lai, T. L. (1998). “Information Bounds and Quick Detection of Parameter Changes in Stochastic Systems”. *IEEE Transactions on Information Theory*, 44, pp. 2917-2929.

Lai, T. L. (2001). “Sequential Analysis: Some Classical Problems and New Challenges”. *Statistica Sinica*, 11, pp. 303-351.

Lorden, G. (1971). “Procedures for Reacting to a Change in Distribution”. *The Annals of Mathematical Statistics*, 42, pp. 1897-1908.

MacDonald, I. L. and Zucchini, W. (1997), Hidden Markov and Other Models for Discrete-valued Time Series. Chapman & Hall, UK.

Madsen, R. W. (1993). “Generalized binomial distributions”. *Communications in Statistics—Theory and Methods,* 1993, 22(11), pp. 3065–3086.

McCracken,A.K., and Chakraborti,S. (2013), "Control Charts for Joint Monitoring of Mean and Variance: An Overview". *Quality Technology and Quantitative Management,* 10, 1, pp. 17-36

Megahed, F. M., Kensler J. L. K., Bedair, K. and Woodall, W. H. (2011). "A Note on the ARL of Two-Sided Bernoulli-Based CUSUM Control Charts". *Journal of Quality Technology*, 43, pp. 43–49.

Mousavi, S. M. and Reynolds, M. R. Jr. (2008), "Monitoring Markov Dependent Observations with a Log-likelihood Based CUSUM". Technical Report 08-3, Department of Statistics, Virginia Tech.

Mousavi, S. M., "Monitoring Markov Dependent Binary Observations with a Log-Likelihood Ratio Based CUSUM Control Chart", Ph.D. Dissertation, Virginia Polytechnic Institute and State University, 2009.

Mousavi, S. M. and Reynolds, M. R. Jr. (2009). "A CUSUM Chart for Monitoring a Proportion with Autocorrelated Binary Observation". *Journal of Quality Technology*, 41, pp. 401–414.

Mori, S., Kitsukawa, K and Hisakado, M (2011) "Moody's Correlated Binomial Default Distributions for Inhomogeneous Portfolios". *Quantitative Finance*, 11, 3 pp. 391-405

Page, E. S. (1954). "Continuous Inspection Schemes". *Biometrika*, 41, pp. 100-114.

Reynolds, M. R. Jr., Lou, J. (2010) "An evaluation of a GLR control chart for monitoring the process mean". *Journal of Quality Technology*, 42, pp. 287–310.

Reynolds, M. R. Jr., Lou, J., Wang, S., Lee, J. (2013) "The Design of GLR Control Charts for Monitoring the Process Mean and Variance". *Journal of Quality Technology*, 45, pp. 287–310.

Reynolds, M. R., Jr. and Stoumbos, Z. G. (1999). "A CUSUM Chart for Monitoring a Proportion When Inspecting Continuously". *Journal of Quality Technology,* 31, pp. 87-108.

Reynolds, M. R., Jr. and Stoumbos, Z. G. (2000). "A General Approach to Modeling CUSUM Charts for a Proportion". *IIE Transactions*, 32, pp. 515-535.

Roberts, S. W. (1959). "Control Chart Tests Based on Geometric Moving Averages". *Technometrics*, 42, 1, *Special 40th Anniversary Issue*, pp. 97-101.

Runger, G. C. and Testik, M. C. (2003). "Control Charts for Monitoring Fault Signatures: Cuscore Versus GLR". *Quality and Reliability Engineering International*, 19, pp. 387-396.

Shepherd, D. K., Champ, C. W., Rigdon, S. E. and Fuller, H. T. (2007). "Attribute Charts for Monitoring a Dependent Process". *Quality and Reliability Engineering International*, 23, pp. 341-365.

Shewhart, W. A. (1931). Economic control of quality of manufactured product, Van Nostrand, New York.

Szarka, J. L., III. and Woodall, W. H. (2011). "A Review and Perspective on Surveillance of Bernoulli Processes". *Quality and Reliability Engineering International*, 27, pp. 735-752.

Wang, N. and Reynolds, M. R., Jr. (2013). "The GLR Chart for Monitoring a Proportion with Autocorrelation". *Journal of Quality Technology*, submitted.

Wang, S. and Reynolds, M. R., Jr. (2013). "A GLR Control Chart for Monitoring the Mean Vector of a Multivariate Normal Process". *Journal of Quality Technology*, 45, pp. 287–310.

Weiss, C.H. (2009) "Group Inspection of Dependent Binary Process". *Quality and Reliability Engineering International*, 25, pp. 151-165.

Westgard, J. O., Groth, T., Aronsson, T. and De Verdier, C. (1977). "Combined Shewhart-CUSUM Control Chart for Improved Quality Control in Clinical Chemistry". *Clinical Chemistry*, 23, pp. 1881-1887.

Willsky, A. S. and Jones, H. L. (1976). "Generalized Likelihood Ratio Approach to Detection and Estimation of Jumps in Linear-Systems". *IEEE Transactions on Automatic Control*, 21, pp. 108-112.

Woodall, W. H (1997). "Control Charts Based on Attribute Data: Bibliography and Review". *Journal of Quality Technology* 29, pp. 172-183.

Woodall, W. H (2006). "The Use of Control Charts in Health-Care and Public-Health Surveillance". *Journal of Quality Technology* 38, pp. 89-104.

Zhao, H., Jin, R., Wu, S., Shi, J. (2011) "PDE-Constrained Gaussian Process Model on Material Removal Rate of Wire Saw Slicing Process". *Journal of Manufacturing Science and Engineering*, 133, 021012-1.